NOTICE

The quality of this microform is heavily dependent upon the quality of the original thesis submitted for microfilming. Every effort has been made to ensure the highest quality of reproduction possible.

If pages are missing, contact the university which granted the degree.

Some pages may have indistinct print especially if the original pages were typed with a poor typewriter ribbon or if the university sent us an inferior photocopy.

Reproduction in full or in part of this microform is governed by the Canadian Copyright Act, R.S.C. 1970, c. C-30, and subsequent amendments.

AVIS

La qualité de cette microforme dépend grandement de la qualité de la thèse soumise au microfilmage. Nous avons tout fait pour assurer une qualité supérieure de reproduction.

S'il manque des pages, veuillez communiquer avec l'université qui a conféré le grade.

La qualité d'impression de certaines pages peut laisser à désirer, surtout si les pages originales ont été dactylographiées à l'aide d'un ruban usé ou si l'université nous a fait parvenir une photocopie de qualité inférieure.

La reproduction, même partielle, de cette microforme est soumise à la Loi canadienne sur le droit d'auteur, SRC 1970, c. C-30, et ses amendements subséquents.

ISBN 0-315-53833-3

SLIDING SHEAR IN LOW RISE SHEAR WALLS UNDER LATERAL LOAD REVERSALS

by
Zbigniew Feliks Wasiewicz

A thesis
submitted under the supervision of
Dr. Murat Saatcioglu

in partial fulfillment
of the requirements for the degree of
Master of Applied Science

Department of Civil Engineering
Faculty of Engineering
University of Ottawa

Abstract

In this investigation, two reinforced concrete walls with aspect ratios of one – quarter and one – half were designed, constructed and tested. The wall with an aspect ratio of one – quarter was reinforced with minimum shear reinforcement, while the other was overdesigned for shear. Specially detailed joint reinforcement was provided at the construction joint in both walls to prevent shear sliding. Both specimens were subjected to inelastic lateral load reversals.

The test data were analytically studied. The load – deflection relationships, crack patterns, moment – rotation relationships and general observations during the test were analyzed. Behaviors of the two specimens were compared with those of the accompanying specimens tested earlier by others.

Both specimens failed in diagonal compression mode. The shear sliding failure, which occurred in two accompanying specimens was eliminated by means of specially detailed sliding shear reinforcement. The use of sliding shear reinforcement was proven to be an effective method of preventing shear sliding, while improving strength and ductility of low rise walls.

Finally, design recommendations were made to prevent shear sliding in low rise shear walls.

Acknowledgements

The author would like to express his gratitude to Dr. M.Saatcioglu for his guidance, advice, and financial support throughout this research project. Appreciations are extended to Mr. C.Pilette and the technical staff of the Civil Engineering Department for the assistance provided during the experimental part of this project.

Thanks are due to Mr. H. Hachem and S. Razvi for their help during the experiments.

Contents

List of Figures

List of Tables

Notations

A_{sv}	=	total area of vertical reinforcement
b	=	wall thickness
c	=	depth of compression zone
C_c	=	compression force in concrete
d	=	effective depth of the cross section
E	=	modulus of elasticity of steel
E_c	=	modulus of elasticity of concrete
F	=	applied force
f'_c	=	maximum compressive stress observed in a cylinder test
f_y	=	yield stress of reinforcement
f_u	=	ultimate stress of reinforcement
G	=	elastic shear modulus of concrete
h_w	=	height of the wall
l_w	=	length of the wall
M	=	applied moment
M_u	=	ultimate moment capacity
s	=	spacing of shear reinforcement
V_c	=	concrete contribution in shear capacity
V_s	=	steel contribution in shear capacity
V_u	=	shear force corresponding to ultimate moment capacity
$\bar{x}$	=	the distance of resultant compression force in the concrete from extreme compression fibre
γ_{xy}	=	angle of shear distortion in plane xy
δ	=	flexural component of deformation
ϵ_0	=	strain corresponding to maximum strain in concrete
ϵ_x	=	strain in concrete in x direction

ϵ_y = strain in concrete in y direction

ϵ_θ = strain in concrete at the plane inclined by θ to plane xz

θ = rotation of the top of the wall

ρ_{sv} = ratio of vertical reinforcement

ρ_{sh} = ratio of horizontal reinforcement

τ_n = nominal shear stress

ϕ = curvature

Chapter 1

Introduction

1.1 General

The primary function of reinforced concrete walls in building structures is to provide required strength and stiffness against lateral loads. The use of walls in earthquake resistant structures prevents nonstructural damage in the event of frequent minor earthquakes. The same walls minimize damage in the event of occasional moderate earthquakes. The walls when properly designed, also prevent structural collapse in the case of major earthquakes. To fulfill these requirements, the walls must be designed to have certain properties desirable in earthquake resistant structures. Among those, the most important are: stiffness, strength, stability, and ductility.

Generally it is difficult to achieve the required ductility in a reinforced concrete structure. However, many properly designed concrete structures withstood severe earthquakes in recent years. In the case of low intensity earthquakes, structural walls behave in elastic range. This provides full protection to nonstructural elements without having to satisfy requirements of

ductility. During strong earthquakes however structural walls respond to earthquake generated inertia forces in the postelastic range. Therefore, only those walls that are carefully designed, detailed and constructed, can develope the required ductility.

The behavior of a reinforced concrete wall is significantly influenced by the aspect ratio. The aspect ratio of a wall may be defined as the ratio of the wall height to wall width. Tall structural walls with an aspect ratio of more than 2 are representative of those that are found in medium–rise and high–rise buildings. The behavior of these walls is generally dominated by flexure. Therefore their design is similar to that for beams. Tall structural walls can be designed to behave in a ductile manner by promoting flexural yielding of vertical reinforcement. This can be achieved by providing shear capacity in excess of that corresponding to flexural strength.

While flexural behavior dominates the response of tall structural walls, squat walls with an aspect ratio of less than 2.0 behave differently. Squat walls are representative of those found in low–rise buildings. Shear and flexure in these members are more intimately interrelated and hence, these walls have to be treated separately. Therefore design of squat walls cannot be based on the conventional beam theory, applicable to tall structural walls.

1.2 Seismic performance of squat shear walls.

Low–rise buildings have periods of vibration shorter than those for high–rise buildings. Therefore, for an earthquake of given duration squat walls may be subjected to larger number of postelastic cycles than tall flexural walls. Accordingly, the demand for cumulative ductility is larger. Because

of increased number of inelastic cycles, stiffness and strength degradation may become critical [20]. In severe earthquakes, the survival of a structure can be assured only by the ability of structural elements to dissipate the largest possible energy, through stable hysteretic behavior. Furthermore, large deformations imposed on structural walls will result in substantial excursions into postelastic range. This calls for stable hysteretic behavior in the large inelastic deformation range, with minimum possible stiffness and strength degradation.

Well rounded stable load – displacement hysteresis loops can be attained in members subjected to high flexure and low shear stresses. This can be easily achieved by allocating major part of internal forces to flexural reinforcement, placed near the ends of the wall section. Yielding of flexural reinforcement, prior to development of high shear stresses ensures a ductile response. For walls with low aspect ratio, the presence of long internal arm, and uniform distribution of vertical reinforcement across the section, does not permit early yielding of flexural reinforcement prior to a built – up of high shear stresses. Hence, squat walls are more susceptible to inelastic shear distortion, which manifests itself by pinched character of load–displacement hysteresis loops.

The hysteretic behavior of squat shear walls may be affected by the following parameters:

- Wall aspect ratio.
- The magnitude of shear stresses.
- Presence and magnitude of axial load.
- Number of inelastic load reversals and their intensity.
- Vertical and horizontal reinforcement layouts.

- Vertical and horizontal reinforcement ratios.
- Presence and construction of boundary elements.
- Presence of a top element (i. e. roof, slab, floor, girder).
- Presence of specially detailed reinforcement or devices preventing shear sliding.
- Joint surface preparation.

There are three major modes of shear failure for squat walls with a rectangular cross section:

1. **Diagonal tension failure**
2. **Diagonal compression failure**
3. **Sliding shear failure**

Diagonal tension failure

This type of failure is caused by yielding of insufficient transverse reinforcement crossing the major diagonal crack, which may develop in the wall. The presence of top element (rigidly attached slab or beam) and wall aspect ratio are interrelated, and have significant influences on development of diagonal tension mechanism. While a squat wall without a top beam can develop a 45° shear failure plane, the same wall with a top beam may not develop the same shear failure plane. The top beam serves as a gigantic stirrup and prevents the 45° diagonal tension failure. In these walls a second failure plane may form between the opposite corners. For walls with a low aspect ratio (for example 1/2 or less), the shear force causing corner to corner diagonal tension failure plane may exceed that causing 45° diagonal tension failure [23]. Failures occur by excessive yielding and eventual

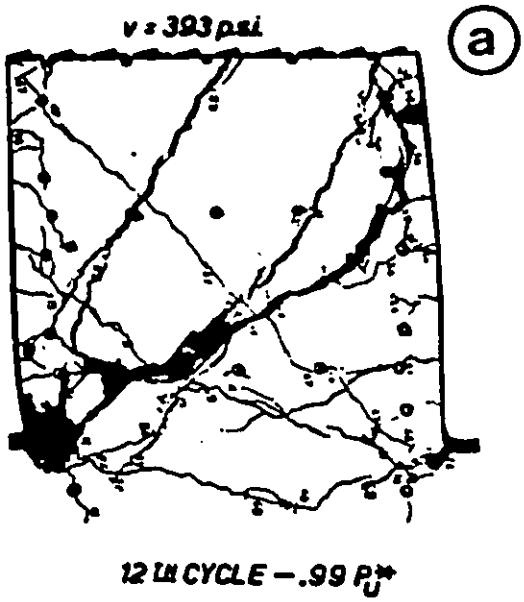

Figure 1.1: Diagonal tension failure of a wall with an aspect ratio of 1.0

fracture of horizontal shear reinforcement before the ultimate flexural capacity is reached. Diagonal tension failure, (considered as a "ductile type of failure") can be prevented by providing sufficient shear reinforcement. A typical 45° diagonal tension failure is shown in Fig. 1.1. A corner to corner diagonal tension failure is shown in Fig.1.2.

Diagonal compression failure

Cycles of load reversals produce two sets of diagonal shear cracks in two opposite directions. Further cycling causes opening and closing of the intersecting diagonal cracks, and consequently reduces the compression strength of concrete. Diagonal compression failure occurs when compressive stresses in diagonal struts exceed compressive strength of concrete. This type of failure is likely to occur when the wall has enough horizontal reinforcement to resist diagonal tension, and all other forms of failure are eliminated. Fig.1.3 illustrates a typical diagonal compression failure.

Sliding shear failure

This type of failure is typical of walls under cyclic loading, when the level of

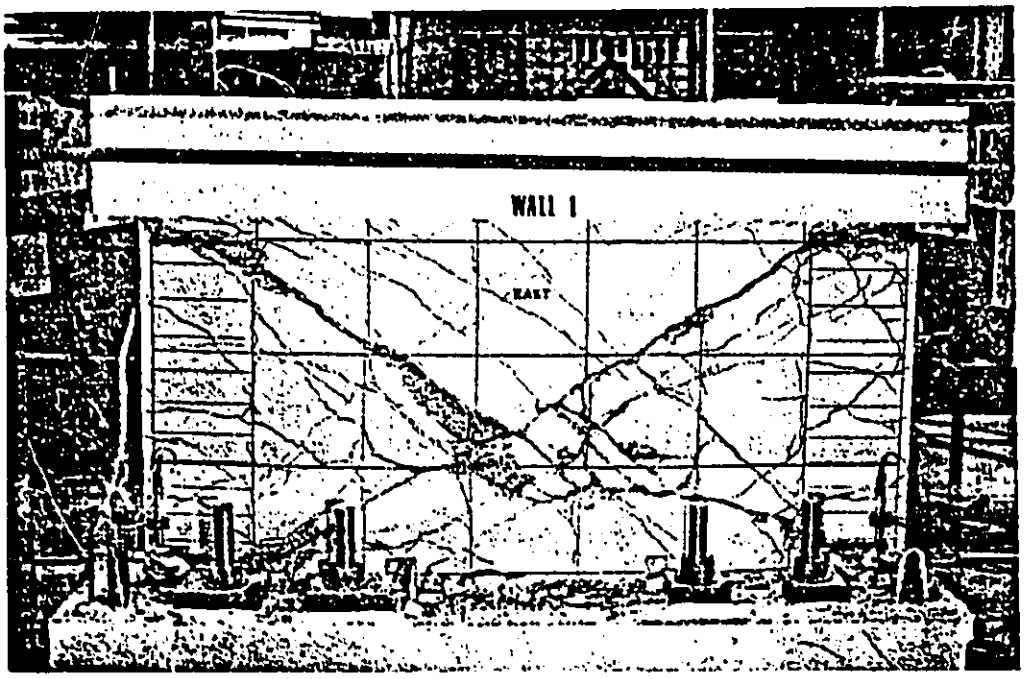

Figure 1.2: Diagonal tension (corner to corner) failure

Figure 1.3: Diagonal compression failure

nominal shear stress is high, and the diagonal tension failure is suppressed by adequate reinforcement while flexural yielding is permitted. When the wall is loaded monotonically, the compression zone usually remains intact until concrete crushing, and permits transfer of diagonal compression forces generated in diagonal struts. However, during cyclic loading, full flexural yielding of the cross section at the base causes opening and closing of flexural cracks. This produces deterioration of the interface roughness (decrement in friction coefficient) at the base . The shear transfer capacity is eventually reduced very significantly and if the applied force is high enough, the upper portion of the wall is forced to slide over the base.

Figure 1.4 illustrates the development of sliding shear mechanism. During the initial loading shown in Fig.1.4(a), high shear force at the base is transmitted across relatively small flexural compression zone. Yielding of flexural reinforcement forms a flexural base crack. During reversed loading, shown in Fig.1.4(b), flexural cracks develop within the previous flexural compression zone. Upon load reversals and applied higher forces, these flexural cracks extend to the middle of the section, forming one continuous crack. Beyond this load stage, shear force has to be transmitted by the dowel action of vertical reinforcement, and by friction forces between the wall panel and the base concrete. This is illustrated in Fig.1.4(c). With subsequent inelastic cycles, deterioration of cracked surfaces results in further reduction in shear friction resistance. Bond transfer along vertical reinforcement diminishes, and crushing of concrete around flexural bars at the joint location takes place. The crushing of concrete adjacent to the bars changes the character of dowel action of flexural reinforcement, and reduces stiffness of dowel shear mechanism. Eventually, the principal mode of shear transfer across the joint is provided only by kinking of vertical bars. This is shown in Fig1.4(d).

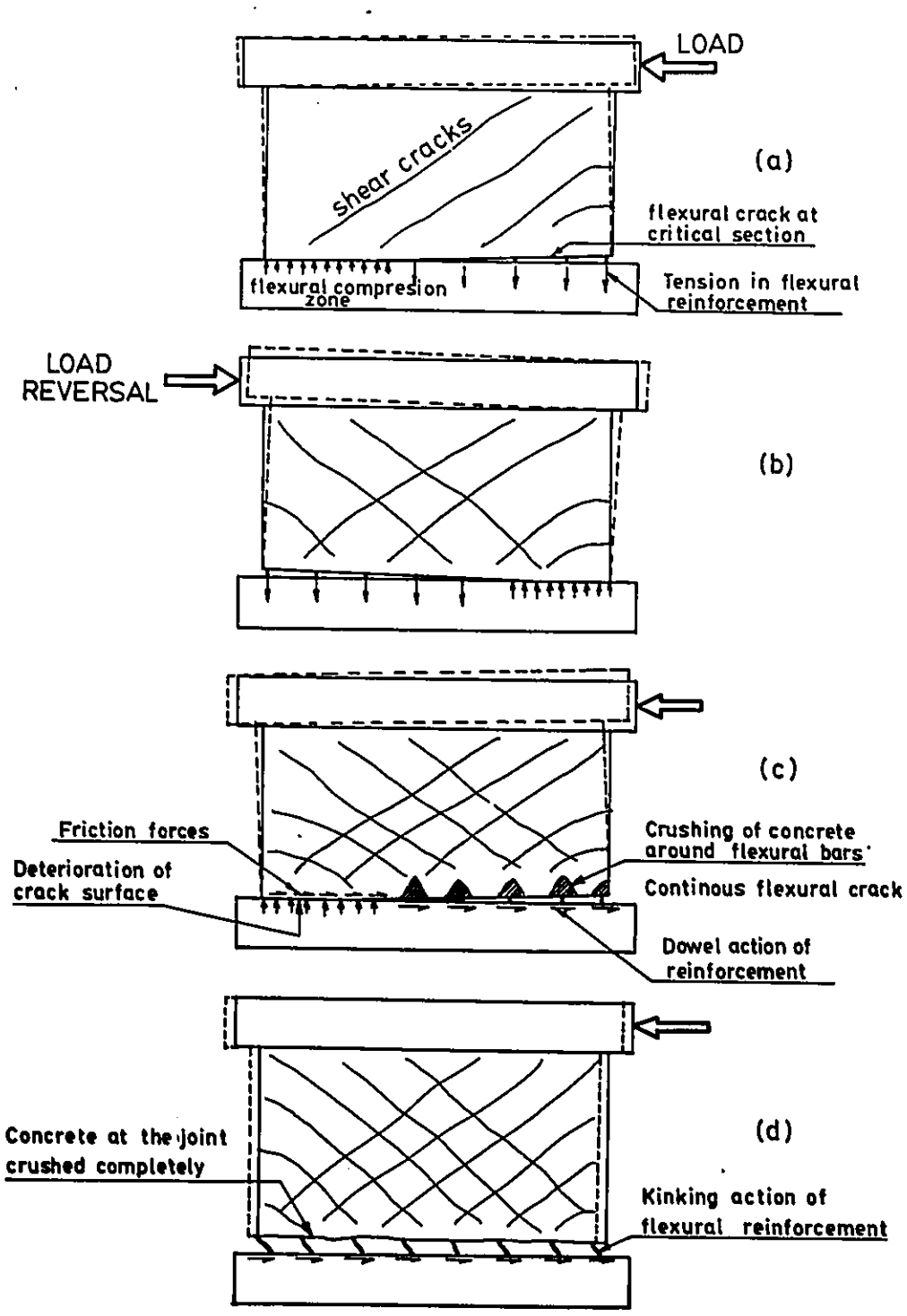

Figure 1.4: Shear sliding phenomena

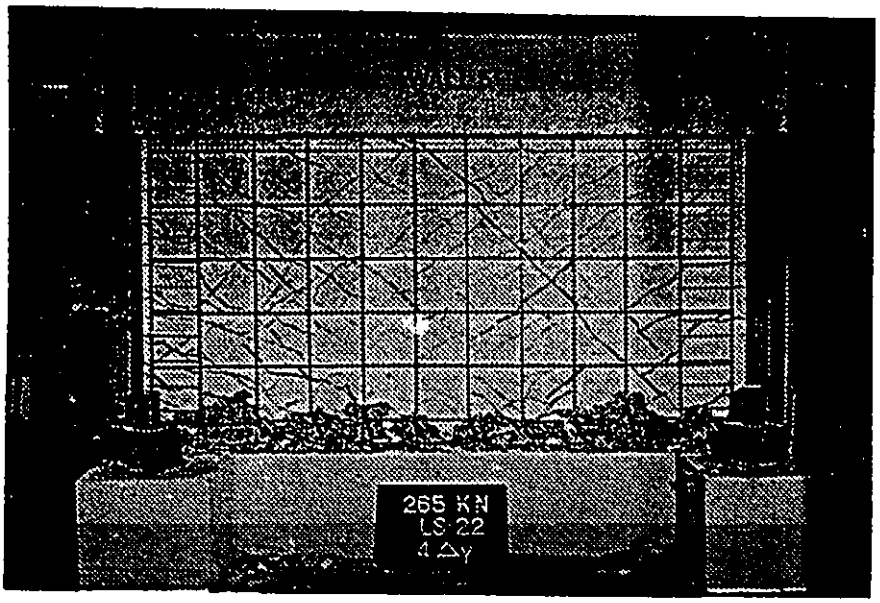

Figure 1.5: Sliding Shear failure

The sliding shear mechanism is not likely to develop in squat walls subjected to low nominal shear stresses. These walls usually have adequate shear transfer capacity at the construction joint. Sliding shear failure observed in a wall specimen is shown in Figure 1.5.

1.3 Previous Research

In 1972 Barda et al. [6] at the Portland Cement Association, Skokie, Ill., tested eight squat walls with boundary elements. Specimens with aspect ratios 1/2 and 1/4 were prepared with top elements representing slab or roof. The main variables included were: aspect ratio, vertical and horizontal steel contents, and type of loading (monotonic vs. cyclic). The main objective was to investigate the shear response of walls. Therefore, the specimens were overdesigned in flexure. The specimens developed very high shear stresses ranging between $0.7\sqrt{f'_c}$ MPa and $1.3\sqrt{f'_c}$ MPa. Sliding shear was not observed mainly because continuous flexural cracks at the

base level could not form.

The following conclusions were reported:

1. For walls with aspect ratios of 1/2 and 1/4 horizontal reinforcement did not contribute to shear strength, but significantly contributed to distribution of cracks.

2. Minimum horizontal reinforcement ratio was found to be essential in all walls.

3. Vertical reinforcement was effective as shear reinforcement in the specimens with aspect ratios of 1/2 and 1/4.

4. Cyclic loading reduced wall strength by about 10%.

5. Shear force was transmitted from the top element to the base through the formation of compressive struts.

In 1973 Alexander et al. [24] at McMaster University, Hamilton, conducted a series of cyclic lateral loading tests on one half scale reinforced concrete shear wall panels. Main parameters of interest were the shape of load deflection curves, stiffness degradation, crack patterns, energy absorption, and ductility capacity. Three walls with an aspect ratio of 1/2 (2750 mm long, 1370 mm high, and 100 mm thick) were tested. One panel included minimum horizontal and vertical reinforcement ($\rho = 0.003$), two other specimens contained single vertical bars at the ends to improve flexural capacity, and some starting bars extending from the base to the panel. One of those improved elements, besides lateral loading, was subjected to axial compression.

The panel with only orthogonal reinforcement failed along the flexural crack at the wall base interface, prior to the formation of shear cracks. The panel

with starting bars showed an improved behavior, and failed in diagonal compression. The panel with axial load sustained approximately 25% higher lateral force. Crack pattern was more uniformly distributed when compared with accompanying specimen without axial compression. Axial load reduced ductility approximately 50%, and improved energy absorption by about 70%.

Main conclusions of that investigation were as follows:

1. Energy absorption improved when inclined cracks were widely dispersed over the panel face.
2. Compressive axial stress reduced panel ductility capacities, but decreased stiffness degradation.
3. Aspect ratios affected panel ductility capacities, with shorter panels having higher ductility capacities.

Trounce and Pristley[28] at University of Canterbery, New Zealand, carried out tests on masonry shear walls. Although the existence of mortar joints in masonry walls affect the crack pattern, it was concluded that the walls behaved in flexure mode. This was achieved by providing steel angles crossing the base crack, which significantly reduced base slip, and improved energy absorption qualities.

Fiorato et al. [13] at the Portland Cement Association in Skokie, Ill., conducted test of 14 large scale structural walls with an aspect ratio of 2.4. Thirteen specimens were tested under reversed loading, one was tested under monotonic loading, and two were repaired and retested. Main variables included: cross sectional shape, amount of main flexural reinforcement, and the amount of hoop reinforcement around the main flexural bars.
The following conclusions were reported:

1. The observed hysteretic behavior and load deformation characteristics of structural walls were similar to those in beams.

2. Isolated structural walls had significant inelastic deformation capacity when subjected to reversed loading.

3. Maximum rotational ductility decreased with increased level of shear stress.

4. Significant increase in the amount of horizontal reinforcement had only a small effect on ductility prior to web crushing.

5. Two specimens under high nominal shear stress of about $0.87\sqrt{f'_c}$ MPa developed web crushing.

6. The load capacity of confined elements was the same as that of a companion specimen without confinement. The hoops around main flexural reinforcement were effective in limiting longitudinal bar buckling.

7. Confinement increased overall top deflection ductility factor by about 5%.

8. All specimens had post yield deflection capacities under reversed loading.

In 1980, Synge [20] at University of Canterbery, New Zealand, tested four squat walls with an aspect ratio of 1/2, under reversed cyclic loading. Two of the specimens had rectangular cross section, and two others were constructed with flanges. One specimen of each type contained only orthogonal reinforcement, while the other contained some diagonal shear reinforcement to resist about 30% of shear force. All walls were designed to have similar flexural capacities in order to produce shear stresses of about $0.6\sqrt{f'_c}$ MPa. All walls, except the one with flanges and diagonal reinforcement,

were designed for shear in excess of that associated with diagonal tension failure. The wall with flanges and diagonal reinforcement contained only about 50% of horizontal reinforcement assigned to the other walls.
The main objectives of the investigation were:
- to show that shear walls with an aspect ratio of 1/2 may behave in flexure mode,
- to show that shear failure could be suppressed,
- to define the role of horizontal reinforcement,
- to assess the susceptibility of squat walls to rapid stiffness degradation due to sliding shear,
- to investigate the effectiveness of providing diagonal reinforcement,
- to limit sliding shear displacement and improve energy dissipation.

All walls tested in the experimental program slid during the test. Diagonal reinforcement in the wall with rectangular cross section delayed sliding displacement up to a ductility factor of 4, compared with ductility factor of 2, in accompanying wall without the diagonal reinforcement. The sliding was reduced by about 50% through the use of diagonal reinforcement. Similar observations were made relative to the specimens with flanges.

Following conclusion were drawn from the tests:

1. Diagonal tension failure was prevented by using the capacity design procedure outlined in the New Zealand Building Code [27].
2. Demand on horizontal reinforcement increased with cumulative ductility imposed on the wall.
3. Horizontal reinforcement carried only about 50% of total shear force at high deformations.

4. Inclusion of diagonal shear reinforcement reduced the magnitude of base slip up to 60%.

5. Hysteretic behavior of squat shear walls was substantially improved by the inclusion of diagonal reinforcement.

6. Energy dissipation by the base slip was substantially increased through yielding of the diagonal bars.

In 1980, Cardenas et al. [11,12] at the Portland Cement Association, Skokie, Ill., conducted an experimental investigation to determine strength of rectangular low rise walls. Seven large scale specimens with an aspect ratio of 1.0 were tested. One of the specimens was subjected to 10 load reversals. Lateral load was slowly applied at the top of the wall through an enlarged monolithic section that simulated a floor slab. There was no vertical load applied.

The conclusions drawn from this investigation were as follow:

1. Load reversals decreased wall strength approximately 7% and had very little effect on the load deflection relationship.

2. Both vertical and horizontal reinforcement contributed to shear strength of walls with an aspect ratio of 1.0 and effectively restrained the growth of inclined cracks.

3. The minimum amount of vertical and horizontal reinforcement ratio of 0.0025 is essential in shear walls.

4. Low rise rectangular walls with an aspect ratio of 1.0 can develop shear stresses in the order of $0.83\sqrt{f'_c}$ MPa, even under load reversals.

5. Walls with an aspect ratio of 1.0, with minimum horizontal shear reinforcement were able to develop a shear capacity of about $0.7\sqrt{f'_c}$ MPa.

In 1985, Wiradinata and Saatcioglu [22,23] at the University of Toronto tested two squat walls with an aspect ratio of 1/2 and 1/4. Results of that investigation, as well the results of the test carried out by Pilette [21],who tested two walls with an aspect ratio of 1/2, at the University of Ottawa in 1987, are discussed later for comparison purposes. The tests conducted at the University of Toronto and the University of Ottawa were part of the same comprehensive investigation on wall response. Therefore these specimens were numbered consecutively, following the sequence in which they were prepared.

1.4 Research needs

It is clear from the limited research available that the behavior and design of squat walls subjected to inelastic load reversals are not well understood. More experimental data are required to establish the nature of different failure modes observed in the previous research. While some design information is available to prevent diagonal tension and compression failures, very little or no information is available for design against sliding shear. Investigation of sliding shear, especially under inelastic load reversals, is essential for earthquake resistant design of shear walls. Therefore there is a definite need for research in this area.

1.5 Objective and scope

The objective of this research program is to investigate sliding shear phenomena in low rise shear walls during strong earthquakes. The objective includes development of design information for prevention of sliding shear failure in seismic resistant shear walls.
The following is the scope of the investigation:

1. Review of previous research and current state of the art on seismic design of squat walls.
2. Identification of the parameters that affect sliding shear in walls.
3. Preparation of an experimental program for large scale testing of walls under simulated seismic loading.
4. Design, construction and instrumentation of two large scale wall specimens with aspect ratios of 1/2 and 1/4.
5. Testing of wall specimens.
6. Evaluation and presentation of results.
7. Development of a design procedure for prevention of sliding shear in earthquake resistant shear walls.
8. Presentation of research findings.

Chapter 2

Experimental program

2.1 General

The specimens tested in this investigation were companion to those tested by Wiradinata [22] in 1985 and Pilette [21] in 1987. Two large scale squat walls, with rectangular cross sections and aspect ratios of 1/4, and 1/2 were prepared for testing. The specimens were labelled as Wall 3 and Wall 6. This chapter describes the details of the test specimens, test set-up, instrumentation, test procedure, and material properties.

2.2 Test specimens

2.2.1 Specimen geometry

Figures 2.1 and 2.2 illustrate overall dimensions of the wall specimens. The thickness of both walls was 100 mm, and the length was 2000 mm. The

height of Wall 3 was 500 mm, resulting in an aspect ratio of 1/4, and the height of Wall 6 was 1000 mm, resulting in an aspect ratio of 1/2.

The specimens were cast with heavily reinforced base to provide full base fixity. The base of each specimen was fixed to the laboratory strong floor prior to testing. Heavily reinforced beams were cast on the walls to facilitate uniform load transfer.

2.2.2 Design of Wall 3

Wall 3 with an aspect ratio of 1/4 was designed to develop nominal shear stress of about $1.13\sqrt{f'_c}$ MPa. Theoretical flexural capacity was calculated based on plane section analysis, using all main vertical reinforcements and measured material properties.[1] The details of flexural capacity calculations and the theoretical moment curvature relationship are included in Appendix A.

The vertical reinforcement consisted of 8 pairs of 10 mm diameter grade 400 deformed bars, placed in two layers. The reinforcements were extended into the top beam and base by at least development length. The reinforcement ratio for vertical steel was 0.008. Seven pairs of sliding shear reinforcement were placed in between the vertical reinforcement to eliminate shear sliding. These bars were embedded into the base by at least development length and extended into the wall by 100 mm. Wall 3 was a companion specimen to Wall 2 [22]. Therefore the vertical reinforcement layout was identical. Three horizontal layers of deformed 6.3 mm diameter, Grade 230 bars were placed uniformly over the full height to provide a shear capacity equal to that of Wall 2. This was equivalent to shear capacity that would be

[1]The sliding shear reinforcement provided at the construction joint was assumed not to contribute in flexural capacity.

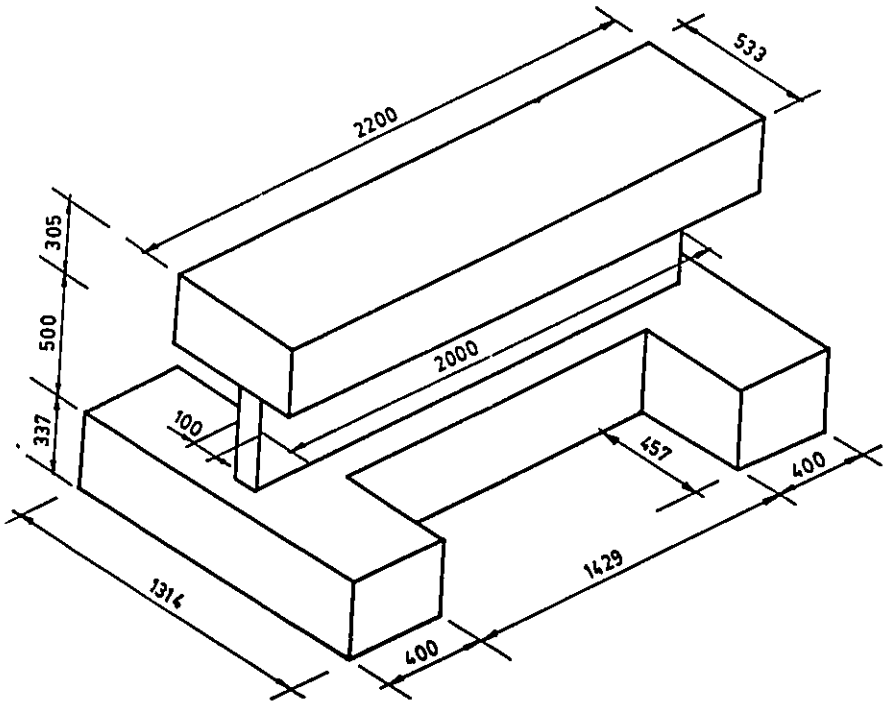

Figure 2.1: Overall geometry of Wall 3

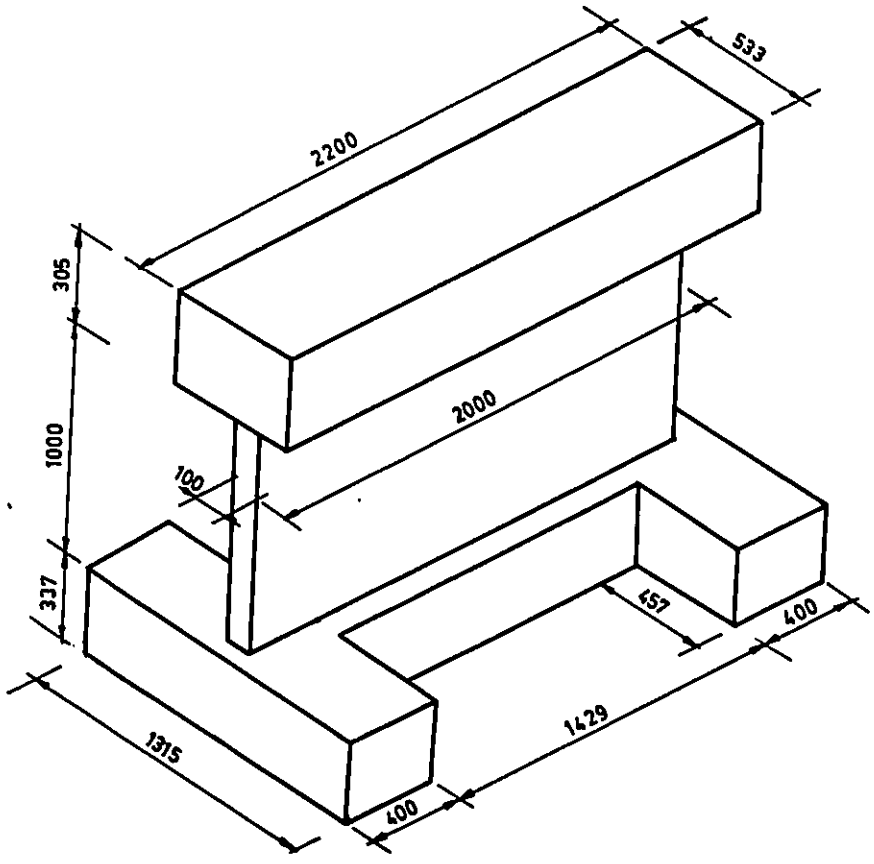

Figure 2.2: Overall geometry of Wall 6

obtained by the use of minimum reinforcement ratio of 0.0025 when the steel grade was 400. The details of shear capacity calculation are included in Appendix A. There were no stirrups provided at the ends of the wall to prevent buckling of vertical reinforcement.
The main differences between Wall 2 [22], and Wall 3 were as follows:

1. Wall 3 included sliding shear reinforcement to prevent shear sliding.
2. The yield strength of flexural reinforcement for Wall 3 was slightly higher than that for Wall 2.
3. The yield strength of horizontal reinforcement for Wall 3 was much lower than that for Wall 2. However number of bars was proportionately adjusted to provide similar shear capacities in both specimens.
4. Wall 3 did not include stirrups to prevent premature buckling of extreme flexural bars.

Material properties of Wall 2 are included in Appendix B. Details of reinforcement cage used in Wall 3 are shown in Figures 2.3 and 2.4.

2.2.3 Design of Wall 6

Wall 6 with an aspect ratio of 1/2 was designed to develop nominal shear stress of about $0.65\sqrt{f'_c}$ MPa. Theoretical flexural capacity was calculated based on plane section analysis, considering all main vertical reinforcements and measured material properties. Main vertical reinforcement layout was identical to that of Wall 3. Seven pairs of sliding shear reinforcement placed in between the main flexural reinforcement to prevent shear sliding. These bars were embedded into the base by at least development length and were extended into the wall by 200 mm. Stirrups were provided at both ends of

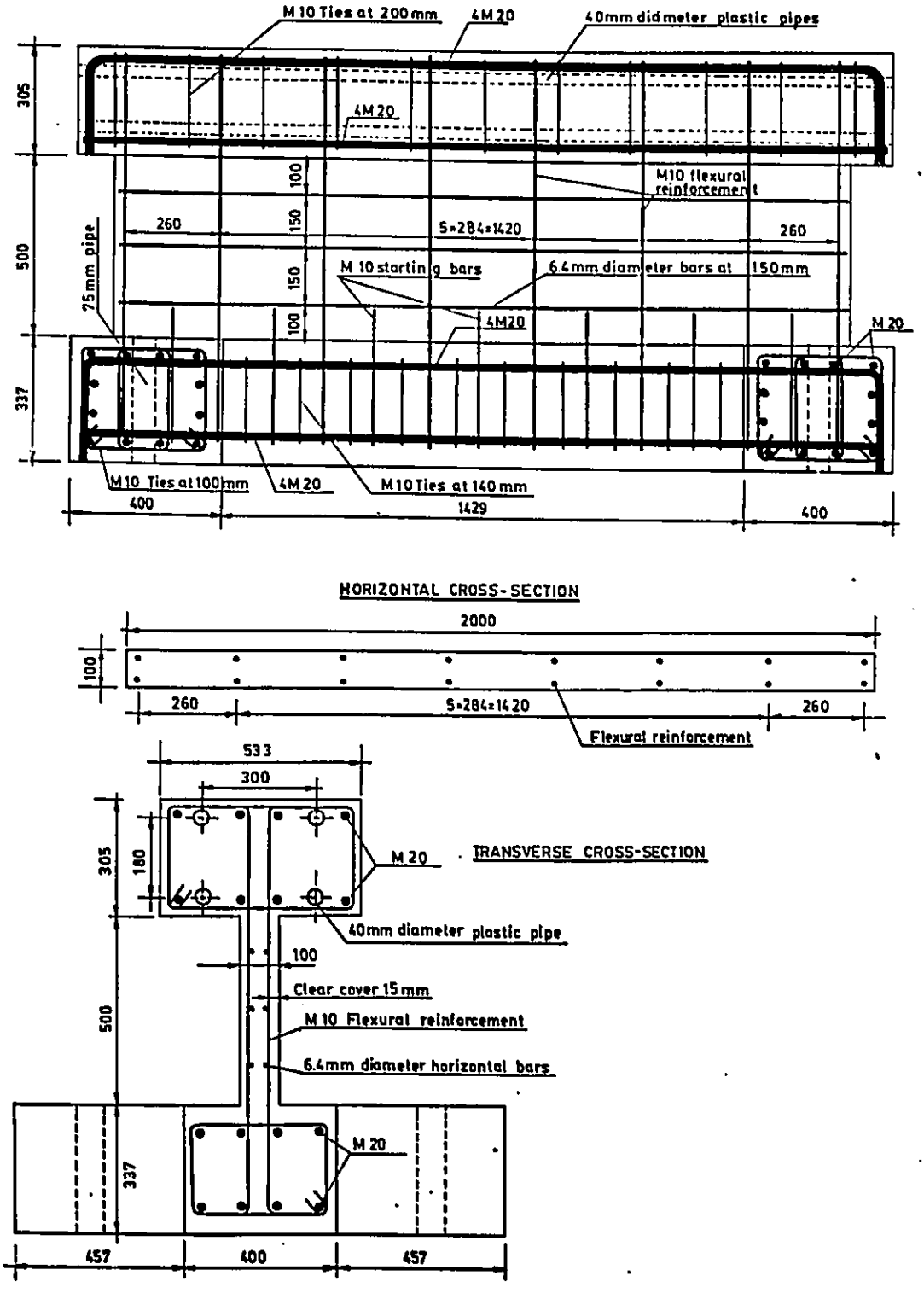

Figure 2.3: Reinforcement layout of Wall 3

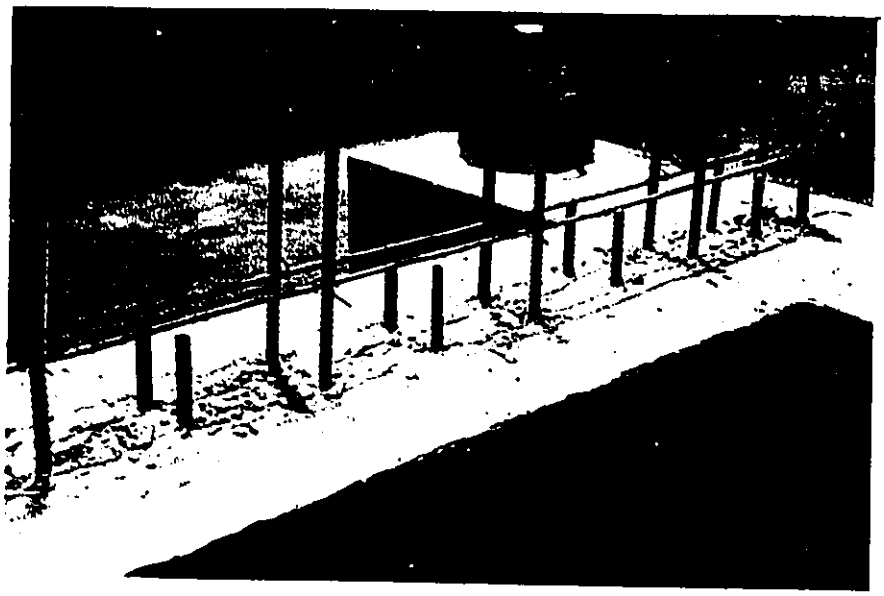

Figure 2.4: Picture of reinforcement layout of Wall 3with base cast

the wall to prevent premature buckling of vertical bars. Shear capacity was provided in excess of that corresponding to flexural capacity by 4 pairs of 10 mm diameter 400 Grade deformed bars, placed uniformly over the full height of the wall. The details of shear capacity calculations are included in Appendix B. Details of reinforcement cage used in Wall 6 are shown in Figures 2.5 and 2.6.

Wall 6 was a companion specimen to Wall 1 [22], and Wall 4 [21] tested earlier in the previous two phases of the same investigation. The main differences between these three specimens were as follow:

1. Wall 1 had minimum horizontal reinforcement ratio of 0.0025, while Wall 6 and Wall 4 had a horizontal reinforcement ratio of 0.008, which provided a shear capacity in excess of that corresponding to flexural capacity.

2. Only Wall 6 included sliding shear reinforcement extending 200 mm into the wall to eliminate shear sliding.

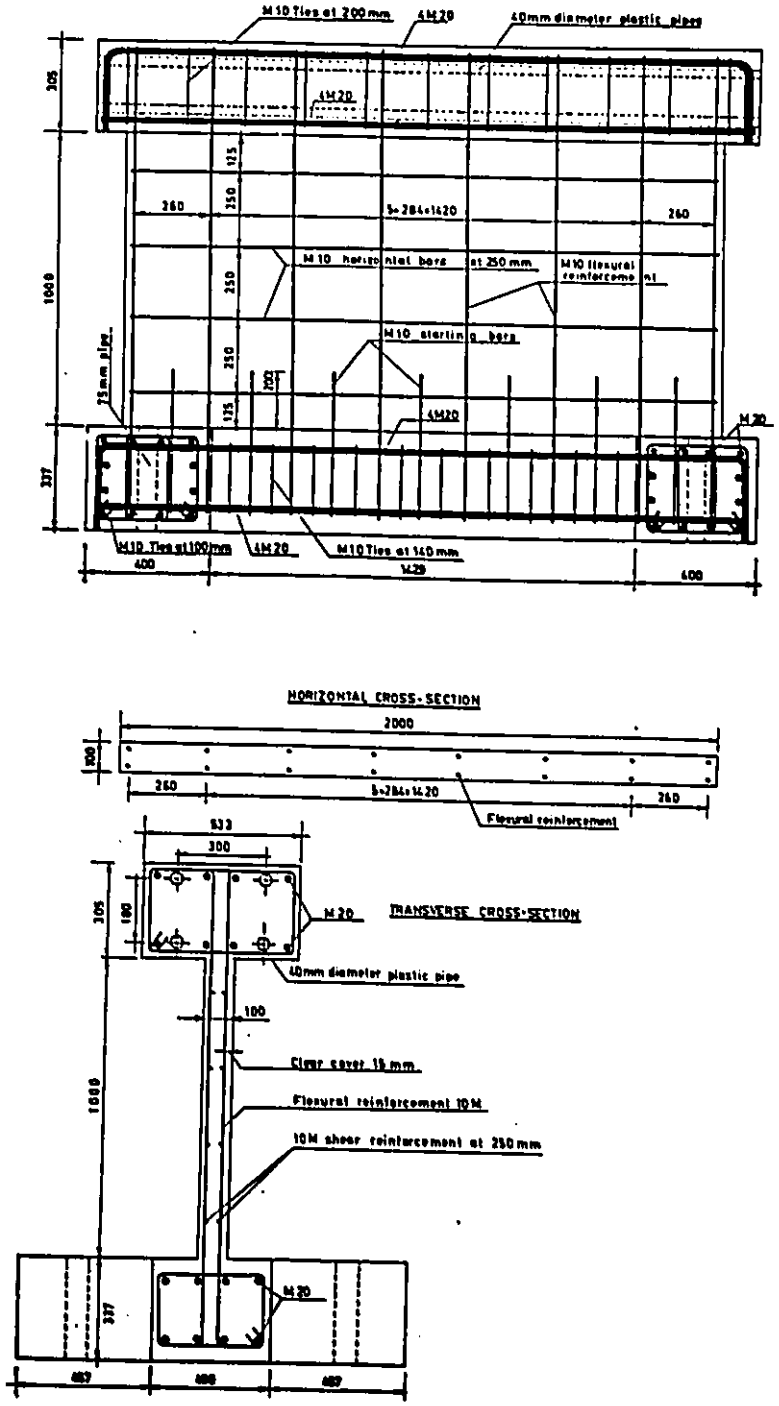

Figure 2.5: Reinforcement layout of Wall 6

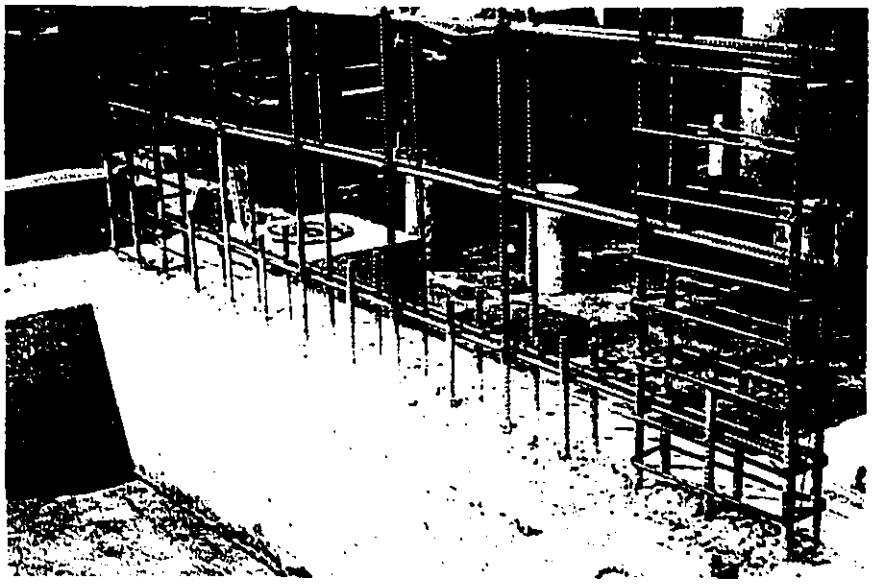

Figure 2.6: Picture of reinforcement layout of Wall 6 with base cast.

2.3 Fabrication of specimens

The specimens were cast in wooden forms. The formwork was built using 20 mm thick plywood, $50mm \times 100mm$ and $100mm \times 100mm$ wood. The forms were treated with preservative. Light coat of form oil was applied before assemblage. Concrete casting simulated the actual construction practice. Accordingly, the base was cast first, and the vertical main reinforcement and sliding shear reinforcement were cast in. The proper roughness of the construction joint was achieved by leaving the area of the joint after pouring concrete without trowelling. This provided rough surface of the joint with a relief depth of about 10 mm, and was consistent with current practice. Joint surface was cured till the wall concrete was poured. The construction joints are shown in Figures 2.4 and 2.6. The wall and the top beam were cast together at a later date.

The wall base was constructed to have an "I" shape. Heavy reinforcement consisting of 20M bars and 10M stirrups was used to resist axial tension,

shear force and bending moment, induced by shear transfer from the top beam to the base. The reinforcement detailing of the base is shown in Figure 2.3 and 2.5. The top beam was also heavily reinforced. This would provide uniform shear transfer across the wall, and ensure integrity of the beam during testing. The reinforcement detailing of the top beam is shown in Figure 2.3 and 2.5. Ready mixed concrete supplied by a local company was used. Concrete was carefully placed and vibrated using a 25 mm vibrator. Twelve control cylinders were cast from each batch of concrete. The form was stripped after six days, and the walls were cured for additional three days. Testing commenced 155 and 13 days after casting for Wall 3 and Wall 6 respectively.

2.4 Test set-up

The test set-up is shown in Figure 2.7. A reaction frame was used to support the hydraulic jack. The reaction frame consisted of two "A" frames, each bolted to two 457 mm deep supporting channels. These two assemblies were connected by vertically placed 50 mm thick plate, which also provided support for the jack. The two way action hydraulic jack, used in the experiment, had a capacity of about 1500 kN, and was controlled by an electric oil pump. The set-up was designed to resist horizontal forces approximately equal to the capacity of the jack in positive and negative directions. It was bolted to the laboratory strong floor by six 75 mm diameter high capacity bolts. A 900 mm long shaft with swivel ends was placed between the hydraulic jack and the top beam of the specimen. The use of a long shaft significantly reduced vertical force component, resulting from vertical displacement of the top beam. To eliminate out of plane movement and associated twisting moment during the tests, specially designed frame

was constructed to provide support for the shaft against any lateral movement in the transverse direction. Figures 2.7 through 2.10 show various views of the test set-up.

Positive loading was applied by extending the jack piston against the test unit. Load in negative direction was applied by pulling the wall towards the reaction frame. Four 35M bars were mounted in plastic pipes and cast in the top beam with a load cell and an end plate at the remote end to apply the load in negative direction. In Wall 3 these bars were initially prestressed to assure continuous contact of bearing plates with the face of the top beam, resulting in a total prestressing force of approximately 200 kN. Since the prestress was completely lost during the test, and the losses had to be recorded at each load stage, no prestress was applied for testing Wall 6. Test units were firmly bolted to the laboratory strong floor by four 75 mm diameter high capacity bolts. Overall pictures of the test set-up for Wall 3 and for Wall 6 are shown in Figs. 2.8 and 2.9 respectively.

2.5 Instrumentation

2.5.1 Introduction

A light reference frame was built around each specimen for instrumentation. The reference frame was connected to the brackets that had been cast in the base. All displacement measuring devices were attached to this frame. Therefore the measurements were taken relative to the base, and any possible sliding of the specimen as a whole over the floor, would have no effect on the measurements. All measuring devices were hooked up to the data acquisition system, and readings were stored as output voltages by a Hewlett- Packard 9845B mini computer. Figure 2.11 shows the data

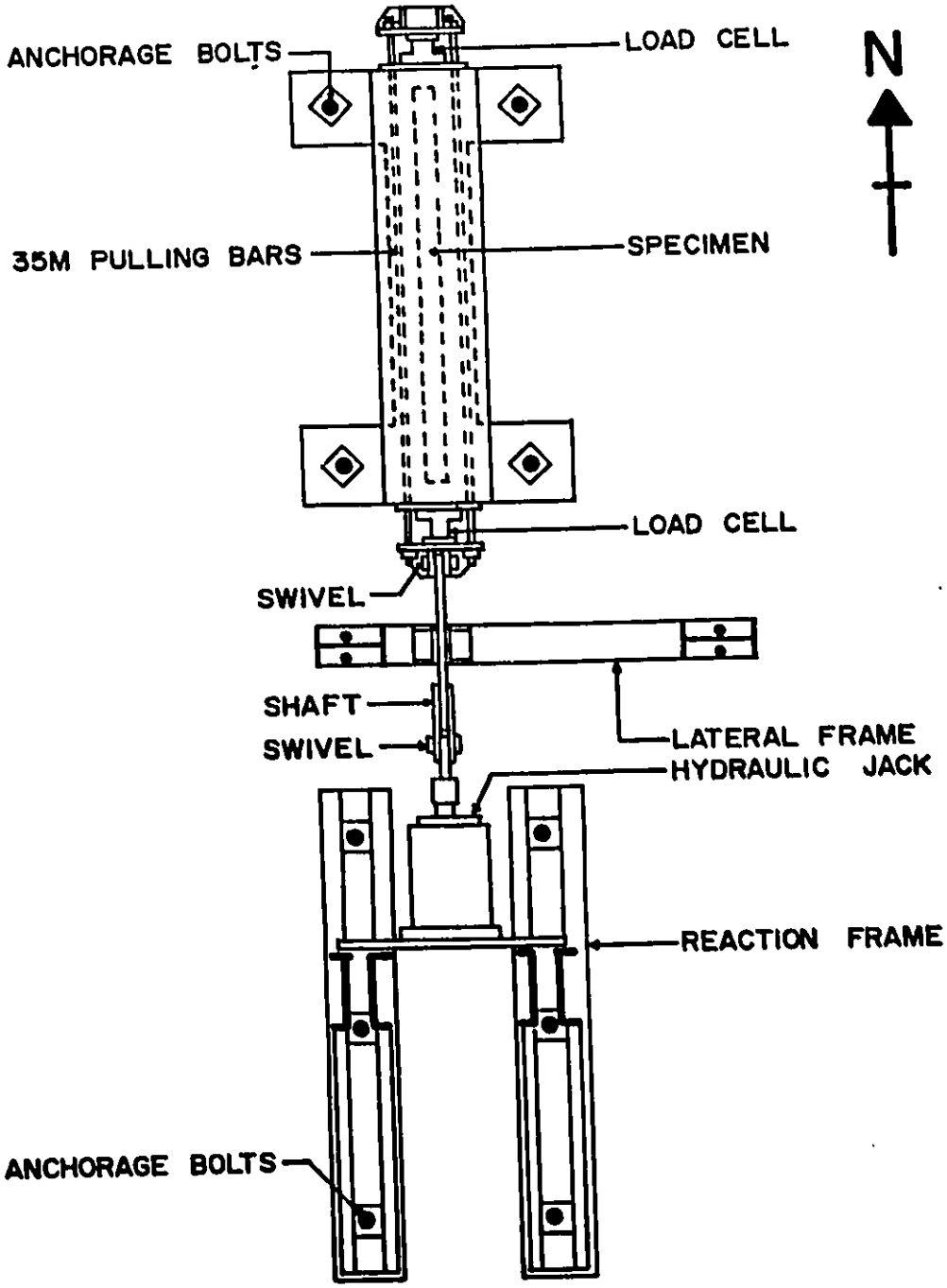

Figure 2.7: Overall view of test set-up

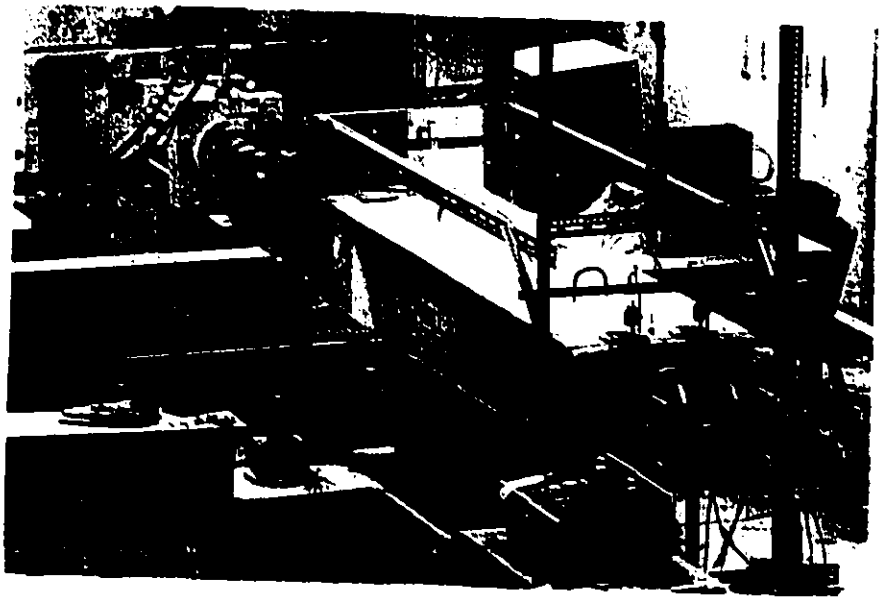

Figure 2.8: Overall picture of test set-up for Wall 3

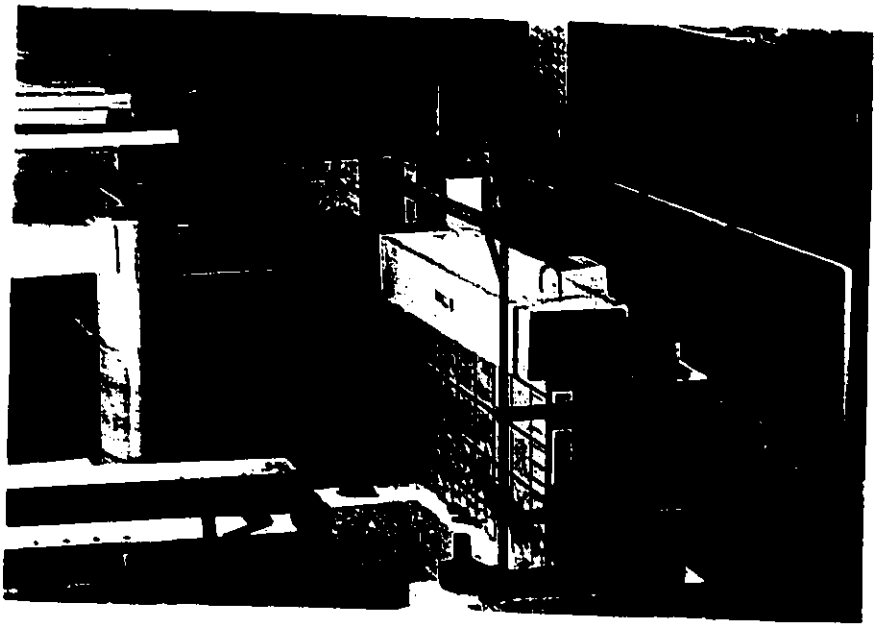

Figure 2.9: Overall picture of test set-up for Wall 6

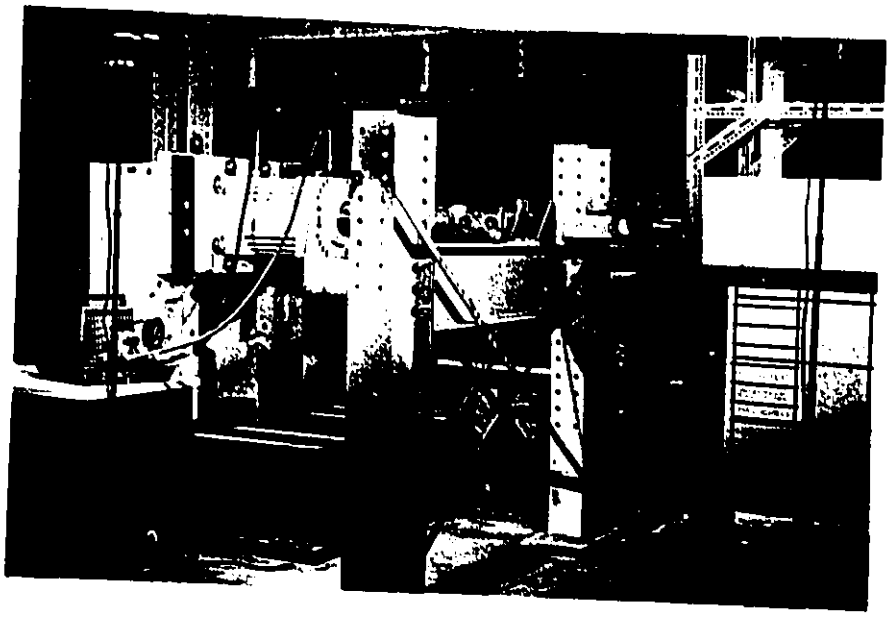

Figure 2.10: Load transfer mechanism and reaction frame acquisition system used during the tests.

2.5.2 Force measurement

A load cell with a static capacity of 1300 kN was placed at each end of the top beam. The load cells were placed between a bearing plate and another plate to which the load was applied. The near–end load cell was used to measure the positive load (pushing against the reaction frame) and the far–end load cell was used to measure the negative load (pulling towards the reaction frame). The load cells were fed into the data acquisition system, and the readings were stored as output voltages. Figure 2.10 shows the loading mechanism.

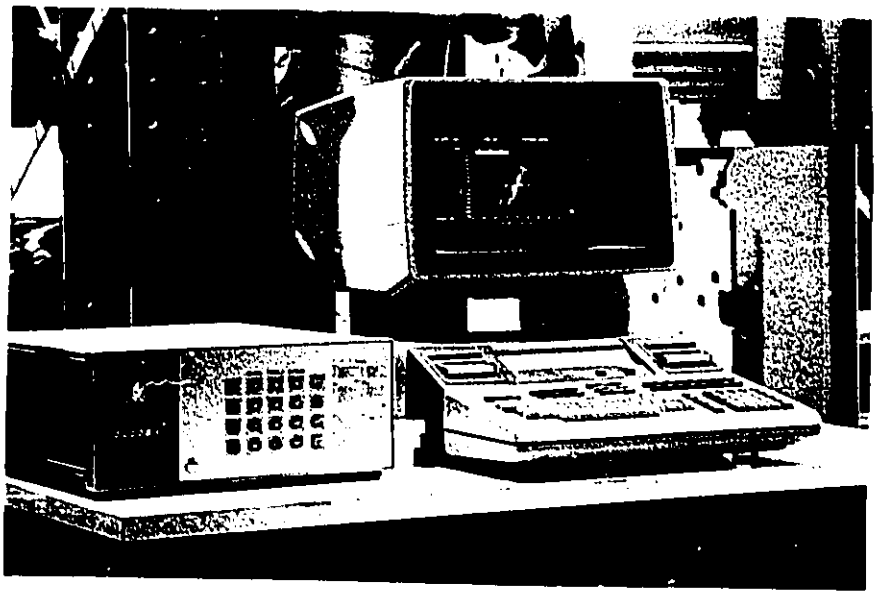

Figure 2.11: Data Acquisition System

2.5.3 Displacement measurements

All displacements of the specimens were measured by 150 mm, and 5 mm stroke linear variable differential transducers (LVDT). Accuracy of LVDTs used was 0.01 mm. All transducers were hooked up to the data acquisition system, and the readings were stored as output voltages. The location of LVDTs used to measure displacements in Wall 3 and Wall 6 are shown in Figures 2.12 and 2.13 respectively. LVDTs were installed on the reference frame, which was attached to the specimen base.

Wall 3

Horizontal displacement of top beam in Wall 3 was measured by a 150 mm stroke LVDT. This is shown in Fig.2.14. Two 150 mm stroke LVDTs were mounted to the base of the wall to measure expected shear sliding. Two 5 mm stroke LVDTs were placed vertically at each end of the wall to measure reinforcement bond slip displacement. Two 5 mm stroke LVDTs

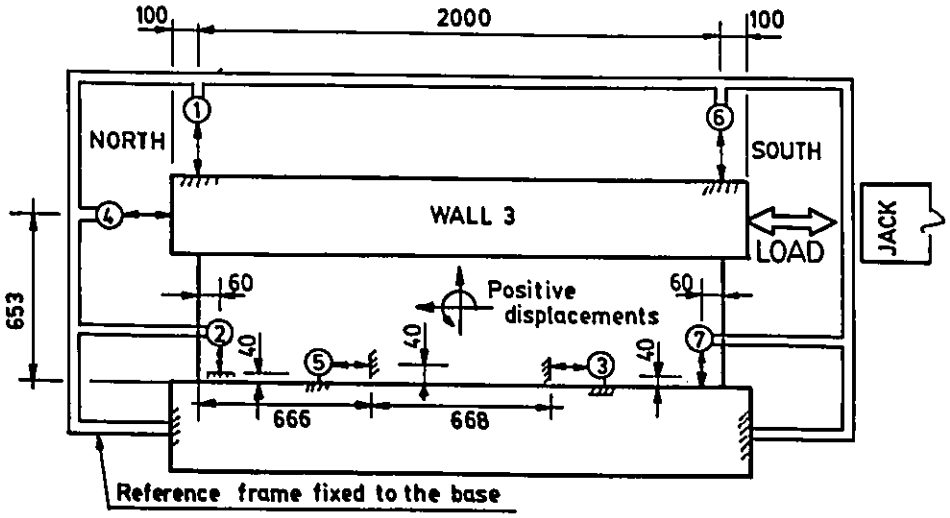

Figure 2.12: Location of LVDTs in Wall 3

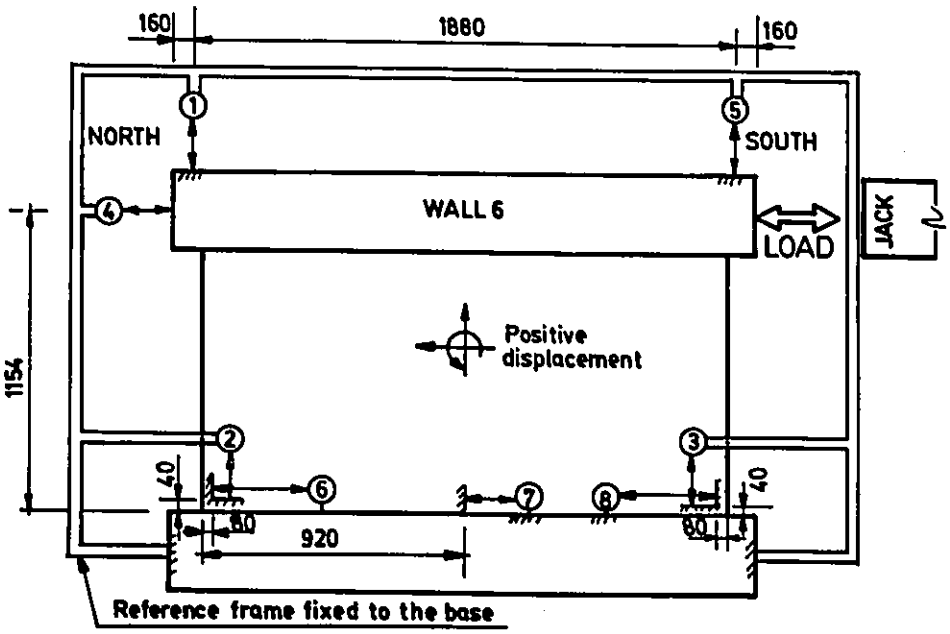

Figure 2.13: Location of LVDTs in Wall 6

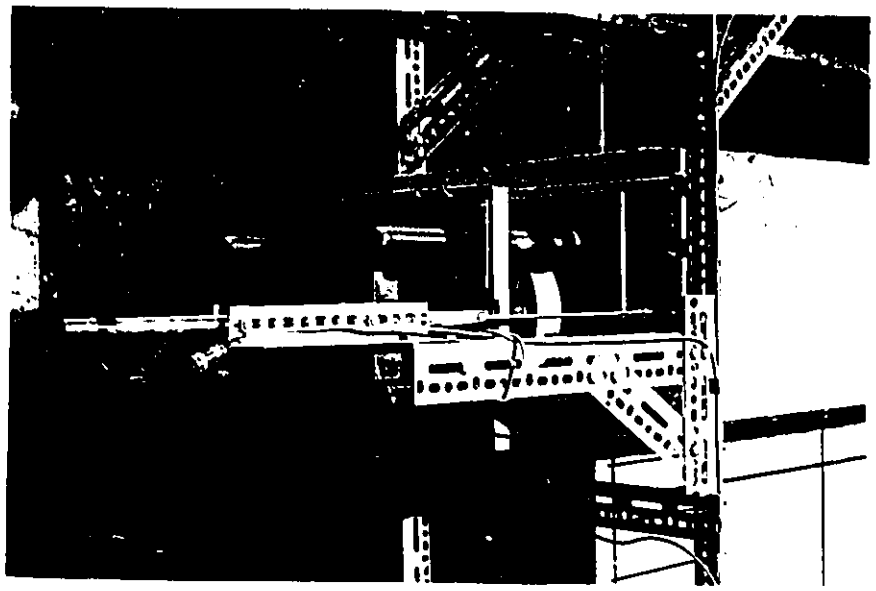

Figure 2.14: LVDT used to measure horizontal displacement of top beam in both walls

were placed above the top beam to measure its vertical movement. These LVDT's were replaced by dial gages at the high deformation range when the LVDT stroke was exceeded.

Wall 6

Horizontal displacement of top beam in Wall 6 was measured in the same manner as in Wall 3. Three 5 mm stroke LVDTs instead of 150 mm, were placed at the construction joint, since the shear sliding was not expected in this specimen. As a backup, a 100 mm stroke dial gage was placed in the center of the joint. Figure 2.14 shows the 150 mm stroke LVDT used to measure horizontal displacement of top beam. The reinforcement bond slip displacement measurement was recorded in an identical manner as that for Wall 3. Because of a relatively large vertical movement experienced in Wall 3, two 150 mm stroke LVDTs were mounted in Wall 6 to measure vertical displacement. This is shown in Figure 2.15.

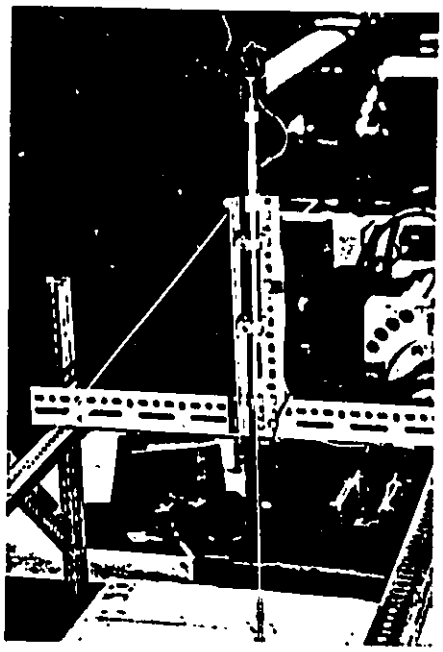

Figure 2.15: LVDT used to measure vertical top displacement in Wall 6

2.5.4 Strain measurements

Electrical resistance strain gages were placed on selected vertical flexural and sliding shear reinforcements, at the construction joint location. The purposes for recording steel strains were:

– to obtain the variation of steel stresses in critical wall section,

– to monitor the contribution of sliding shear reinforcement towards flexural resistance,

– to assess yield displacement of the wall.

A total of 25 strain gages were placed on the reinforcement in Wall 3, and 13 strain gages were placed in Wall 6. Locations of strain gages in Wall 3 and Wall 6 are shown in Figures 2.16 and 2.17 respectively. All areas to be gauged on the rebars were first ground. The reduction of the cross sectional area of the rebar was in the range of about 1.5%. Strain gages and terminals were glued by the use of an adhesive agent. Two

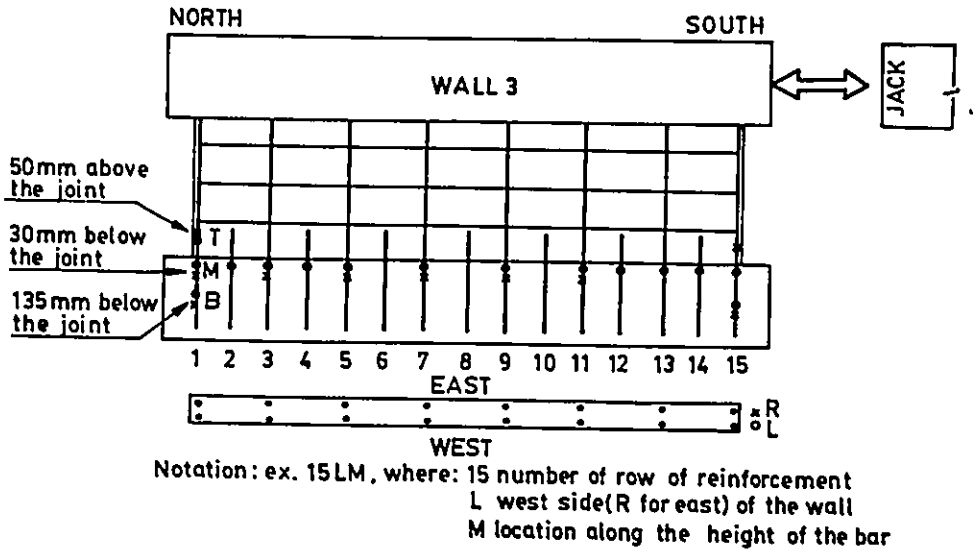

Figure 2.16: Location of strain gages in Wall 3

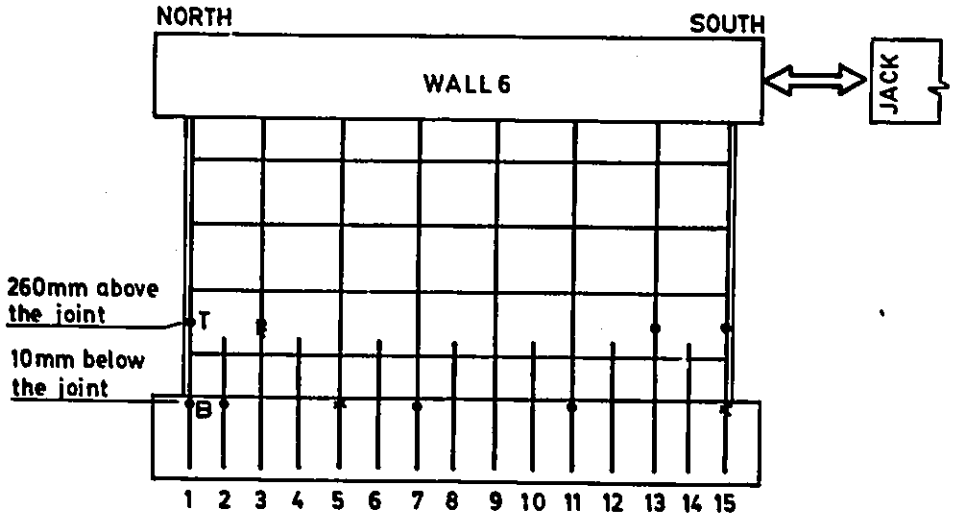

Figure 2.17: Location of strain gages in Wall 6

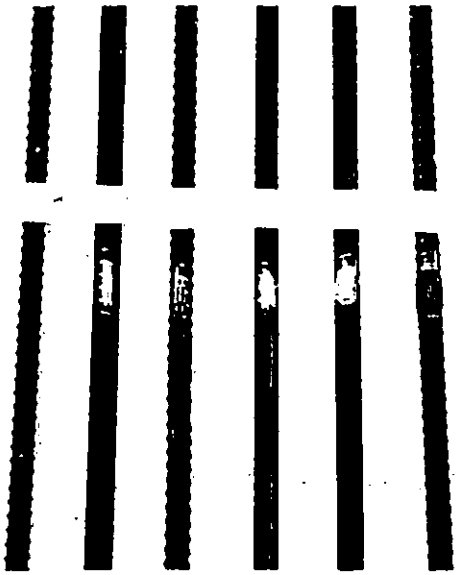

Figure 2.18: Strain gages preparation

layers of waterproof compound were used to cover the gages. The strain gages and terminals were covered by "stay soft" putty and were taped. All strain gages were connected to the data acquisition system, and strain readings were stored as voltage excitations. Consecutive stages of strain gage preparation are shown in Figure 2.18.

2.5.5 Shear deformation measurements in Wall 3

Shear deformations were measured by means of four targets forming a rectangular grid on the wall surface. It was previously reported that [22], use of "Zurich" targets with fine grid, showed significant localized effects due to cracking and crushing. Therefore in Wall 3 the targets were placed to cover almost the whole side area of the wall. This solution averaged the localized effects. Figure 2.19 shows the location of targets in Wall 3.

Total of six readings were taken manually, using specially constructed rulers from which an average shear deformation could be computed at a given load

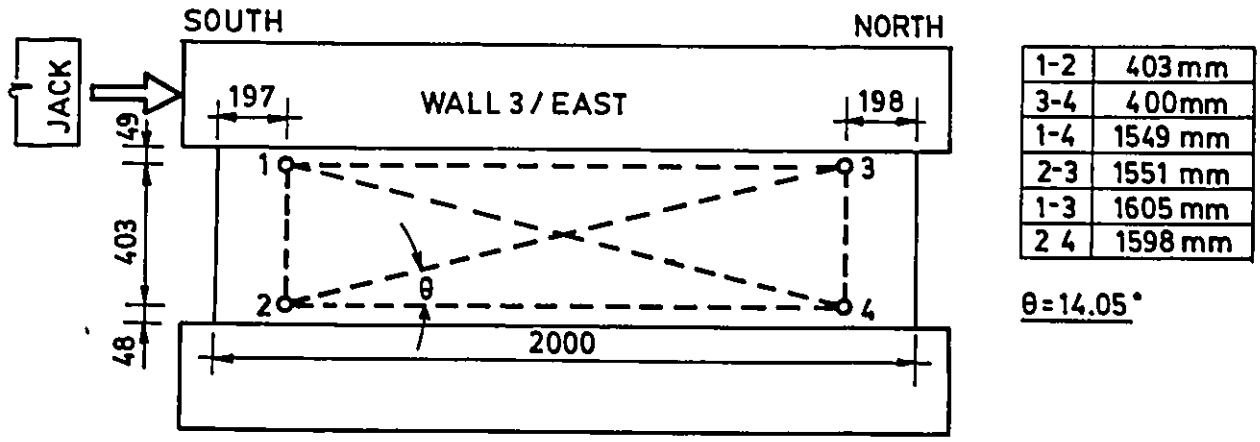

Figure 2.19: Location of shear deformation targets in Wall 3

stage. The readings were taken at zero, peak, and ±100 kN loads of each cycle. Two vertical, two horizontal, and two diagonal readings formed one set. The shear deformation was then calculated using these readings and transformation equation. The complete procedure is included in Appendix C.

2.6 Loading program

The intended loading program for both specimens followed the procedure used by Wiradinata [22], and Pilette [21]. This enabled comparison of results with the companion specimens tested by others. The loading program is illustrated in Fig.2.20.

In the first three cycles, the specimens were loaded up to the cracking load, which corresponded approximately to half of the theoretical ultimate load. Therefore the first three cycle were load controlled. The following load

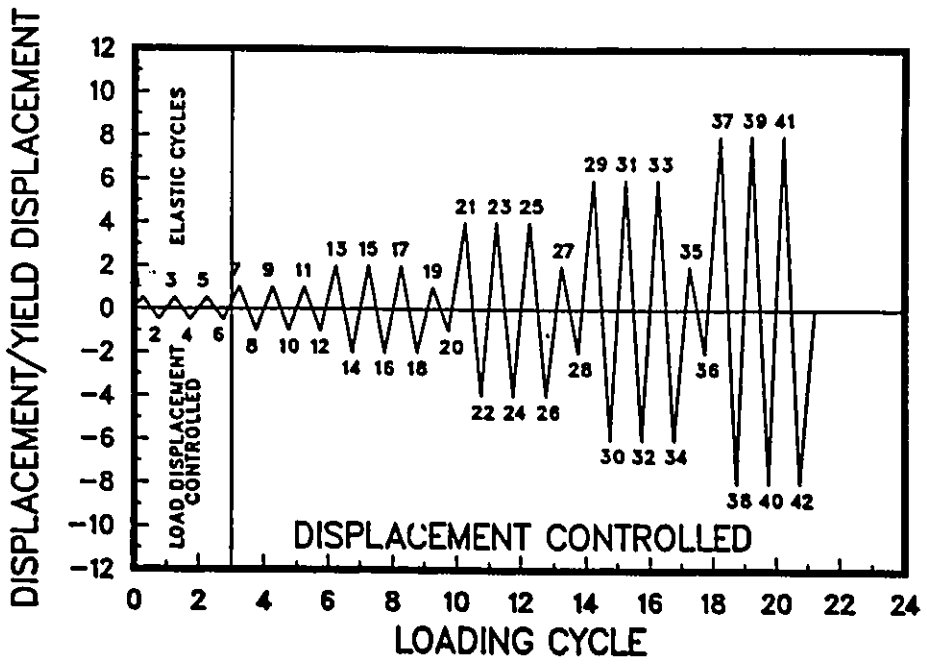

Figure 2.20: The intended loading program for both walls

stage was the yield load. Theoretically, flexural yield point for both walls was defined as the displacement at which half of the flexural bars in tension zone were yielding. Theoretical flexural displacement at yield point was 0.27 mm, and 0.60 mm for Wall 3 and Wall 6 respectively. Shear displacement using 20% of gross shear rigidity was about 1.20 mm and 2.0 mm for Wall 3 and Wall 6 respectively. Since the shear component of top displacement formed a major portion of total displacement, and its value is very sensitive to the estimation of inelastic shear rigidity, the computed displacement components were taken only as initial estimations of the yield displacement. During the test the load vs displacement curve was monitored and attention was paid to steel strains in flexural reinforcement. The actual yield displacement was experimentally determined, when the rate of change of displacement increased significantly under almost constant load. At this load stage, it was observed that the first three rows of vertical bars were yielding at the construction joint. The yield displacement for Wall 3 was determined as 2.5 mm, and for Wall 6 as 4.0 mm. These values corresponded to drift ratios of 0.5% for Wall 3 and 0.4% for Wall 6. During the

subsequent cycles of loading the specimens were subjected to incrementally increasing deformation cycles as shown in Fig.2.20. Three large and one small cycles were applied at each deformation level. The test continued until a significant drop in load resistance was recorded.

2.7 Material properties

Concrete

Ready mix concrete, obtained from a local plant was used in both specimens. Regular concrete with a 28 days target strength of 30 MPa, 75 mm slump, and maximum aggregate size of 12 mm was requested for Wall 3. Concrete made from high early strength cement, with a 28 days target strength of 30 MPa, 100 mm slump, and maximum aggregate size of 12 mm, was requested for Wall 6. Twelve control cylinders were cast from each batch. The cylinders were tested at different ages to determine the gain in strength with time. Representative stress-strain relationships for concrete obtained under repeated and monotonic loading are shown in Figures 2.21 and 2.22.

Steel

Grade 400, 10M reinforcing bars were used as flexural and sliding shear reinforcement in both walls. Bars from the same batch were also used as shear reinforcement in Wall 6. The yield strength, yield strain and elastic modulus were 480 MPa, 0.0024, and 200000 MPa respectively. The ultimate strength and corresponding strain were 773 MPa and 0.15% respectively. The stress-strain relationship of these bars is shown in Figure 2.23.

Deformed bars with 6.4 mm diameter were used as shear reinforcement in

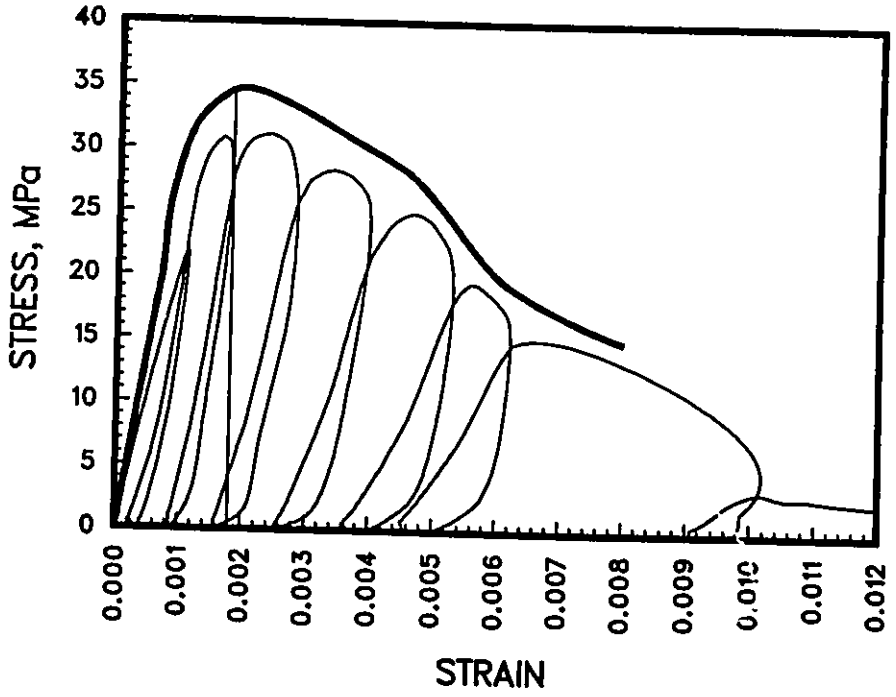

Figure 2.21: Stress–strain relationship for concrete of Wall 3 under repeated and monotonic loading

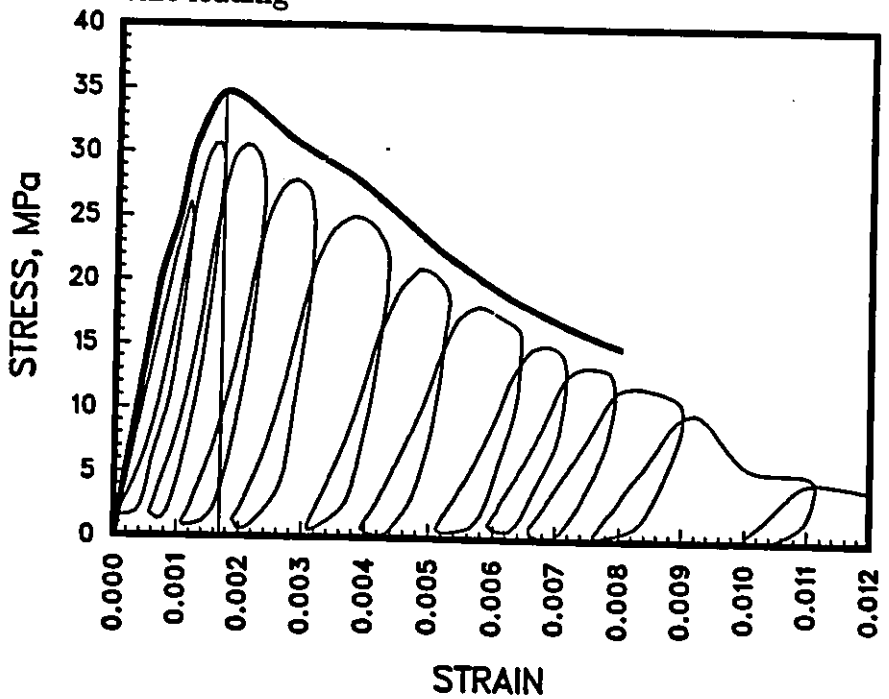

Figure 2.22: Stress–strain relationship for concrete of Wall 6 under repeated and monotonic loading

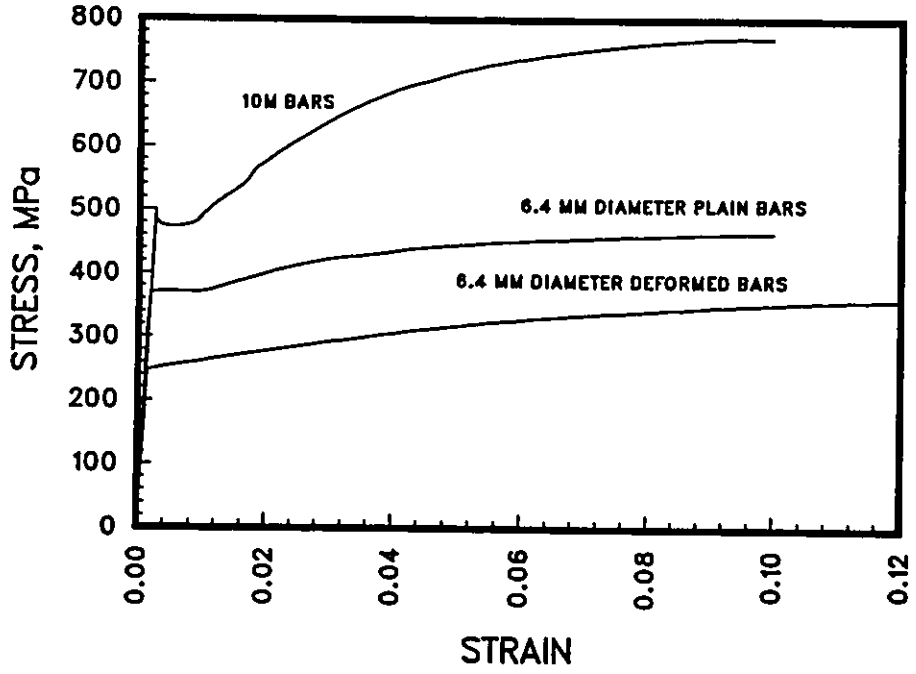

Figure 2.23: Stress–strain relationship for all reinforcement used in both walls.

Wall 3. Yield strength of these bars was 248 MPa, and yield strain was 0.0015 resulting in elastic modulus of 170000 MPa. Figure 2.23 illustrates the stress–strain relationship for 6.4 mm diameter bars.

Plain bars, with 6.3 mm diameter, were used as stirrups to prevent premature buckling of exterior flexural bars in Wall 6. The stress–strain relationship for these bars is also shown in Figure 2.23.

Chapter 3

Observed behavior and test results

3.1 Introduction

This chapter describes performance of each specimen during testing. Crack patterns at each load stage are discussed. Test results, in the form of force displacement hysteresis curves, as well as load vs. strain relationships for some strain gages are presented. The displacement components, either as measured or computed from recorded data, are illustrated.

3.2 Observed Behavior of Wall 3

Wall 3 with an aspect ratio of 1/4, and minimum horizontal reinforcement ratio of 0.0025, was subjected to the loading program shown in Fig. 3.1. The actual loading program differed somewhat from the intended shown in

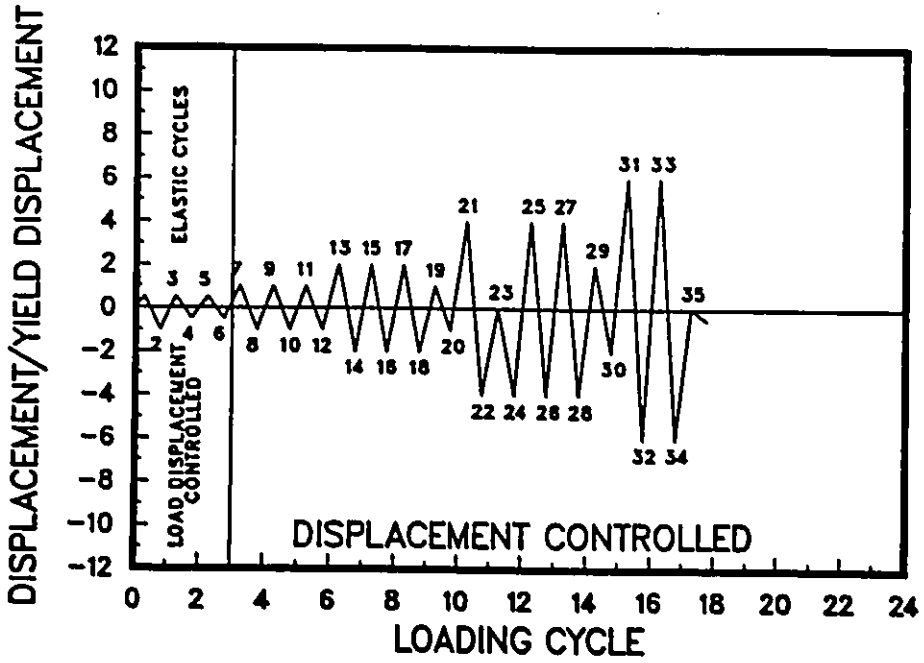

Figure 3.1: Actual loading history for Wall 3

Fig. 2.20. The specimen was accidentally loaded up to $1\Delta_y$, during the first cycle in the negative direction. Furthermore, during the test, because of technical problems, the test had to be stopped while loading in the negative direction towards $4\Delta_y$, (load stage 22). The test was restarted later on by repeating the first negative loading towards $4\Delta_y$. However, these disruptions are not expected to have any effect on the behavior of the specimen.

The predicted monotonic load capacity, based on plane section analysis, was 1080 kN. This would translate into nominal shear stress of about $1.13\sqrt{f'_c}$ MPa. The horizontal displacement of the top beam was recorded during the test using a 150 mm stroke LVDT. The force vs top displacement relationship is shown in Figure 3.2.

During the first three elastic cycles, the specimen was subjected to approximately one half of the predicted ultimate load. The applied peak load in the positive direction was 487 kN. The first peak load in the negative direction was 587 kN. In the latter case, the wall was slightly overloaded during

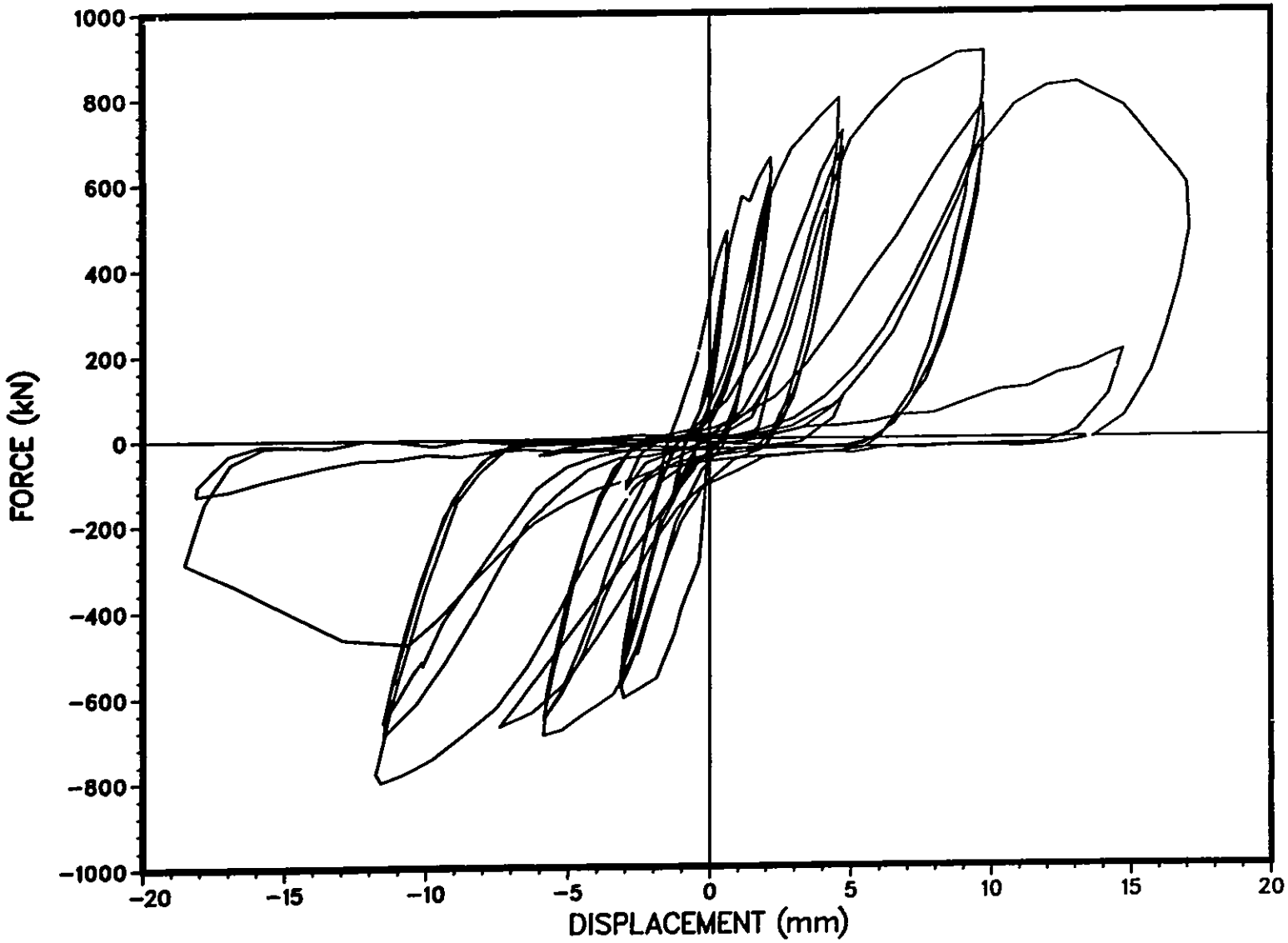

Figure 3.2: Load vs top displacement for Wall 3

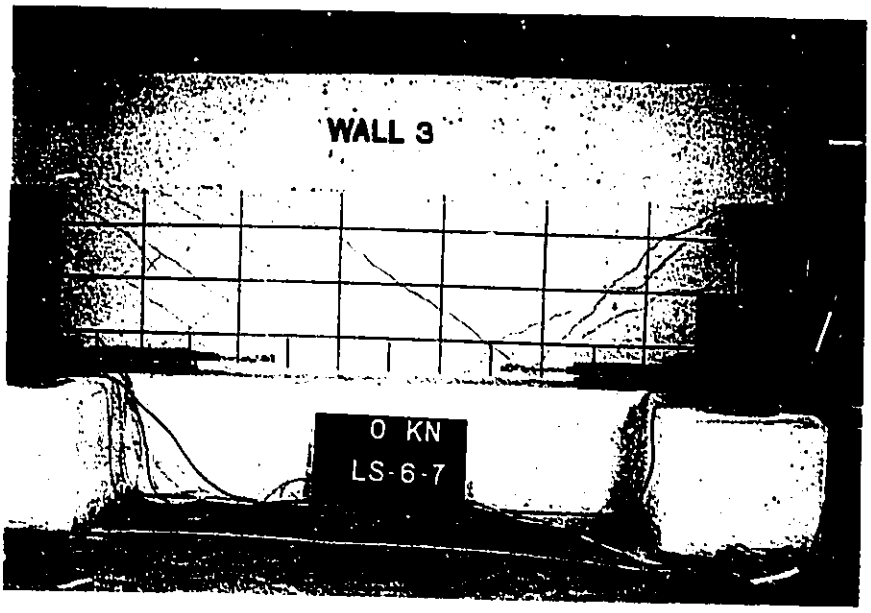

Figure 3.3: The Wall 3 at the end of elastic cycles

the first cycle and hence the consecutive negative loads in the elastic range were applied in displacement control mode. The peak negative displacement at this stage was 1.2 mm. This level of displacement corresponded to the yield displacement in the positive direction. The first set of shear cracks appeared at a load of ±400 kN. This was close to the calculated theoretical cracking load of 390 kN. The shear cracks were essentially inclined at 45° and were passing above the joint reinforcement, propagating toward flexural reinforcement location at the base. There were some flexural cracks at the ends of the wall. These small flexural cracks became continuous with shear cracks between the first two rows of flexural bars. Hysteresis loops were following each other, and neither strength, nor stiffness degradation was observed. Figure 3.3 shows the specimen at the end of the elastic cycles.

After the initial three cycles, application of horizontal load was displacement controlled. The deformation level at this load stage was the yield displacement. The yield displacement, $1\Delta_y$, was equal to 2.5 mm and was

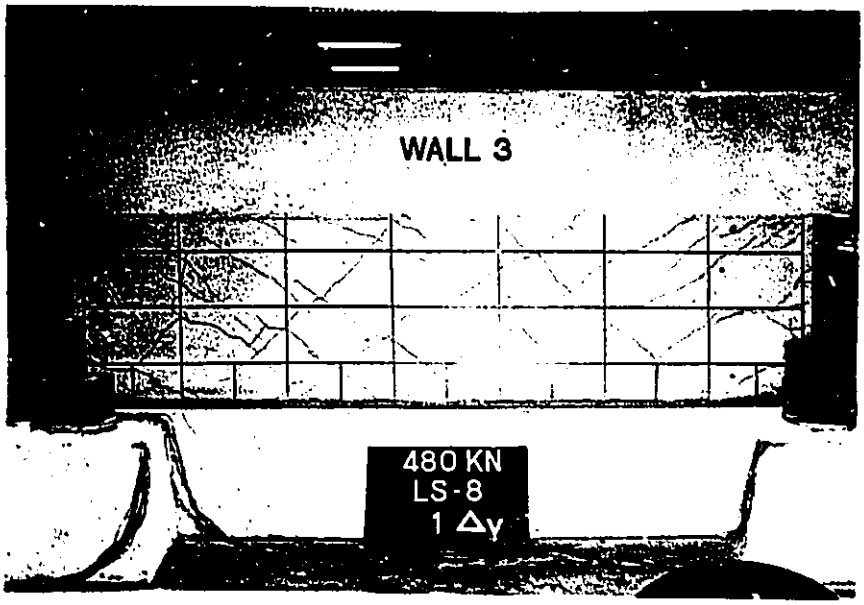

Figure 3.4: Wall 3 crack pattern at $1\Delta_y$

attained at 650 kN[1] in the positive direction and -580 kN, in the negative direction. Additional shear cracks occurred during the first positive loading. The crack pattern remained unchanged during the subsequent cycles at $1\Delta_y$. The cracks were passing through the tips of the sliding shear reinforcement, forming concrete "pyramids" between the cracks and the construction joint. Figure 3.4 illustrates the crack pattern at $1\Delta_y$. There was a slight strength degradation of about 8% during each of the subsequent two cycles at yield displacement. Hysteresis loops were shooting towards the previous maximum displacement, showing only slight stiffness degradation. The path of unloading was essentially the same in all yield displacement cycles.

The next deformation level was $2\Delta_y$. Additional shear cracks formed during the first cycle of this deformation level. The crack pattern became completely uniform and symmetrical. This crack pattern remained essentially

[1]The load of 480 kN, shown in Fig.3.4 does not include the effect of prestressing in steel bars through which the load was applied.

unchanged until the next deformation level. The peak load was 800 kN in the positive direction, and -700 kN in the negative direction. Strength degradation was in the range of 10% and 15% during the second and third cycles of this deformation level respectively. Hysteresis loops were very similar to those of $1\Delta_y$. Reloading paths were shooting towards the previous maximum point and unloading paths were identical. Hysteresis loops showed significant pinching, with very small load resistance in the ± 2 mm displacement range, followed by a pronounced strength increase. The shear cracks in the center of the wall increased in width, reaching 0.5 mm to 1 mm. There were some shear–flexure cracks in the midhight of the wall at both ends, extending to the third row of flexural reinforcement. Shear – flexure cracks were passing above the first sliding shear reinforcement, and propagating toward the junction of the base and the second row of flexural reinforcement. These cracks were approximately 3 mm in width during the peaks, and did not close completely at zero load showing a width of approximately 2 mm. There was a slight sign of formation of flexural cracks along the construction joint. These cracks formed at load stages 14 and 15, and were extending only up to the first row of joint bars. The bottom portion of the wall, consisting of concrete pyramids formed around the sliding shear bars, remained intact. The average length of flexural cracks at either end of the wall critical section was about 70 mm. Figure 3.5 shows the crack pattern at load stage 14.

After three cycles at $2\Delta_y$, the specimen was subjected to one small cycle at $1\Delta_y$. The load resistance at $1\Delta_y$was approximately 30% of the peak load at the first $1\Delta_y$ cycle at load stage 12. The specimen was next subjected to three deformation cycles at $4\Delta_y$. The load was 910 kN in the positive and -800 kN in the negative directions. The drop in load resistance during the second and third cycles was about 14%, and 24% respectively. The character of the tip of hysteresis loop of the first cycle reveals that the

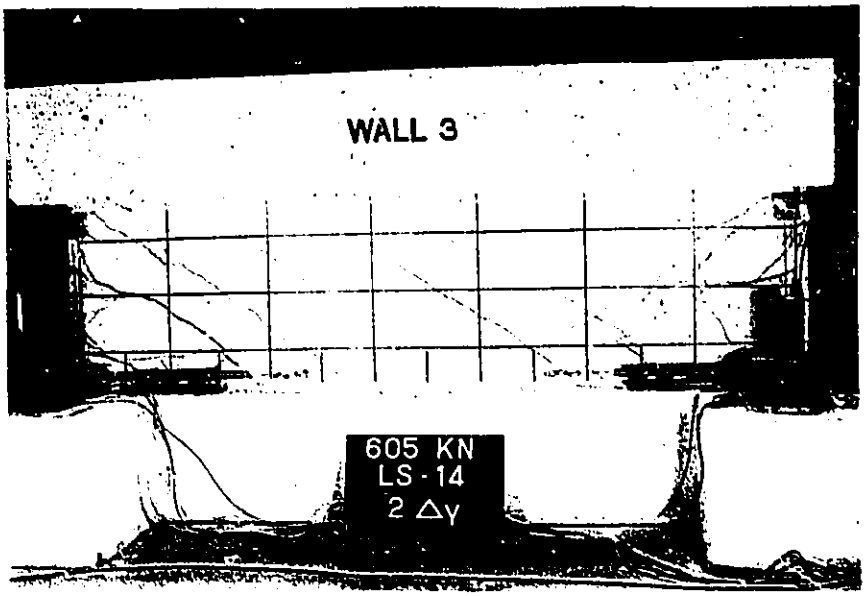

Figure 3.5: Wall 3 – crack pattern at $2\Delta_y$

specimen fully attained its flexural capacity. Increased pinching was observed in the hysteresis loops. There were many new shear cracks observed at the first cycle of this deformation level. The crack pattern remained essentially unchanged during the two repeated cycles. Shear crack widths at the peak loads were ranging between 1 mm in the center of the wall and 8 mm at the ends of the specimen. Intersection of the shear cracks led to concrete spalling. There was a visible permanent deformation at load stage 21. At load stage 22, the exterior flexural bars in compression zone started to buckle, producing complete spalling of concrete. The same situation occurred at the opposite side when the wall was loaded in the positive direction at load stage 23. Significant deformations along major shear cracks were observed at this deformation level. This was visible by discontinuity of lines marking the horizontal reinforcement. Figure 3.6 shows the specimen at the negative peak of the last cycle at $4\Delta_y$. Figure 3.7 shows the buckling of exterior row of flexural reinforcement. There was no significant damage in the bottom portion of the wall. This was attributed to the concrete pyramids formed around the sliding shear reinforcement which functioned

as shear keys. Figure 3.8 shows a close up view of the formation of shear keys around the sliding shear bars.

Based on the intended loading history, a small cycle with a deformation level of $4\Delta_y$ was applied prior to three cycles at $6\Delta_y$. The hysteresis loop for this small cycle followed the last cycle at 4 Δ_y. However, the load resistance at the peak was 15% of the resistance at load stage 18 when the specimen was subjected to $2\Delta_y$ for the first time.

During the first cycle of $6\Delta_y$, the wall developed a maximum load of about 830 kN, before reaching the desired level of deformation. As the displacement was increased, a drop in load resistance was observed. There was visible swelling of concrete in the compression zone extending approximately a third of the wall width. The load dropped suddenly, and displacement was uncontrollable. This behavior was attributed to diagonal compression failure. Similar situation but in lesser intensity occurred when the load was reversed. The wall first reached a maximum load of about -460 kN which then dropped suddenly. There was massive spalling of concrete in the previously overstressed compression region. The test was continued with another cycle at $6\Delta_y$. In this cycle, the specimen sustained only about 200 kN in the positive direction, and about -120 kN in the negative direction. Progressive spalling and deterioration of concrete occurred above the sliding shear reinforcement. The bottom portion of the wall, where the shear keys formed, remained essentially intact. Figure 3.9 shows the specimen at $6\Delta_y$, when failure occurred. Figure 3.10 shows the specimen at the end of the test.

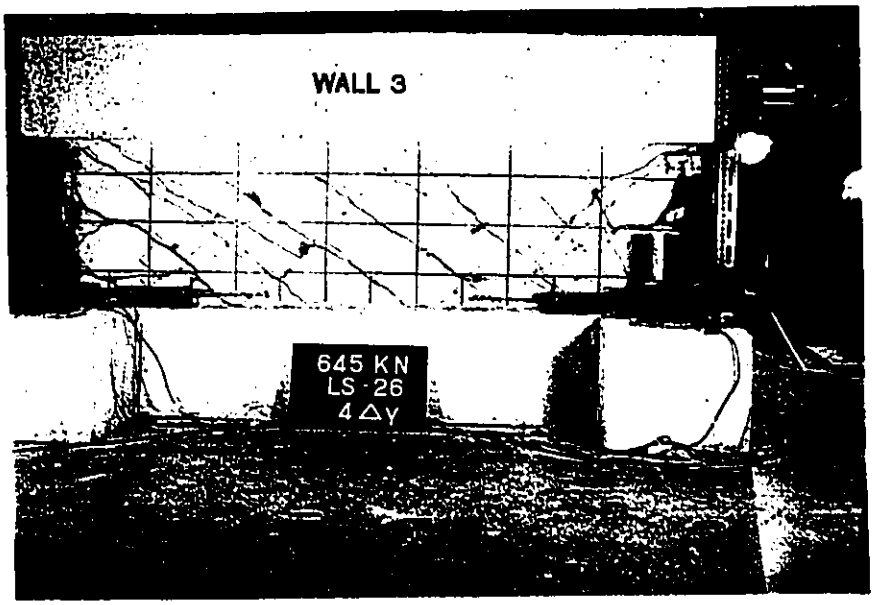

Figure 3.6: The specimen at $4\Delta_y$

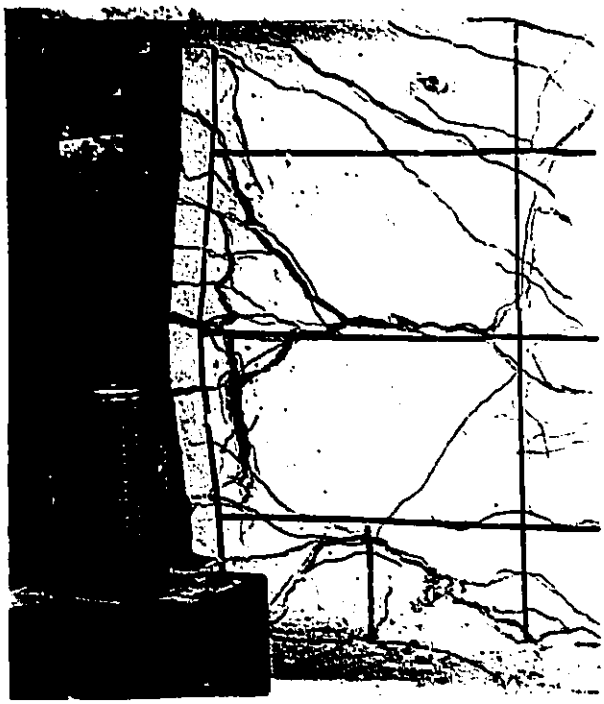

Figure 3.7: Buckling of exterior flexural bars

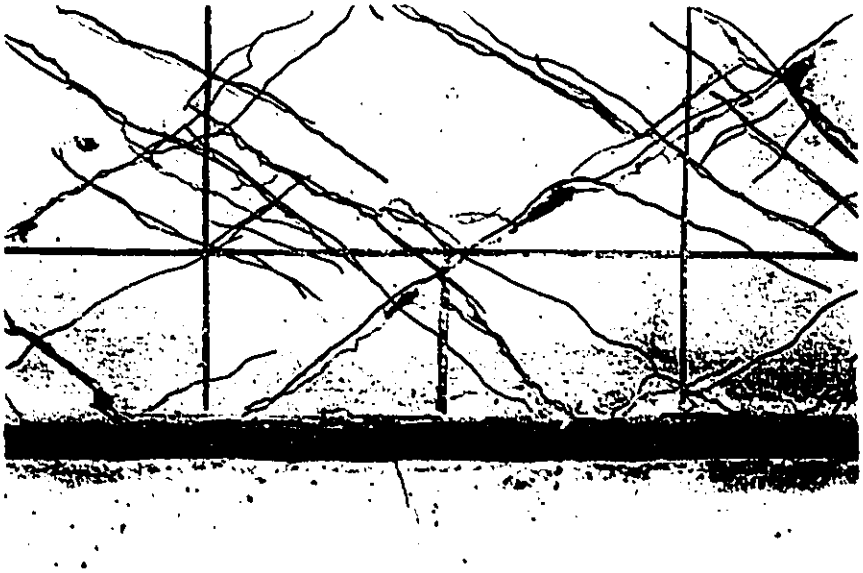

Figure 3.8: Bottom portion of the Wall 3 at $4\Delta_y$.

3.3 Displacement Components of Wall 3

3.3.1 Sliding Shear Displacement

Two 150 mm stroke LVDTs were mounted on the base to measure shear sliding. The location of LVDTs can be seen in Figure 2.12. However, there was no sliding observed during the test. LVDT readings indicated a maximum displacement of about 2 mm, which resulted from cracking in the bottom portion of the wall and was not related to sliding shear. Inclined shear cracks propagated into the bottom portion of the wall where pins for LVDT readings were mounted. These cracks produced deformations that were picked up by the LVDTs. These displacements are shown in Figures 3.11 and 3.12.

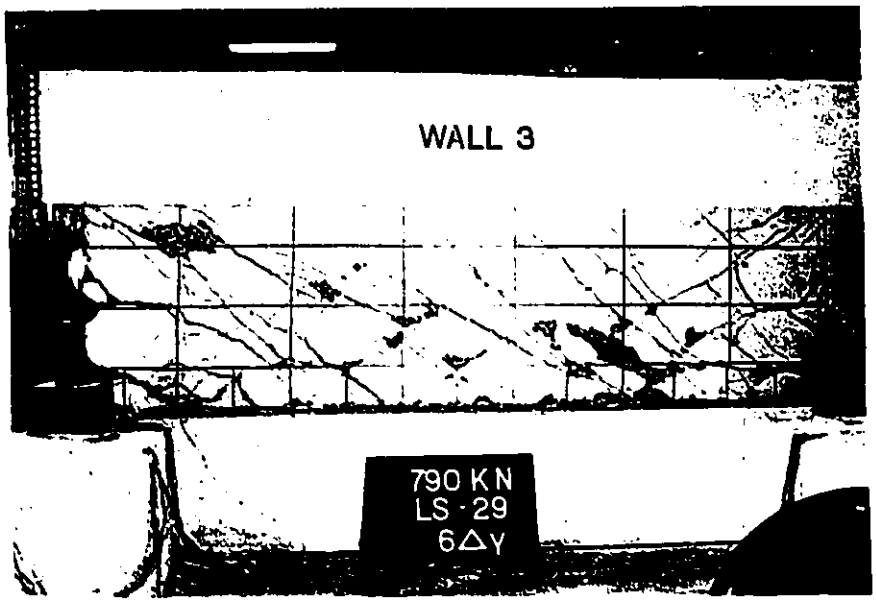

Figure 3.9: Wall 3 at failure

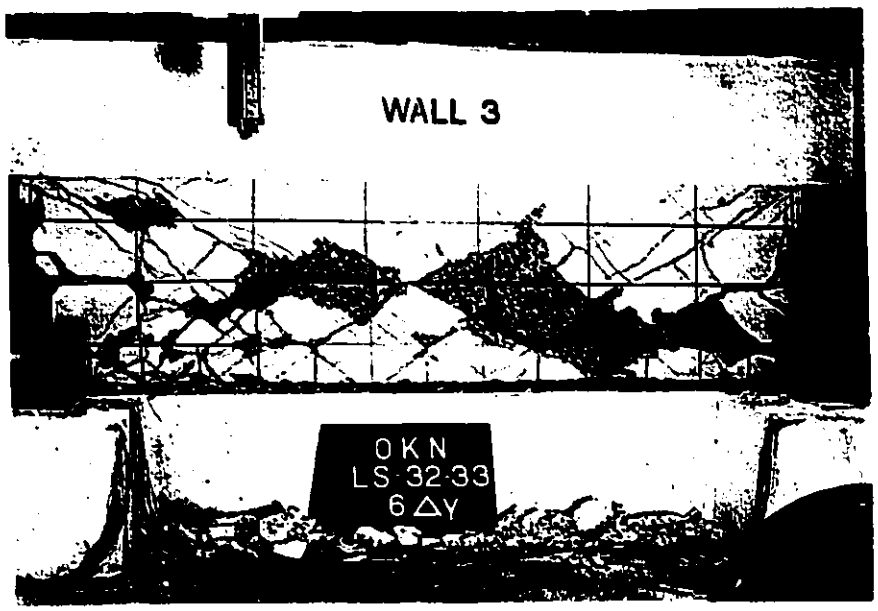

Figure 3.10: Wall 3 after the test

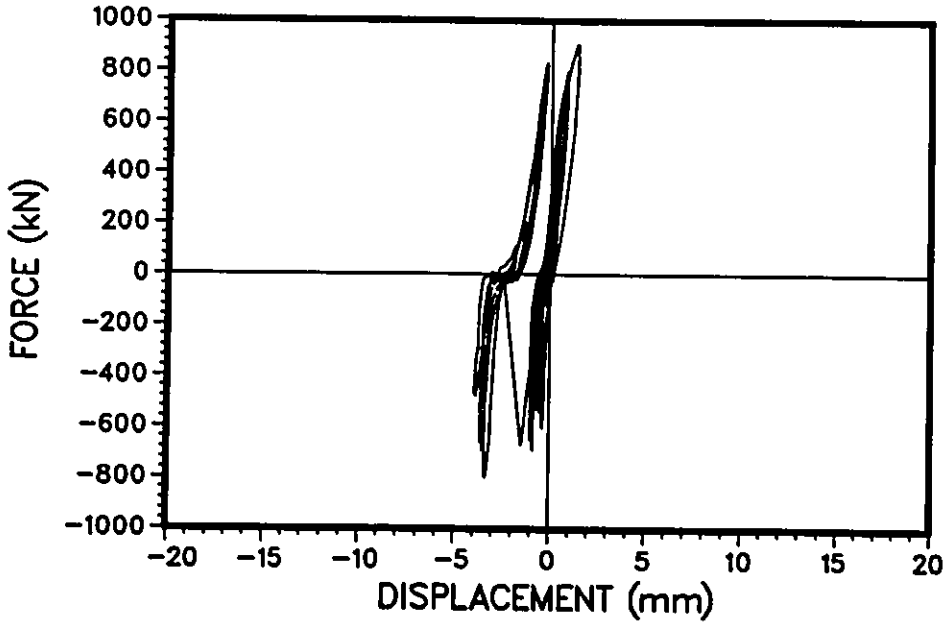

Figure 3.11: Force–displacement relationship recorded by LVDT 3 in Wall 3

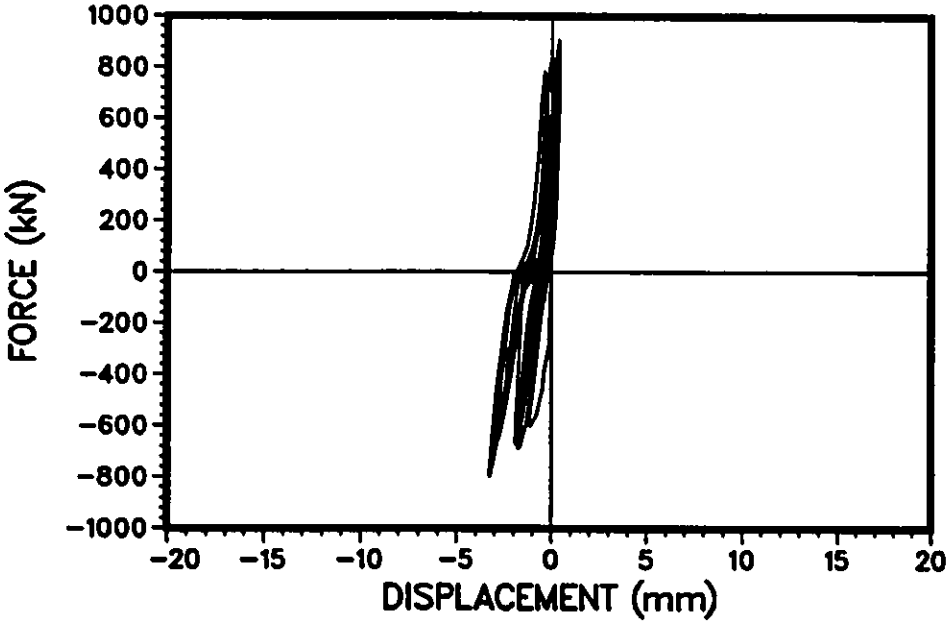

Figure 3.12: Force–displacement relationship recorded by LVDT 5 in Wall 3

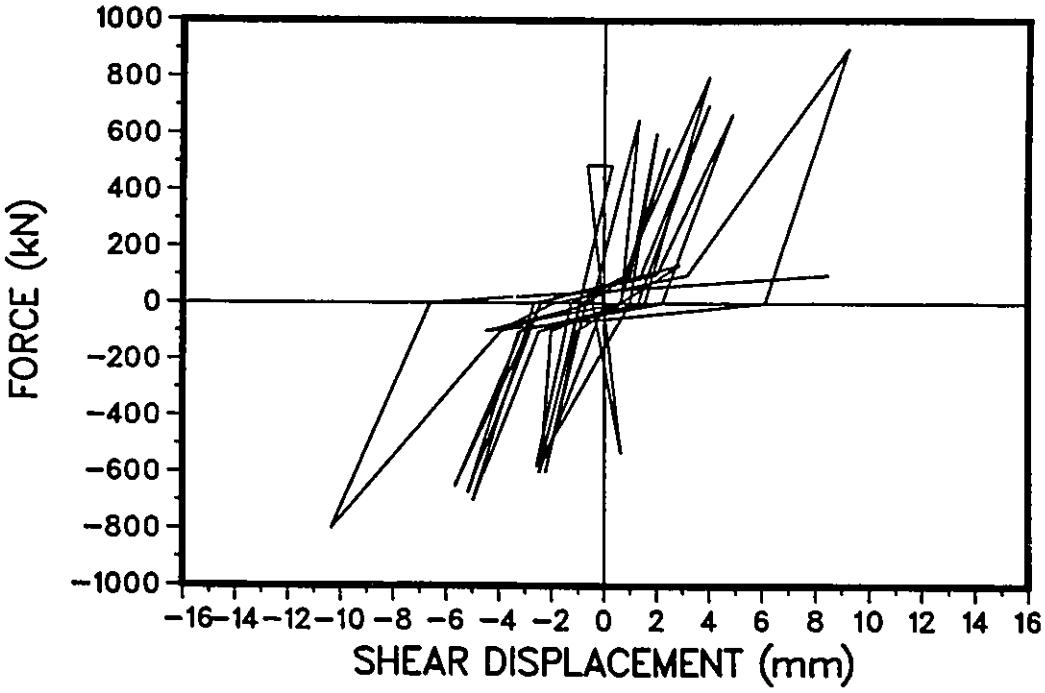

Figure 3.13: Load vs shear displacement in Wall 3

3.3.2 Shear displacement

The instrumentation used for shear deformation measurements is described in section 2.5.5. Detailed calculation of shear displacements using horizontal, vertical and diagonal displacement data is included in Appendix C. Figure 3.13 shows the load vs shear displacement relationship. The readings were terminated after the first cycle at $4\Delta_y$, due to loss of one of the pins in the wall. The instrument used for shear displacement measurements is shown in Figure 3.14.

3.3.3 Displacement due to bar extension

Two 5 mm stroke LVDTs (numbers 2 and 7 in Figure 2.12) were installed vertically at bottom corners of the wall to measure anticipated extension of vertical reinforcement in the base. These measurements would essentially include displacements resulting from local slippage of flexural reinforcement

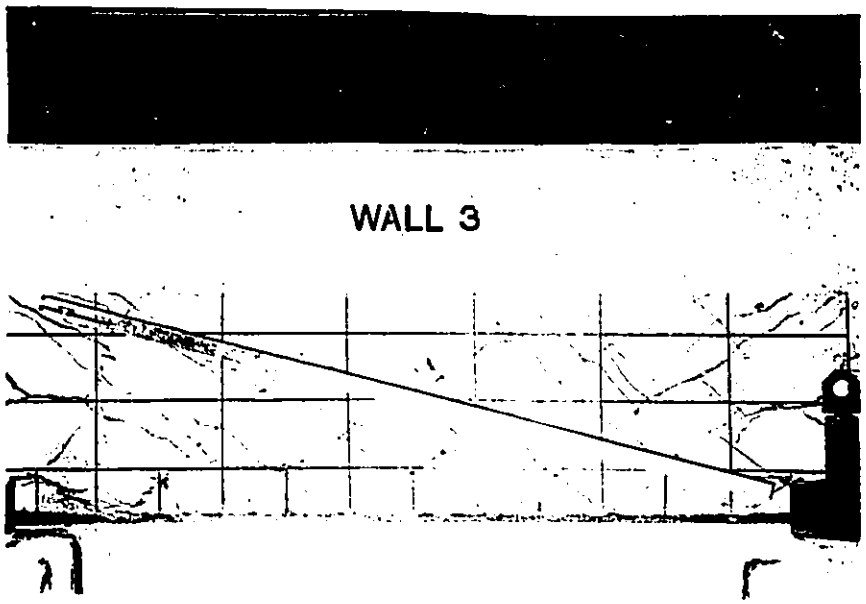

Figure 3.14: Measurement of shear deformation components in Wall 3

within the wall base. This data could then be used to compute horizontal displacement component of wall due to the bar extension. Any possible errors in these readings would include the following additional deformations:

1. Displacement due to bending of the flanges of "I" shaped base, since the instrumentation frame was connected to the base in the vicinity of anchorage bolts.
2. Crushing of concrete in compression toe.
3. Localized effect of cracks in the immediate vicinity of pins to which the LVDTs were connected.

The character of hysteresis loops reveals significant extension of flexural reinforcement within the base and shows permanent deformations after unloading. The load vs bar extension displacement relationships are shown in Figures 3.15 and 3.16.

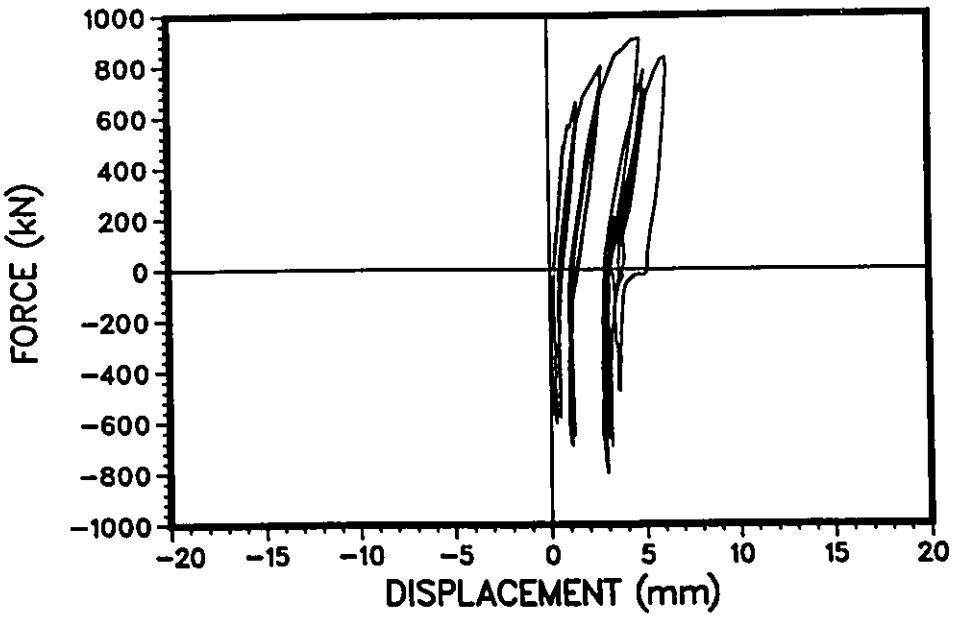

Figure 3.15: Load vs Bar Extension displacement in Wall 3 – LVDT 7

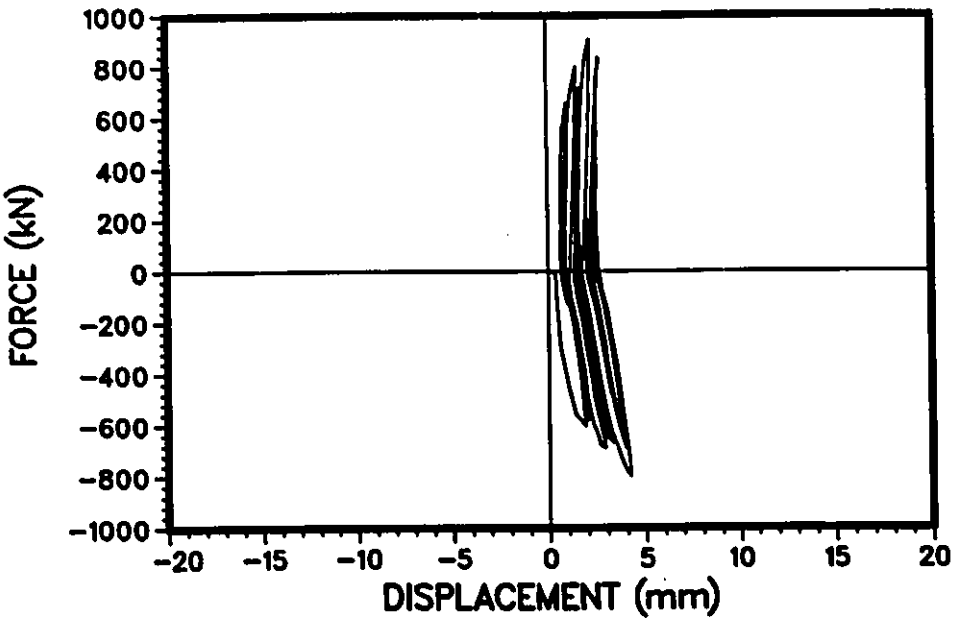

Figure 3.16: Load vs Bar Extension displacement in Wall 3 – LVDT 2

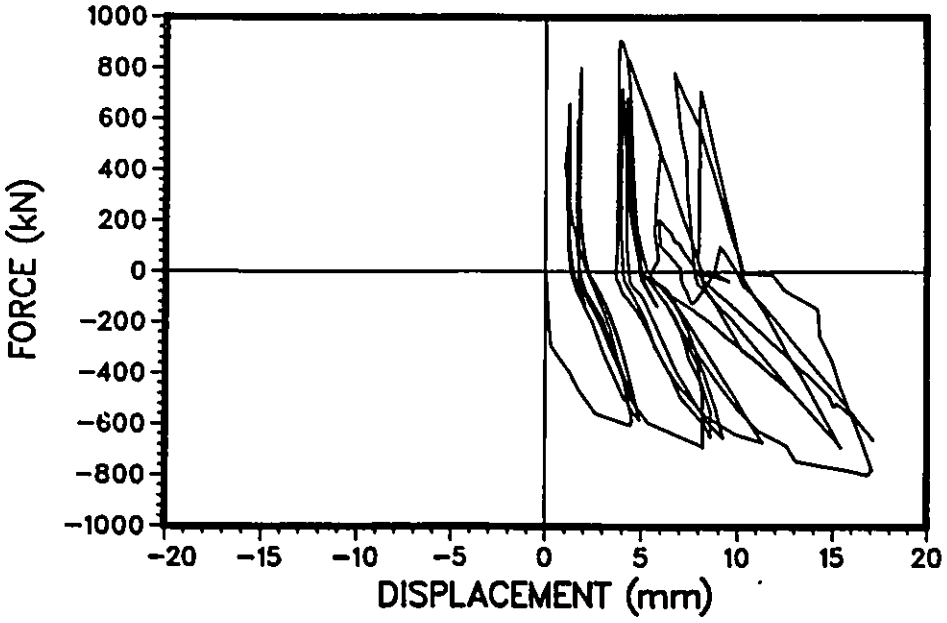

Figure 3.17: Total vertical movement in Wall 3 (LVDT 1)

3.3.4 Flexural Displacement

Flexural displacement of the wall was measured by means of vertical LVDT's recording the vertical displacement of the top beam at the ends. These LVDT readings would provide total rotation of the top beam relative to the base. However, they would include rotations caused by the extension of vertical reinforcement in the base. Therefore, flexural rotation of the top beam could be obtained by subtracting the rotation resulting from reinforcement extension from total rotation.

Vertical displacement of the top beam was monitored during the test by two 5 mm stroke LVDTs (LVDT 1 and LVDT 6 in Figure 2.12). Vertical displacement exceeded the range of LVDT's at load stage 22 ($4\Delta_y$). Therefore, dial gages were used beyond this load stage and the rest of the readings were taken manually. The load vs top vertical displacement relationships recorded during the test are shown in Figures 3.17 and 3.18. The hysteresis loops reveal that permanent deformations increase with increasing level

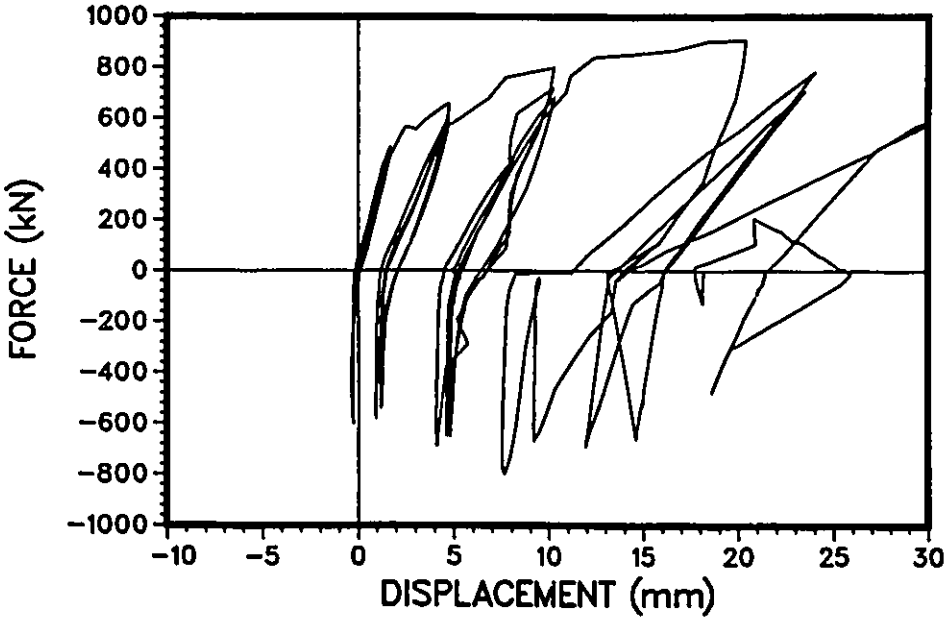

Figure 3.18: Total vertical movement in Wall 3 (LVDT 6)

of horizontal displacement. Furthermore, the vertical displacements at the corner closer to the hydraulic jack show higher rate of increase than those of the opposite corner. It was noted during the test that the summation of crack width on each side of the wall was pretty well matching the recorded displacement.

Hysteretic moment–rotation relationship, obtained experimentally, is shown in Fig.3.19. This plot gives base moment vs. top beam rotation, excluding the rotation of the wall at the construction joint, due to bar extension.

Fig.3.19 shows asymmetric behavior of wall in flexure. This is attributed to vertical component of lateral load, generated during loading. The lateral load was applied by pushing against south face and pulling the north side of the specimen. When the load was applied in the north direction, an upward vertical component, exceeding 5% of the applied load was observed at high deformation range. This is illustrated in Fig. 3.20. This upward vertical load increased moment and caused more rotation. When the load was applied in the opposite direction, the reverse effect was observed. Pulling

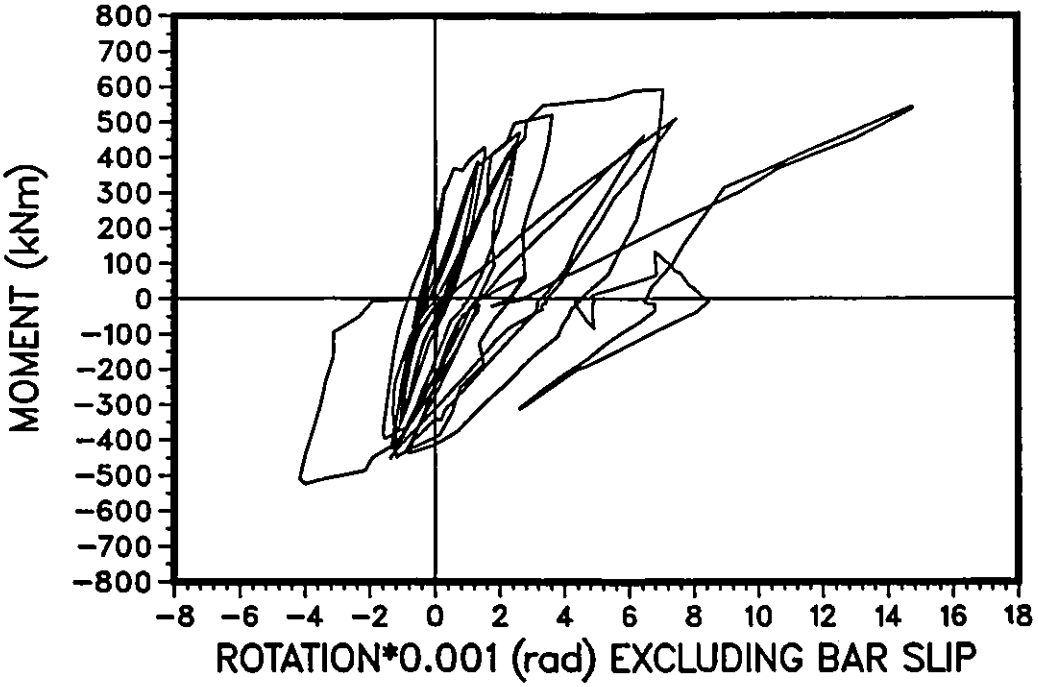

Figure 3.19: Experimental moment-rotation relationship, excluding rotation due to bar extension

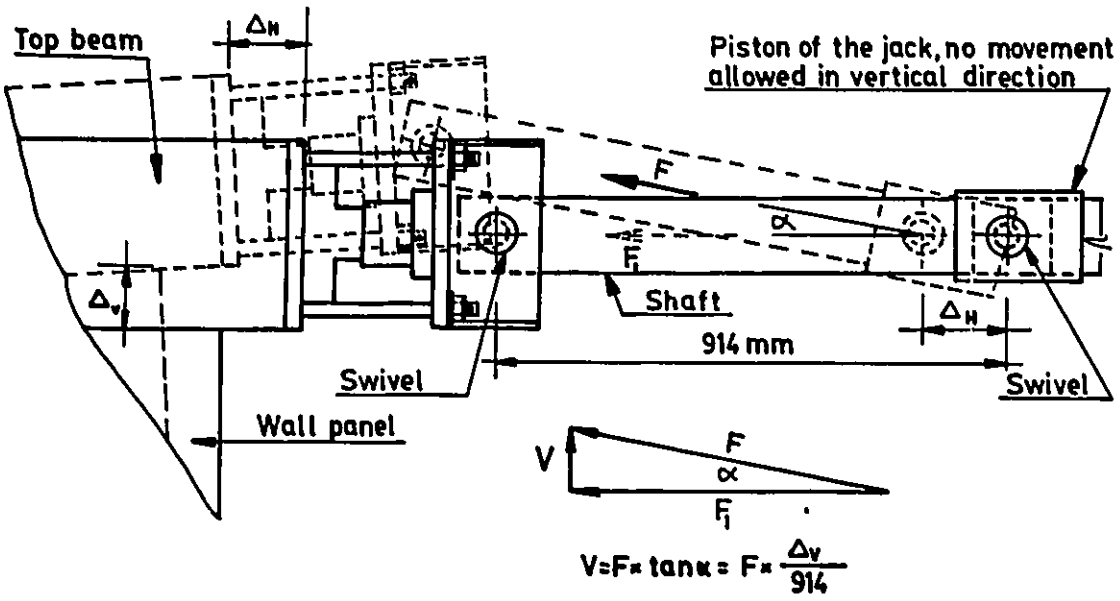

Figure 3.20: Formation of vertical component of applied force

force on the north face produced a downward vertical component which reduced the bending moment and the corresponding rotation.

The horizontal displacement of the top beam due to flexure was computed from the experimental data. It was found that this component was very small in comparison to total displacement and was within the experimental error margin in most cases.

3.4 Steel strain measurements in Wall 3

Strain measurements on selected reinforcing bars were taken by means of strain gages. The locations of strain gages placed on flexural and sliding shear reinforcement are shown in Figure 2.16. Figures 3.21 through 3.28 show the recorded strain gage data. The following observation can be made based on the steel strain data :

1. Strains in sliding shear reinforcement at joint location, were less than or equal to 40% of the yield strain.
2. Yielding of extreme flexural bars did not extend to a distance of 140 mm below the construction joint.
3. All flexural bars yielded during the test at a location 30 mm below the construction joint.

3.5 Observed behavior of Wall 6

Wall 6 with an aspect ratio of 1/2 and a shear capacity in excess of that corresponding to flexural capacity was subjected to the loading history

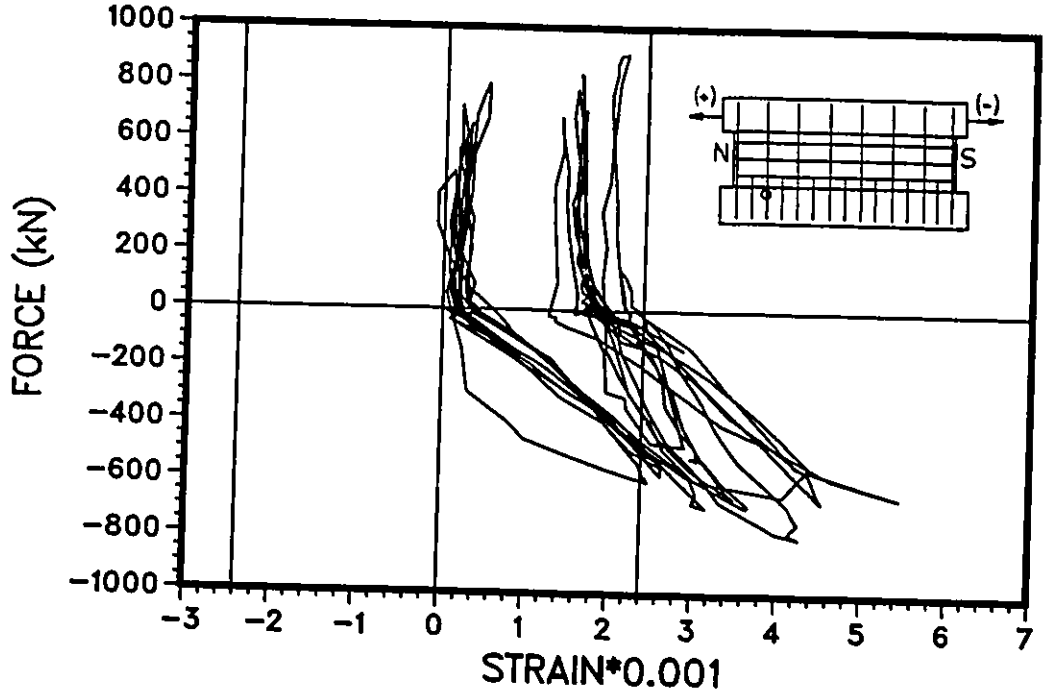

Figure 3.21: Load vs strain relationship in flexural reinforcement at location 3R in Wall 3

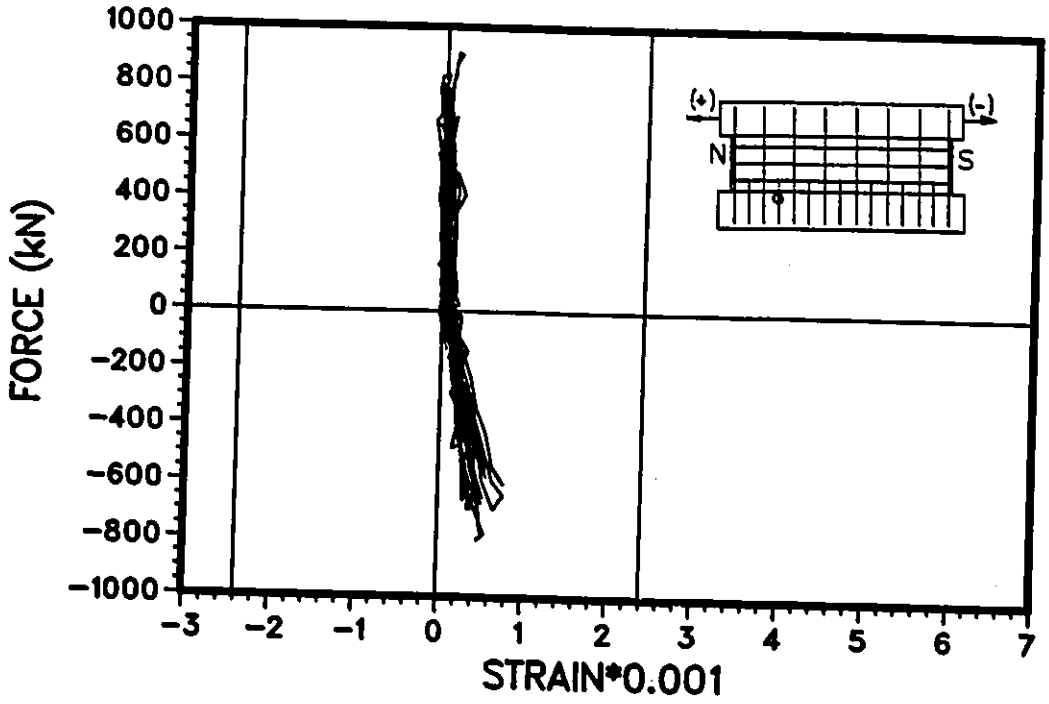

Figure 3.22: Load vs strain relationships in shear sliding reinforcement at location 4R in Wall 3

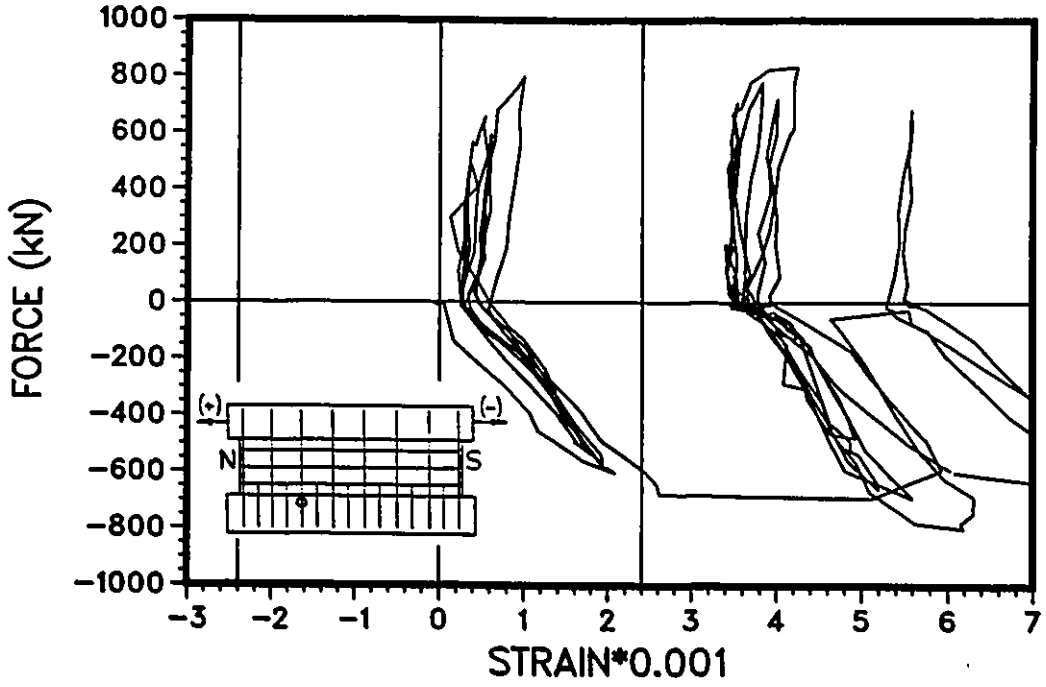

Figure 3.23: Load vs strain relationship in flexural reinforcement at location 5R in Wall 3

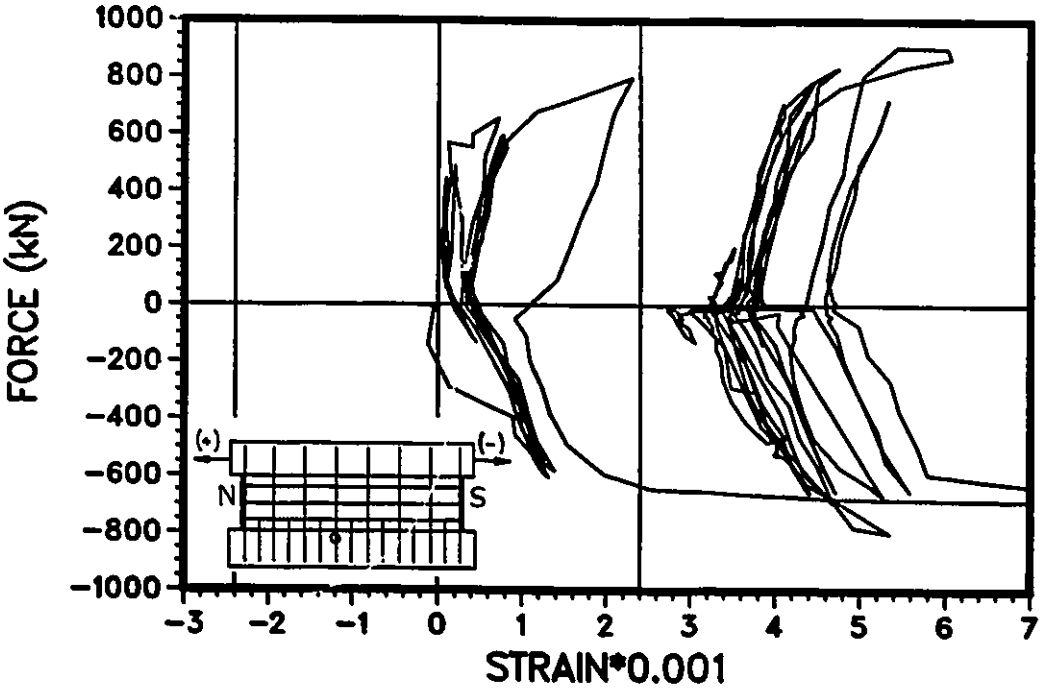

Figure 3.24: Load vs strain relationship in flexural reinforcement at location 7L in Wall 3

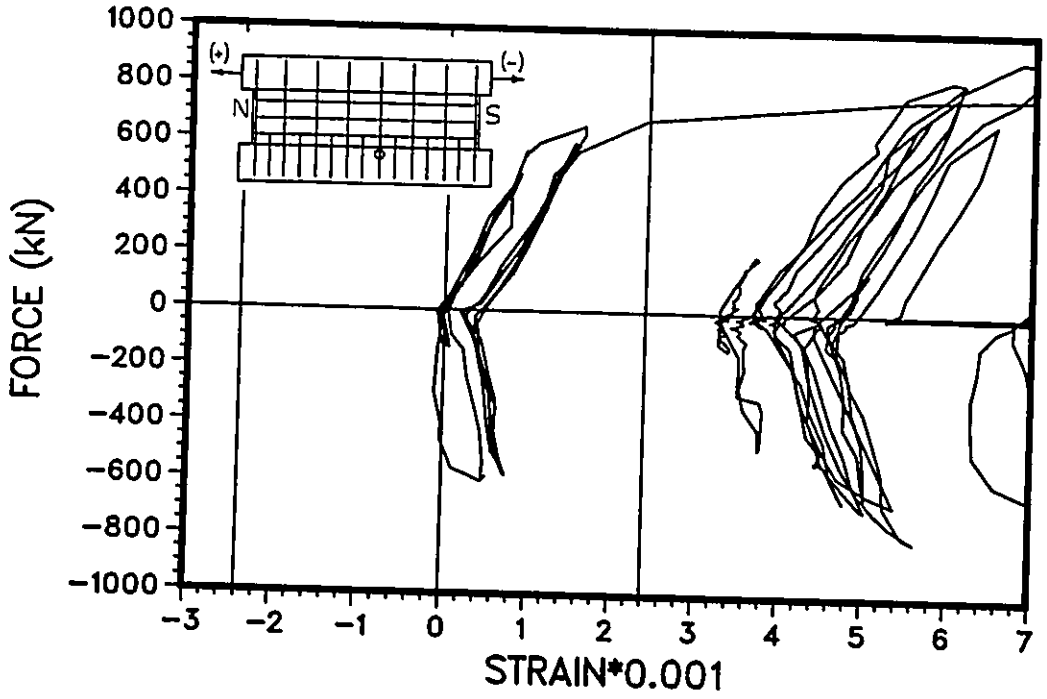

Figure 3.25: Load vs strain relationship in flexural reinforcement at location 9R in Wall 3

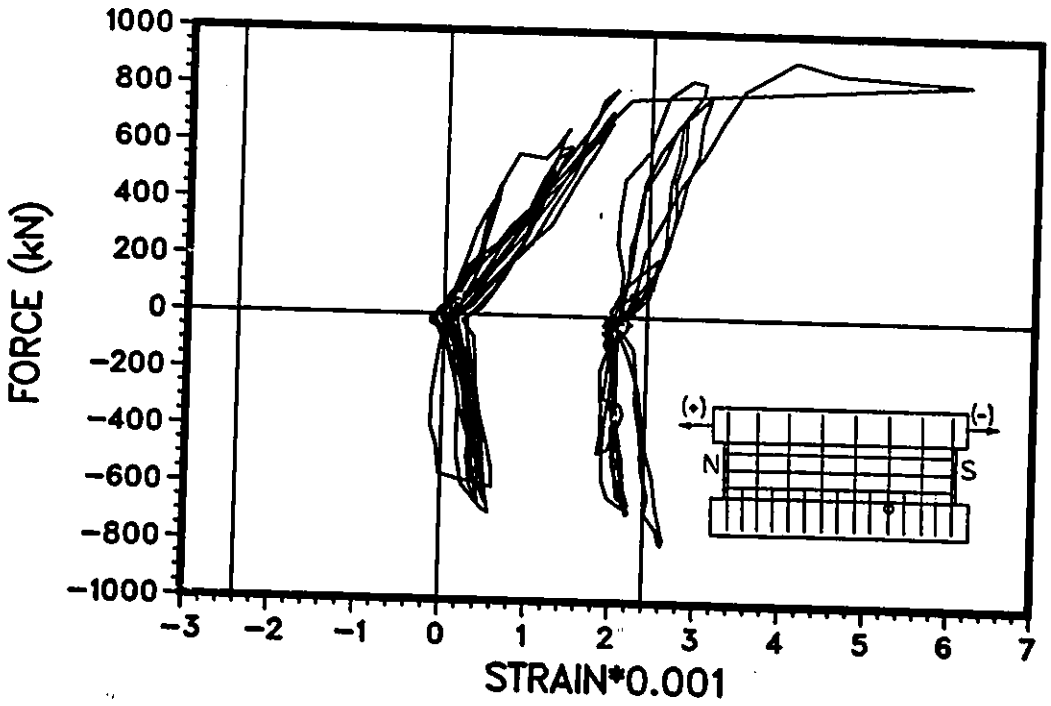

Figure 3.26: Load vs strain relationship in flexural reinforcement at location 11R in Wall 3

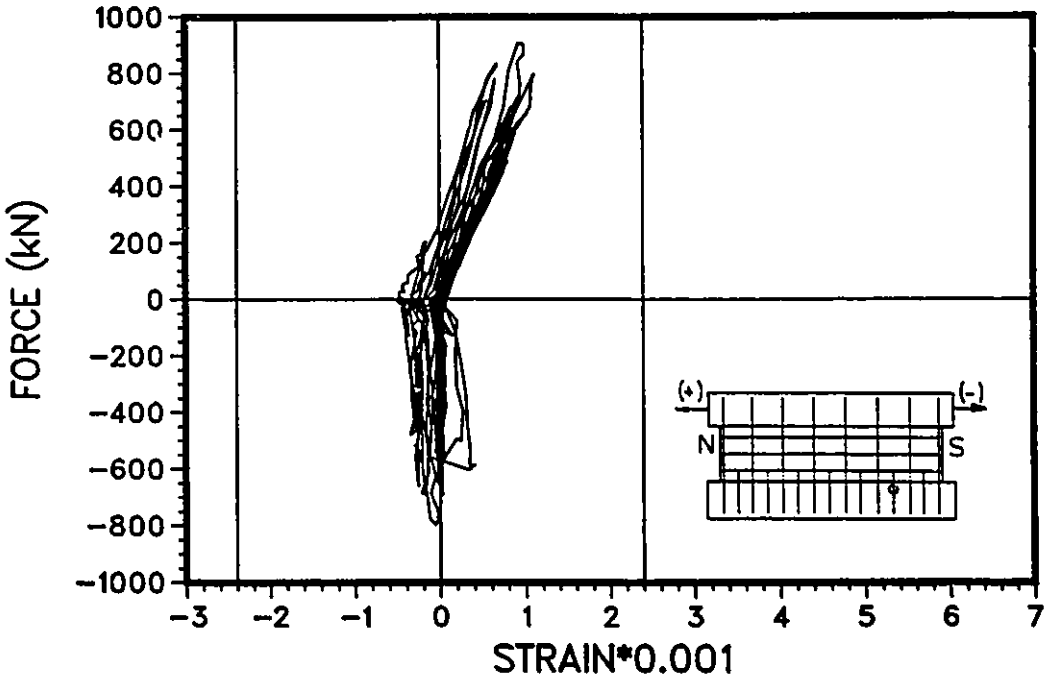

Figure 3.27: Load vs strain relationships in shear sliding reinforcement at location 12 R in Wall 3

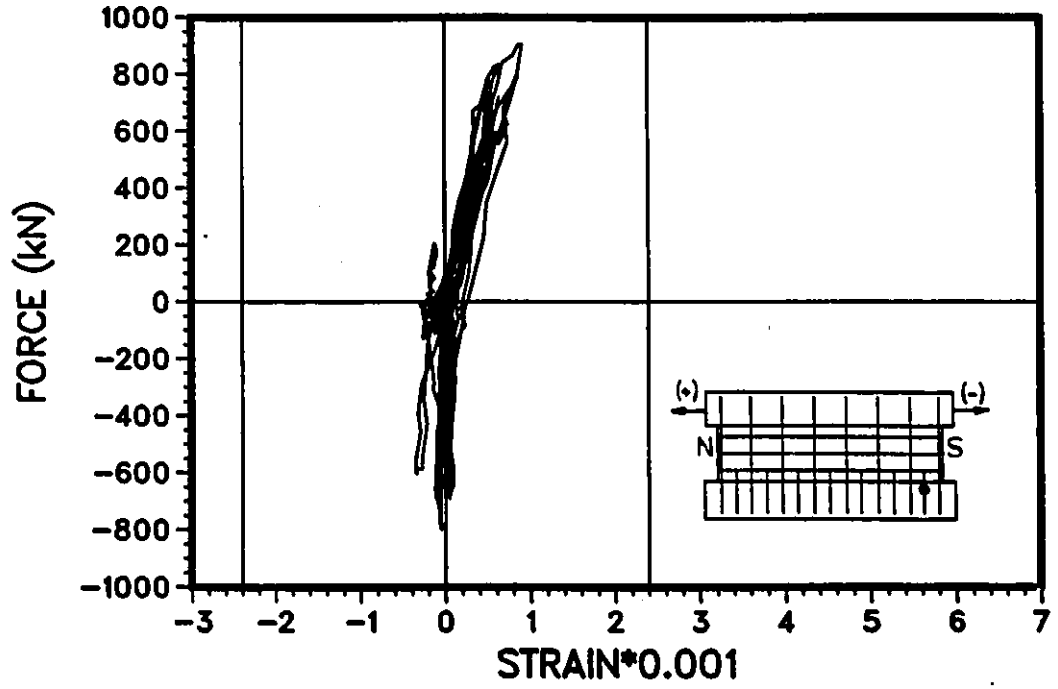

Figure 3.28: Load vs strain relationships in shear sliding reinforcement at location 14R in Wall 3

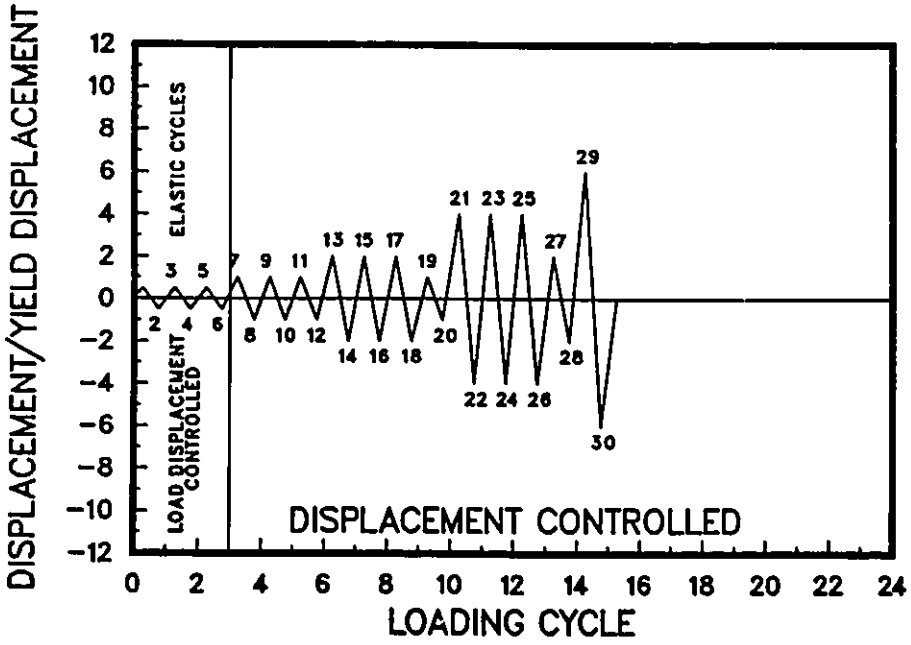

Figure 3.29: Actual loading history for Wall 6

shown in Figure 3.29. The predicted monotonic load capacity based on plane section analysis was 612 kN. This value corresponded to nominal shear stress of $0.65\sqrt{f'_c}$ MPa.

The horizontal displacement of the top beam was monitored during the test using a 150 mm stroke LVDT. The force vs top displacement relationship is shown in Figure 3.30.

During the first three cycles the specimen was subjected to lateral forces of 245 kN in the positive and -280 kN in the negative directions. The first shear crack appeared in the lower portion of the wall at a shear force of 150 kN. Shear cracks at the midhight formed at a shear force of 200 kN. Some flexural cracks occurred at the very ends of the specimen. Flexural cracks had a tendency to follow stirrups at the ends of the wall, and pass above the sliding shear reinforcement. Figure 3.31 shows the crack pattern at the end of the elastic cycles.

After the elastic cycles, the load was applied in displacement control mode.

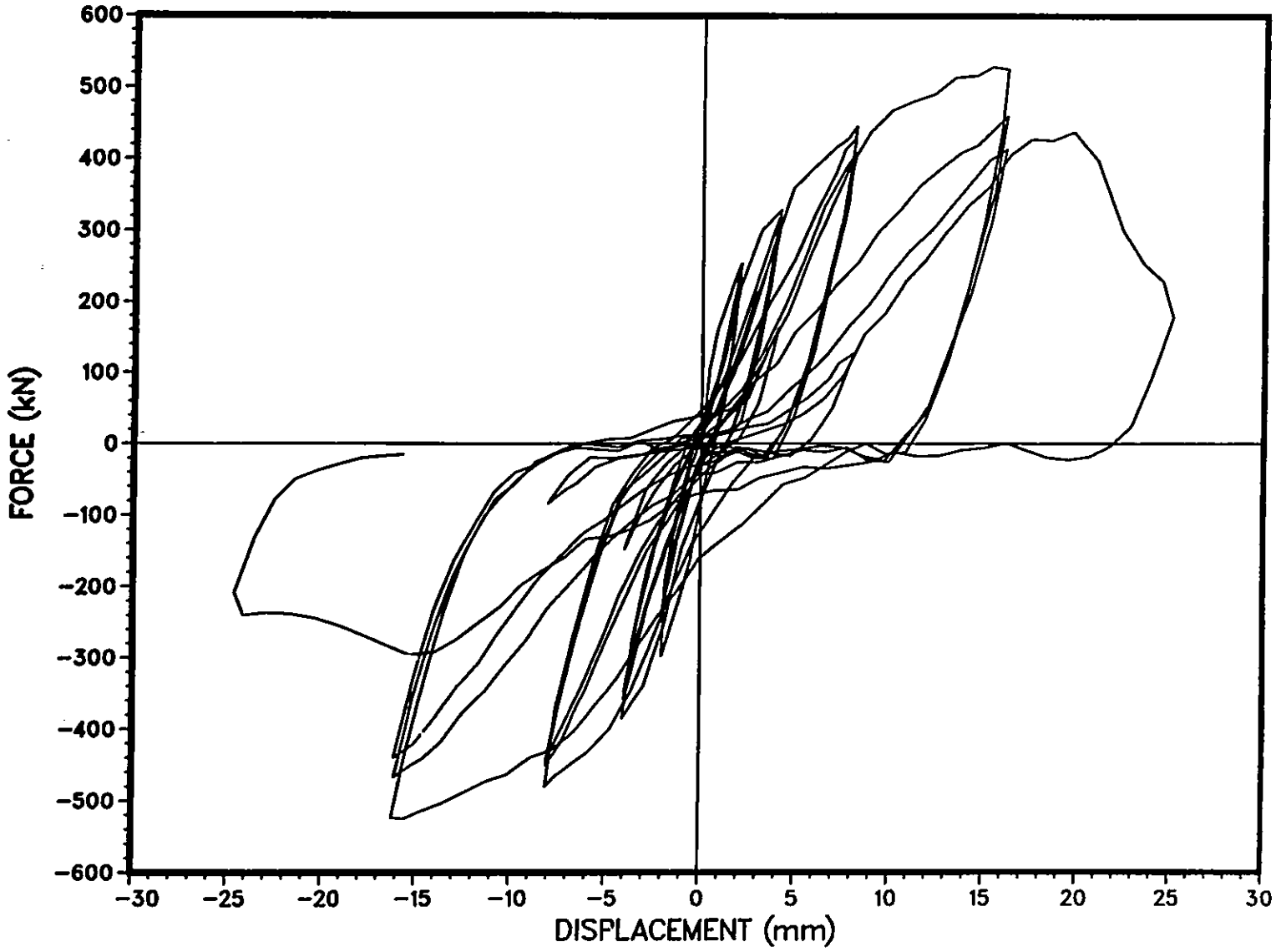

Figure 3.30: Load vs top displacement relationship of Wall 6

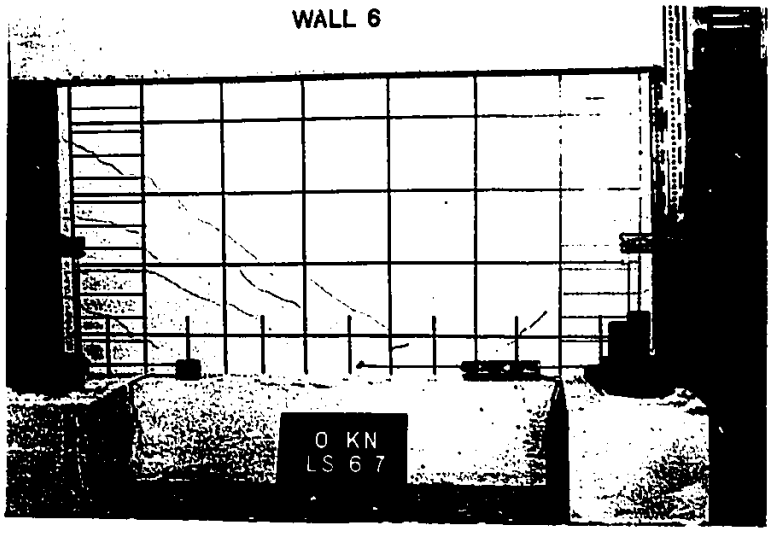

Figure 3.31: Wall 6 at the end of elastic cycles

The wall was subjected to three cycles at yield displacement. The yield displacement ($1\Delta_y$) was equal to 4.0 mm and was reached at a horizontal load of 320 kN in the positive direction and -375 kN in the negative direction. Additional shear cracks started to occur when the load exceeded previously reached maximum, i. e. 280 kN. Some of these cracks propagated to join the existing cracks. There was a sign of formation of flexural crack at the joint. This crack extended only about 70 mm at the south side where the wall was loaded. The crack pattern remained unchanged during the subsequent cycles at yield displacement. Strength degradation in each consecutive cycle was very small (in the range of about 7%), and the loading path was aiming at approximately the previous maximum. Figure 3.32 illustrates the crack pattern at the end of the cycles at $1\Delta_y$.

The next deformation level was $2\Delta_y$. The specimen developed load resistance of 440 kN in the positive direction, and -465 kN in the negative direction. Strength degradation of 6%, and 11% occurred during the subsequent two cycles of this deformation level. The loading path was shooting

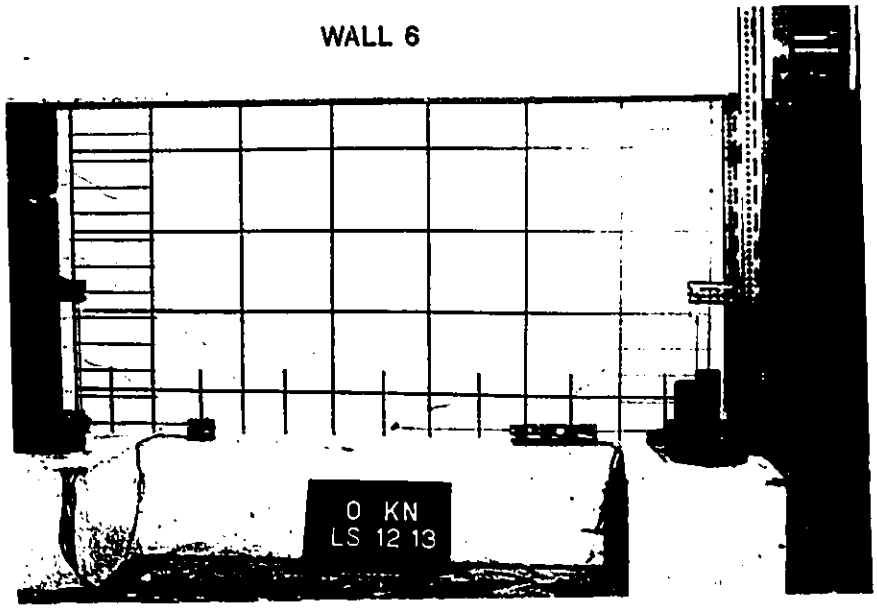

Figure 3.32: Wall 6 at the end of cycles at $1\Delta_y$

towards the previous maximum, and following an identical path. Some pinching of hysteresis loops occurred during the third cycle of $2\Delta_y$. Significant flattening of the top portion of hysteresis loops was observed, forming an extension of the loading path commenced at $1\Delta_y$ cycles. The loops indicated well pronounced strength increase. Additional shear cracks occurred at the first cycle of this deformation level. The flexural crack at the construction joint extended to the second row of flexural reinforcement on the south side, at load stage 13. A similar crack started to form at the peak of load stage 14, but extended only to the first row of joint bars. It was noticeable, that the congestion of shear cracks in the bottom portion of the wall was low. The crack pattern had a tendency to form "shear keys" similar to those observed in Wall 3. Figure 3.33 shows the specimen at the end of $2\Delta_y$ cycles.

Following three cycles at $2\Delta_y$, a cycle with deformation level of $1\Delta_y$(load stages 19 and 20) was introduced to the wall. The hysteresis loop followed the last cycle of $2\Delta_y$, exhibiting strength degradation of approximately

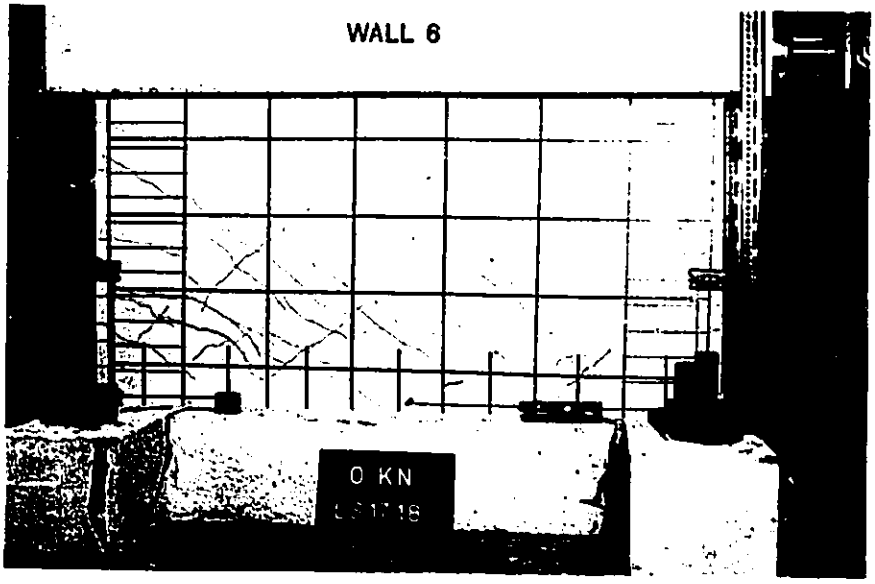

Figure 3.33: Wall 6 at the end of cycles at $2\Delta_y$

50%, compared with the previous cycle at $1\Delta_y$(load stage 12).

The specimen was next subjected to deformation cycles at $4\Delta_y$. The load resistance during the first cycle was 515 kN in the positive direction, and -512 kN, in the negative direction. Relatively high degradation of strength was observed in the subsequent cycles, i. e. 14% and 23% respectively. More pronounced pinching effect was also observed. Complete flattening of the hysteresis loop at this deformation level revealed that the wall reached its maximum capacity. There were new shear and flexural cracks formed immediately above the sliding shear reinforcement. Only a few cracks occurred in the bottom portion of the wall, where the sliding shear reinforcement was placed. The cracks at the joint remained essentially unchanged. The increased congestion of diagonal cracks above the sliding shear reinforcement was very pronounced. The bottom portion, surrounded by "shear keys" remained almost intact. The crack width immediately above the sliding shear reinforcement was ranging from 5 mm at the edge of the wall, to 1 mm in the center. Figure 3.34 shows the bottom portion of the wall at load stage

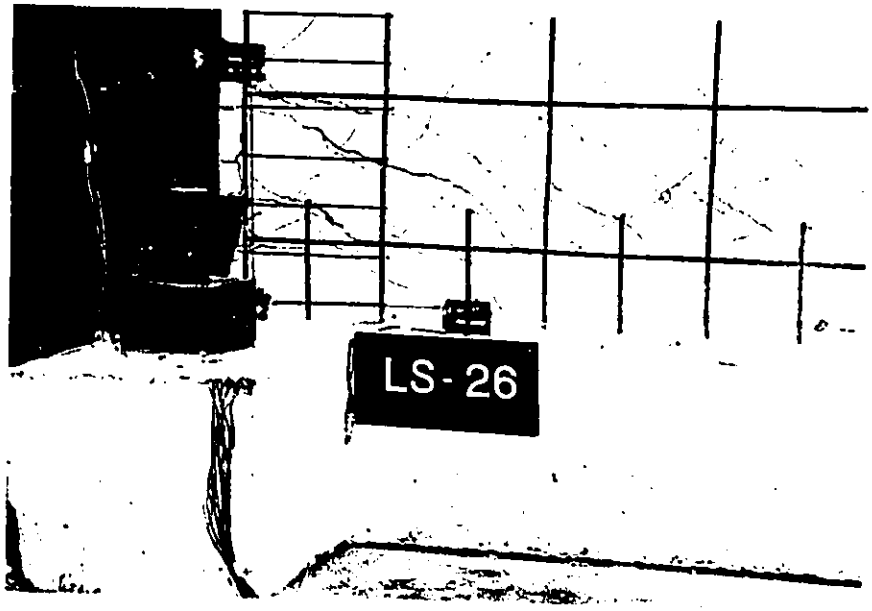

Figure 3.34: Bottom portion of Wall 6 at $4\Delta_y$

26 ($4\Delta_y$). The pinching effect became very significant at this deformation level, showing negligible load resistance when the wall was subjected to -7 to 10 mm displacements. Figure 3.35 shows the wall at the end of cycles at $4\Delta_y$.

A small cycle with a deformation level of $2\Delta_y$was introduced to the wall following the cycles at $4\Delta_y$. Strength degradation in this cycle when compared with load stage 17, was approximately 73%.

In the next deformation level the specimen was subjected to cycles at $6\Delta_y$. The wall developed a load resistance of about 430 kN when diagonal compression failure occurred at approximately $5\Delta_y$. The load dropped suddenly to about 150 kN at a deformation level of $6\Delta_y$. Figure 3.36 shows the damage at this load stage. When the load was reversed, the wall reached -300 kN load at $4\Delta_y$, which dropped to -230 kN at $6\Delta_y$. Massive spalling of concrete occurred in the previously overstressed area. After unloading to zero load the test was terminated. Figure 3.37 shows the specimen at the end of the test.

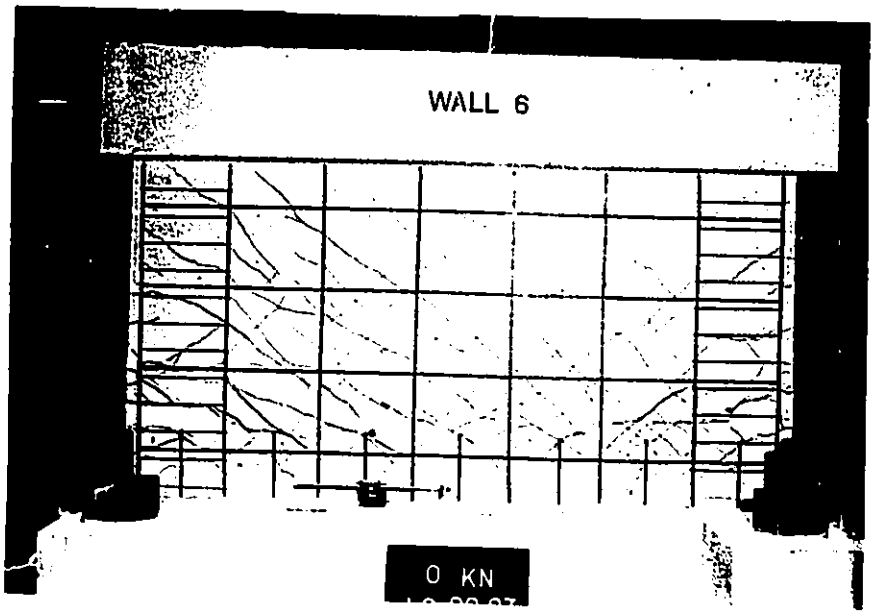

Figure 3.35: Wall 6 at the end of cycles at $4\Delta_y$

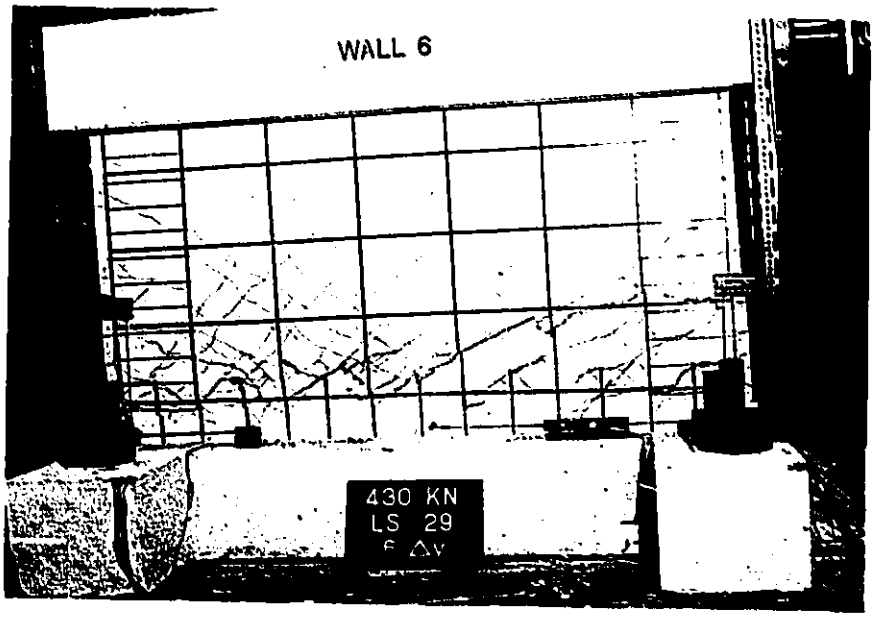

Figure 3.36: Wall 6 at failure

Figure 3.37: Wall 6 at the end of the test

3.6 Displacement components of Wall 6

3.6.1 Sliding Shear Displacement

Three 5 mm LVDTs were installed along the construction joint to measure sliding shear displacement. The location of LVDTs is shown in Figure 2.13. As a backup, 150 mm stroke dial gage was placed in the center of the joint. However, there was no sliding shear phenomena observed during the test. Two LVDTs placed at both ends of the joint (LVDT 6 and 8), showed deformations not exceeding 1 mm, and LVDT 7 placed in the center of the joint, showed deformations of 2.5 mm. LVDT 7, in the center, showed well formed hysteresis loops, and some permanent displacement. There was almost no displacement in the negative direction. Figures 3.38, 3.39, 3.40 show the load vs measured relative displacement between the wall panel and its base.

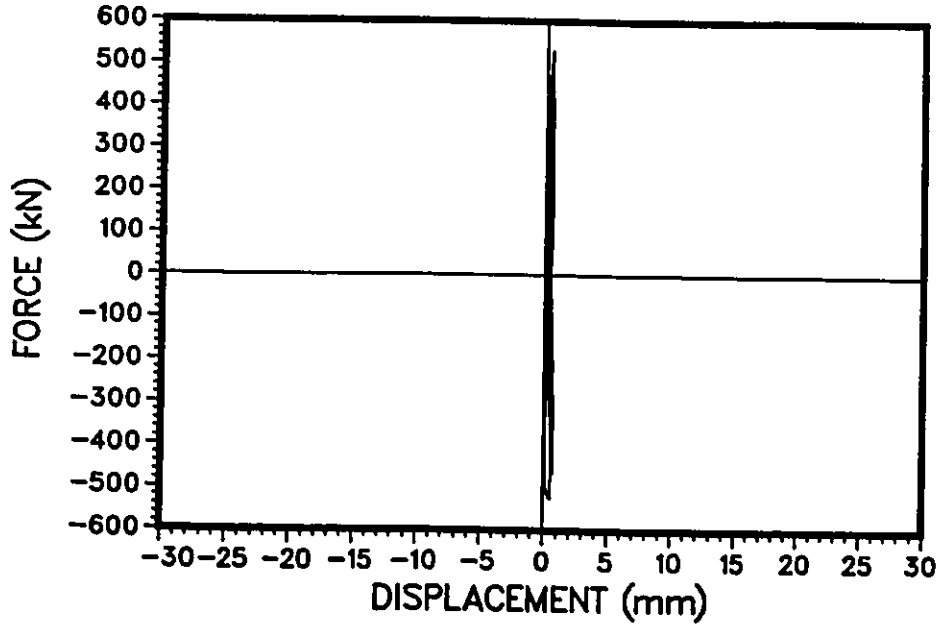

Figure 3.38: Load vs displacement at the base – LVDT 6

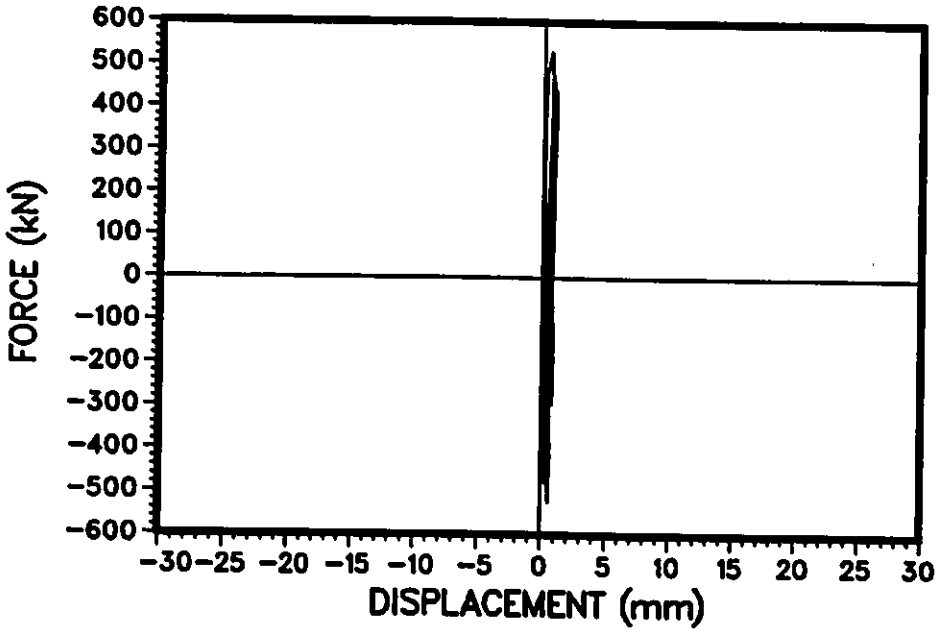

Figure 3.39: Load vs displacement at the base – LVDT 8

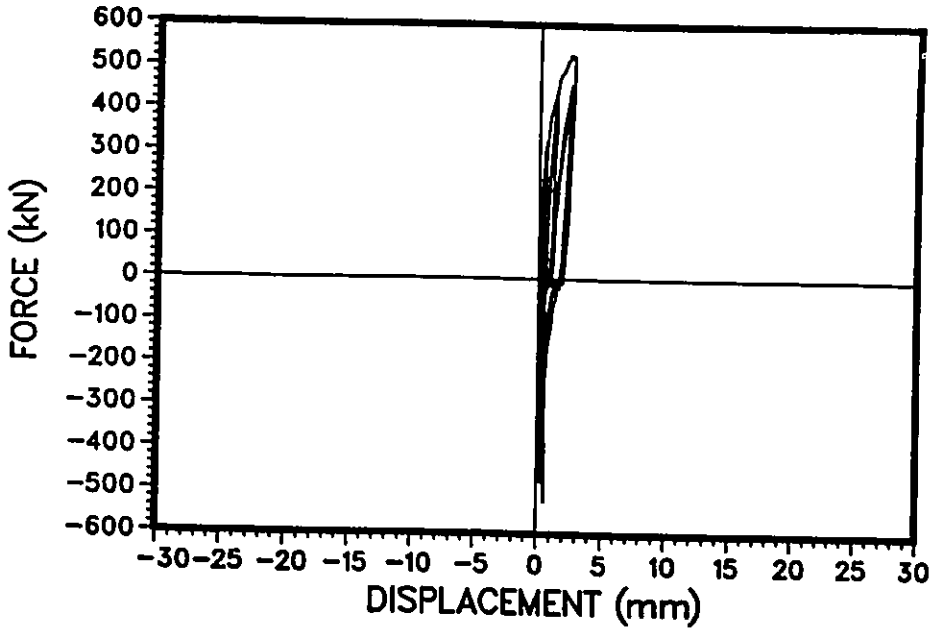

Figure 3.40: Load vs displacement at the base – LVDT 7

3.6.2 Shear Displacement

Shear displacement of Wall 6 was determined using the LVDT readings. The LVDT readings provided deformations of each corner of the wall. This data was used, along with geometric relationships, to determine average strains in two orthogonal as well as diagonal directions. The details of shear deformation calculations using the experimental data are given in Appendix C. Shear force – shear displacement hysteretic relationship is shown in Fig. 3.41.

3.6.3 Displacement due to Bar Extension

Two 5 mm stroke LVDTs (LVDT 2 and 3 in Figure 2.13) were placed at the bottom corners of Wall 6 to measure extension of vertical reinforcement in the footing. Well developed hysteresis loops, observed in Figs. 3.42 and 3.43, reveal yielding of flexural reinforcement and existence of permanent

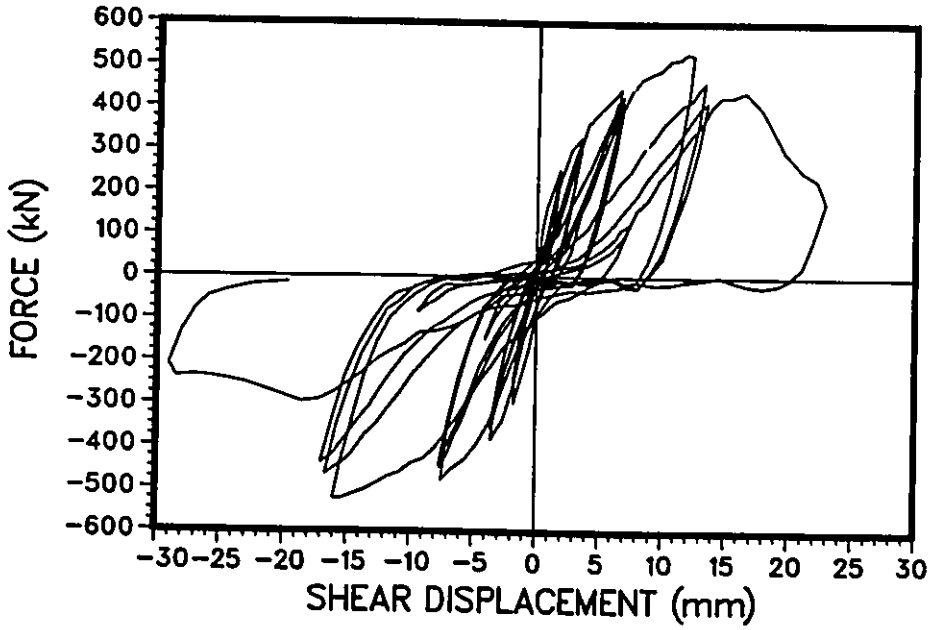

Figure 3.41: Experimental shear force – shear displacement hysteretic relationship of Wall 6

deformation after unloading. Contribution of this displacement to overall wall displacement is discussed later, in sec.4.7.

3.6.4 Flexural Displacement

Flexural deformation of Wall 6 was obtained by means of vertical LVDT's, providing vertical movement of the top beam. Two 150 mm stroke LVDTs were installed to measure vertical movements in Wall 6 (LVDT 1 and 5 in Figure 2.13). The hysteresis loops recorded at both ends of the top beam are fairly symmetrical, with the exception of the LVDT located at south end which showed about 15% higher deformations. There was an increase in permanent deformation with an increase in imposed deformation. Figures 3.44 and 3.45 show recorded relationships between the loads and total vertical movements of the top beam.

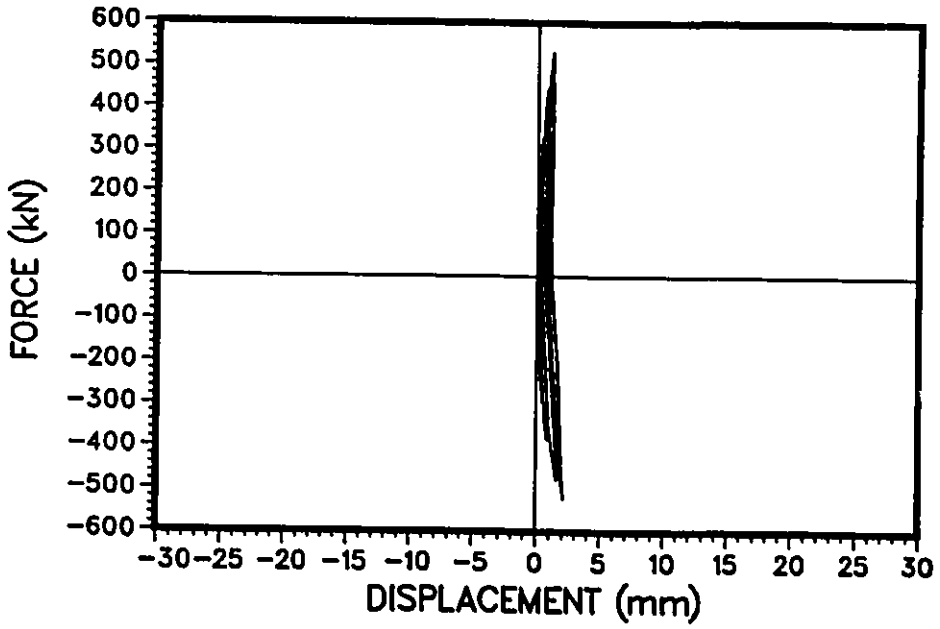

Figure 3.42: Load vs Bar Extension displacement in Wall 6 (LVDT 2)

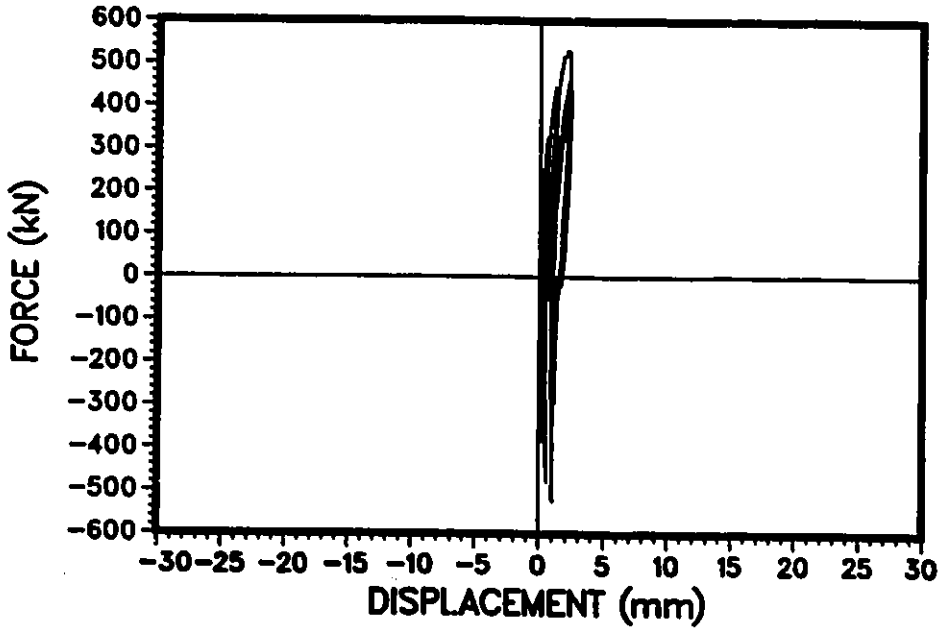

Figure 3.43: Load vs Bar Extension displacement in Wall 6 (LVDT 3)

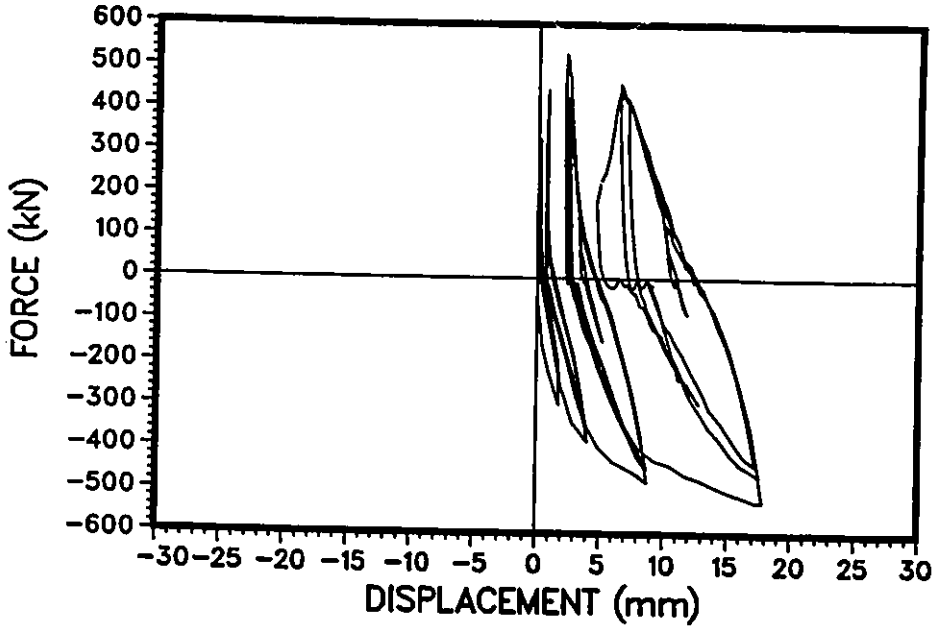

Figure 3.44: Total vertical movement vs load in Wall 6 (LVDT 1)

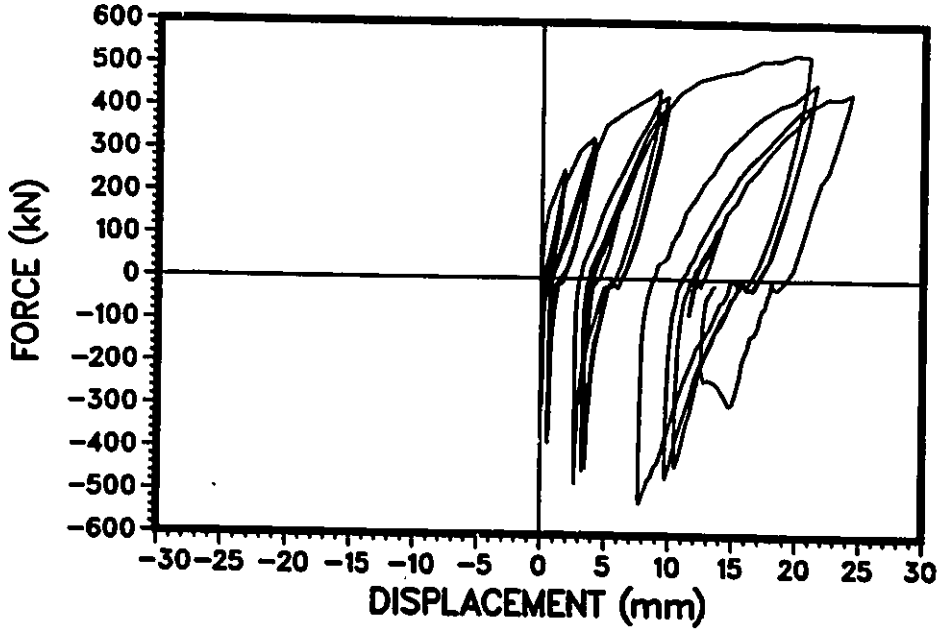

Figure 3.45: Total vertical movement vs load in Wall 6 (LVDT 5)

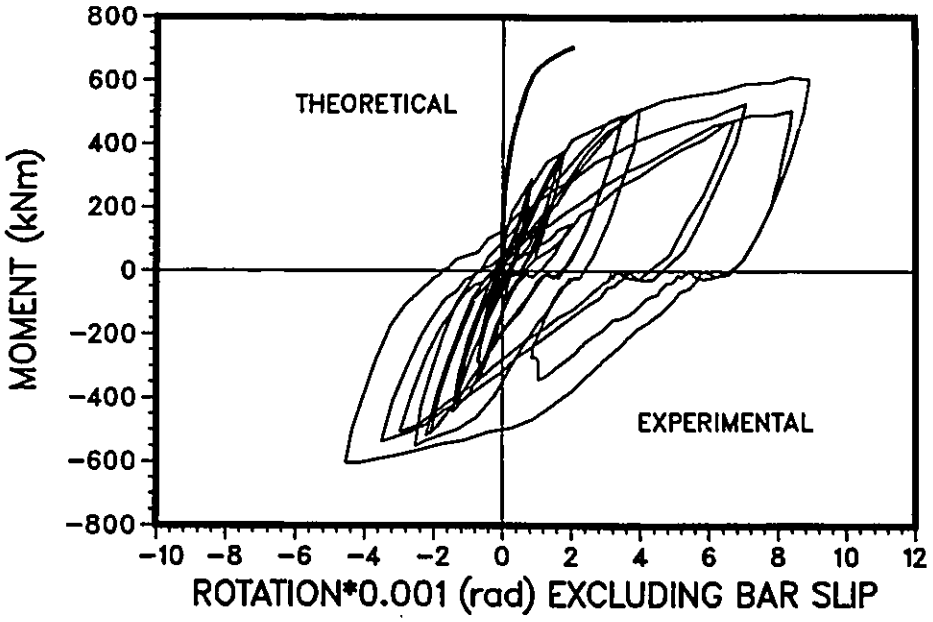

Figure 3.46: Experimental hysteretic moment–rotation relationship for Wall 6

Hysteretic moment– rotation relationship, obtained experimentally, is shown in Fig 3.46. This plot gives base moment vs. top beam rotation, excluding the rotation of the wall at the construction joint due to bar extension. The observed asymmetry in the curve is attributed to the vertical component of lateral load, as explained for Wall 3 in section 3.3.4.

The wall rotation was used to compute corresponding horizontal displacement at the top due to flexure. The hysteretic force flexural displacement relationship is shown in Fig 3.47.

3.6.5 Steel Strain Measurements in Wall 6

Strain measurements on selected reinforcing bars were taken by means of strain gages. The locations of strain gages placed on some flexural and sliding shear reinforcement are shown in Figure 2.17. The relationship between

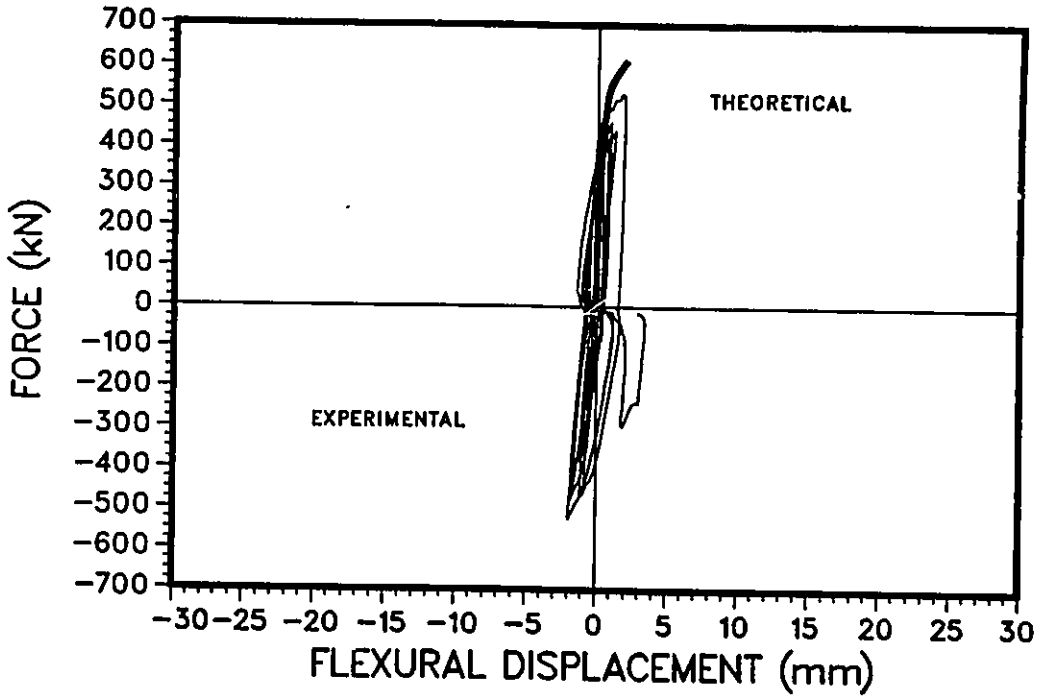

Figure 3.47: Experimental hysteretic force–flexural displacement relationship for Wall 6

the load and strain in selected flexural and sliding shear reinforcement are shown in Figures 3.48 and 3.49. The analysis of hysteretic loops representing force – strain relationship for reinforcing bars reveal that :

- The strains in sliding shear reinforcement measured at the joint location, were in excess of 70% of the yield strain.
- Two rows of flexural bars in the center of the wall did not yield at the joint location.

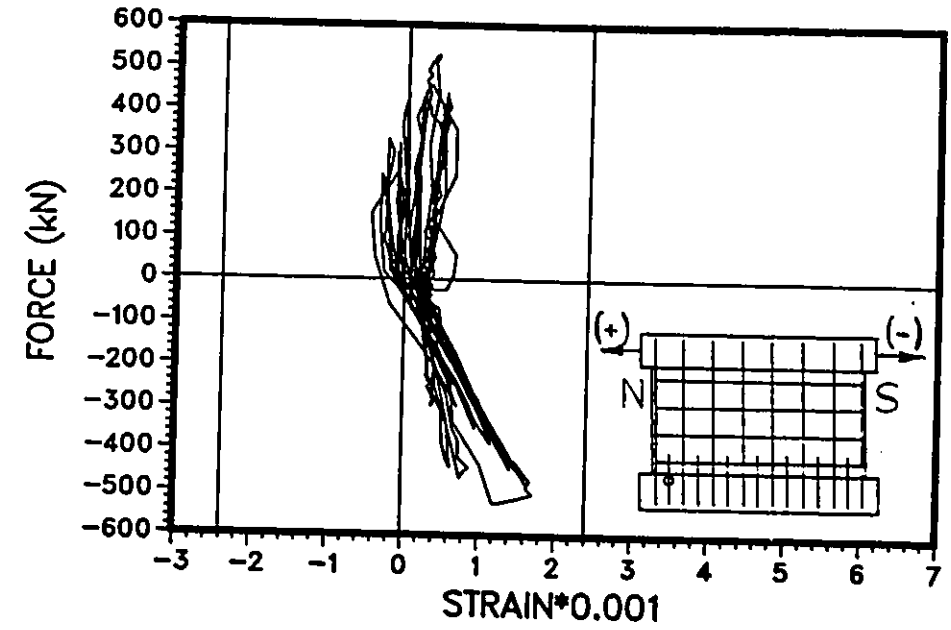

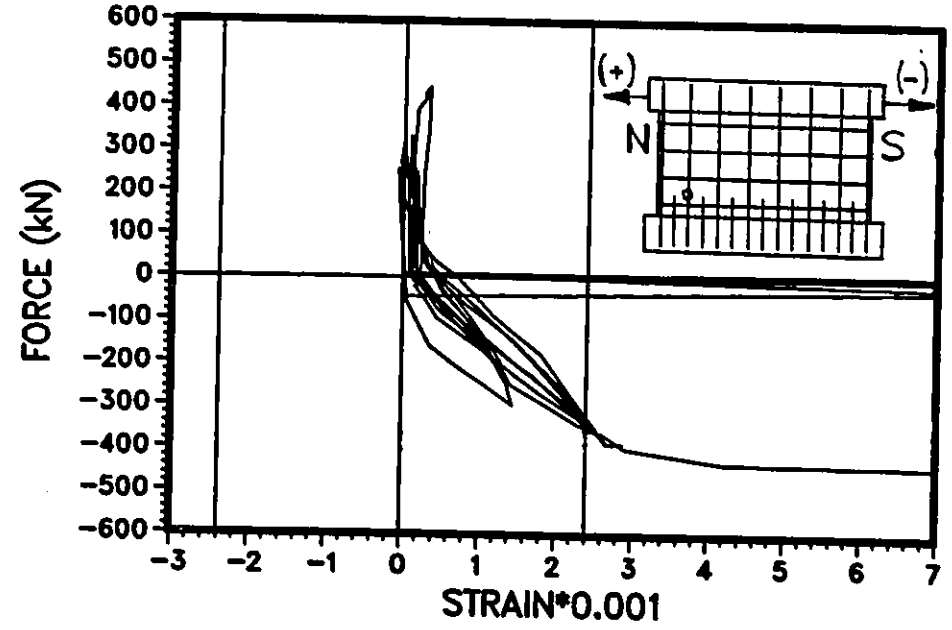

Figure 3.48: Load vs strain in selected bars in Wall 6

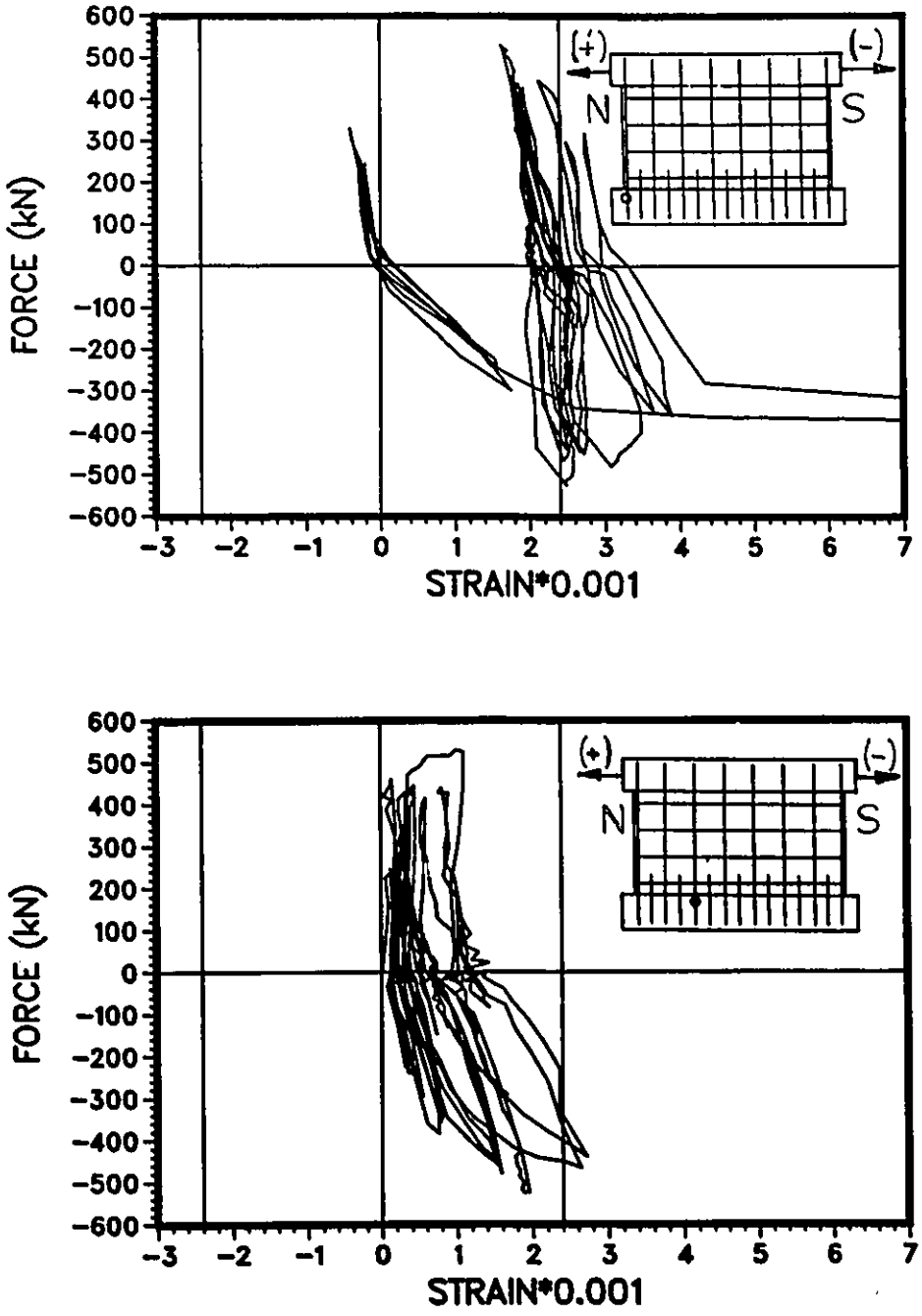

Figure 3.49: Load vs strain in selected bars in Wall 6

Chapter 4

Analysis of Test Results

4.1 General

The test data reported in Chapter 3 are analyzed to understand the mechanism of load resistance in squat shear walls. Significance of flexure and shear response is examined. Effectiveness of specially provided sliding shear reinforcement in resisting shear sliding is studied. Contribution of each component of deformation to overall wall response is illustrated. Finally, an overall assessment of wall response is made for each specimen and their responses are compared with those of the companion specimens tested by others.

4.2 Mechanism of Load Resistance in Wall 3

4.2.1 Flexural Response

Flexural behavior of Wall 3 is determined by examining the strain gauge data taken from vertical reinforcement, as well as by examining the moment–rotation relationship, recorded by LVDTs.

Some of the recorded strain data for vertical reinforcement of Wall 3 are reported in sec.3.4. Progression of yielding in vertical reinforcement at the critical section is illustrated in Fig 4.1. Experimentally obtained strain profiles are shown in Fig 4.2 at different load stages. Moment – curvature relationship, obtained from this data is compared with that obtained theoretically, in the same figure. The theoretical curve is based on the beam theory and is intended for members where shear effect is negligible. The comparison indicates that a substantially softer response was obtained in the test than that indicated by the beam theory. This is attributed to the flexure – shear interaction which is very significant in a squat member, such as Wall 3.

The moment – rotation relationship, obtained from LVDT data is shown in Fig 3.19. This relationship excludes the rigid body rotation of the wall caused by extension of vertical reinforcement in the base and hence gives the flexural response. The envelope of the experimental hysteresis curves is compared with that obtained by integration of theoretical moment – curvature relationships, in Fig 4.3. The comparison indicates softer response in flexure than that predicted theoretically. Furthermore, the wall strength observed experimentally is less than that predicted theoretically. The difference between the experimental and theoretical moment – rotation relationships is attributed largely to shear – flexure interaction which

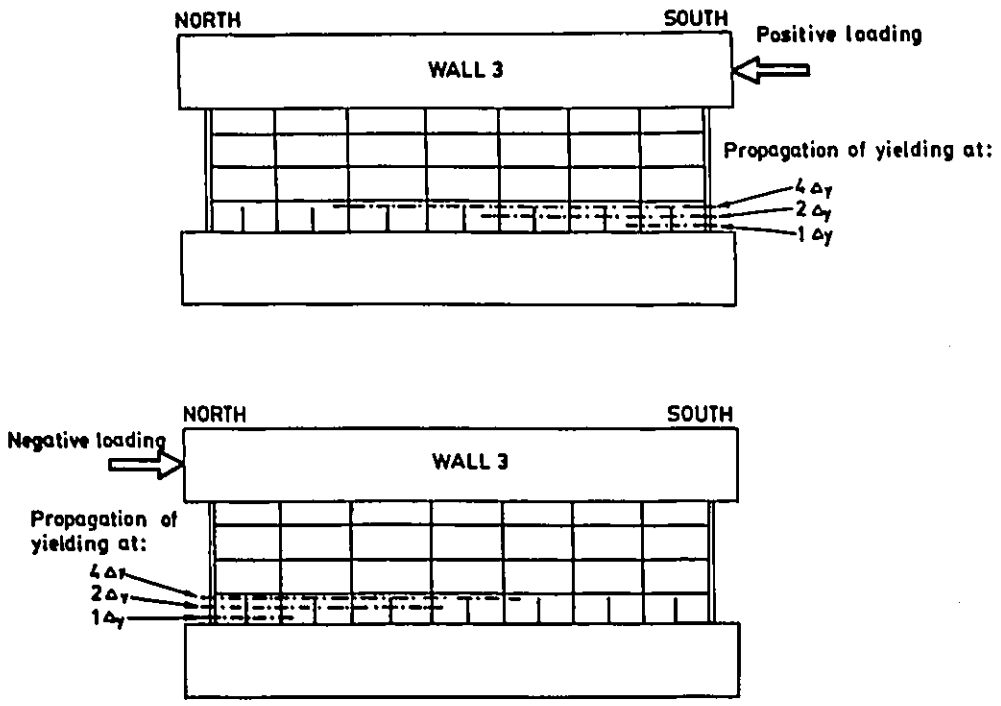

Figure 4.1: Progressive yielding of flexural reinforcement along with consecutive ductility imposed

is not accounted for in the theoretical prediction. Furthermore, the theoretical prediction is based on the assumption that the wall is fully fixed at the base along the entire length. The experimental setup, on the other hand was such that the wall was fully fixed only at the ends. Furthermore additional softening in the wall was caused during the experiment by the vertical component of lateral load as discussed in sec 3.3.4.

4.2.2 Shear Response

Wall 3 with an aspect ratio 1/4 was critical in shear. Shear deformations were measured during the test as discussed in sec 3.3.2. Shear force – shear displacement hysteretic relationship is shown in Fig 3.13. Examination of this relationship indicates a significant degradation of shear stiffness under cyclic loading. Pinching of force – displacement hysteresis loops is evident, indicating sliding of cracked surfaces under shear.

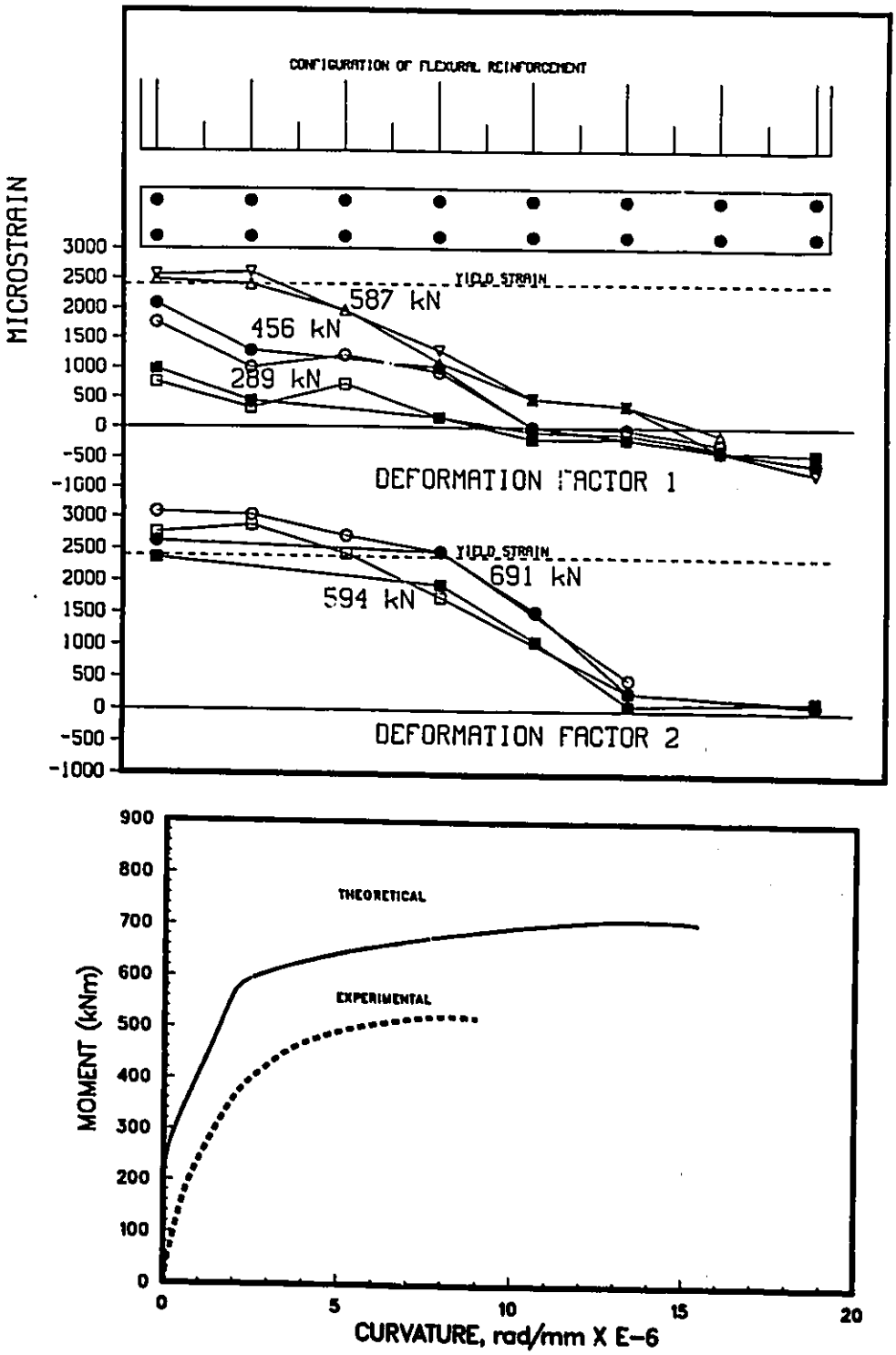

Figure 4.2: Strain profiles in flexural reinforcement and experimental and theoretical moment – curvature relationship in Wall 3

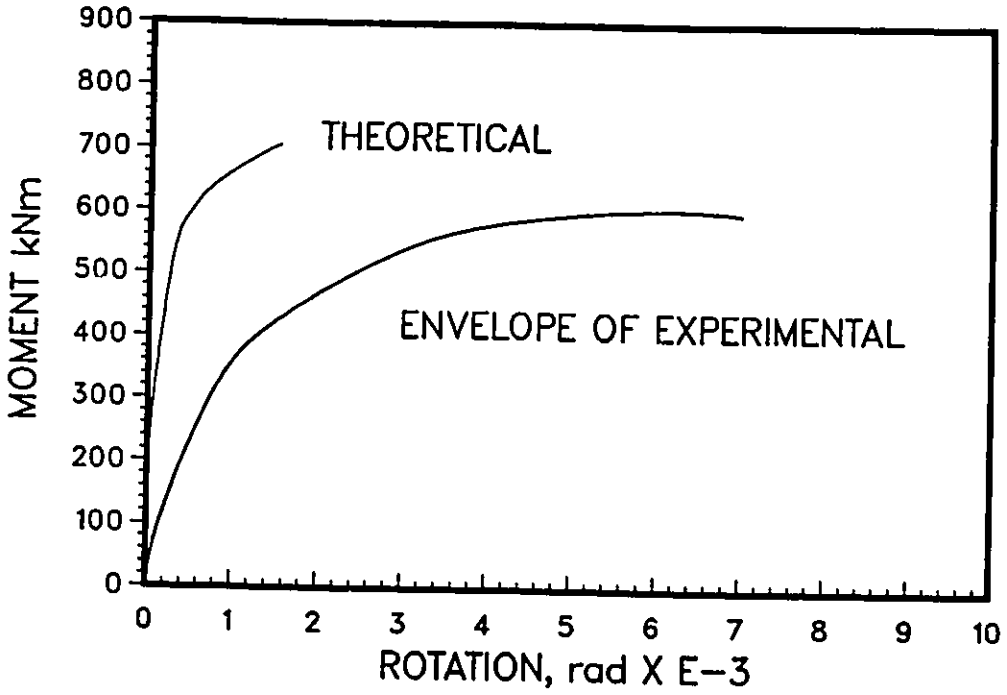

Figure 4.3: Theoretical and envelope of experimental moment – rotation relationships for Wall 3

Examination of strain gage data taken from the horizontal reinforcement indicates first yielding of these bars at $2\Delta_y$. At this load stage, inclined shear cracks in the mid – portion of the wall developed approximately 1mm crack width. The crack width reduced to 1/2 mm upon unloading. Shear crack width ranged between 2.0 to 5.0 mm at $4\Delta_y$ indicating significant yielding of reinforcement. Inspite of the increase in crack width, diagonal tension failure was prevented because of the presence of top beam. Cyclic loading reduced diagonal compression capacity of the wall and resulted in diagonal compression failure.

4.2.3 Contribution of sliding shear reinforcement

Sliding shear failure was observed in one of the walls tested earlier [22]. This wall, labelled as Wall 2 was companion to Wall 3. The main difference between the two walls was the presence of sliding shear reinforcement in

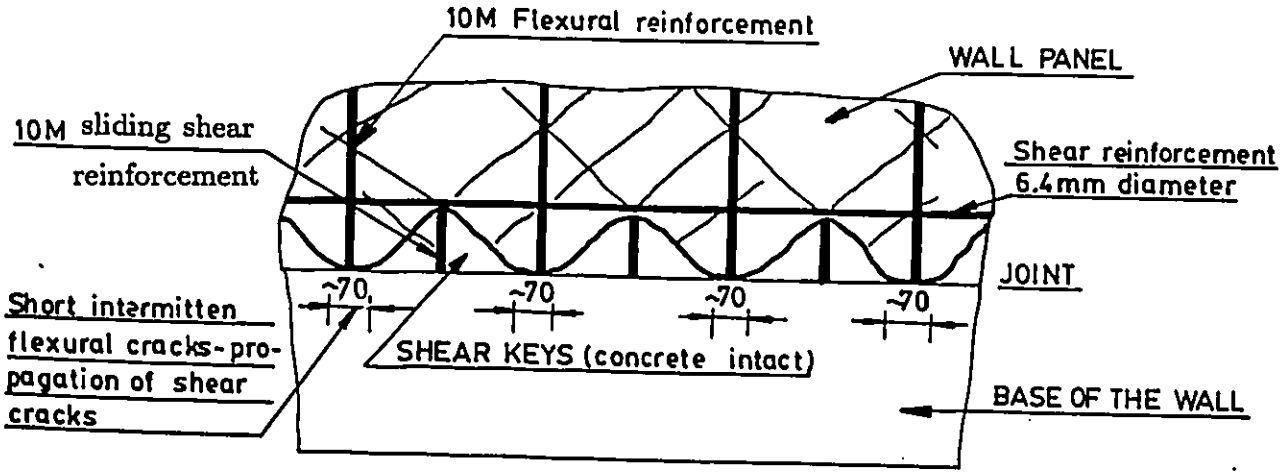

Figure 4.4: The mechanism of formation of "shear keys in Wall 3

Wall 3 at the construction joint.

The details of the sliding shear reinforcement are discussed in sec. 2.2.2. These bars extended into the wall by about 100 mm. Their short lengths would prevent them to develop their full strengths and hence would not contribute to the flexural capacity appreciably.

The strain gage data indicate that the sliding shear reinforcement developed a maximum stress of approximately 40% of the yield stress. At $1\Delta_y$ it was observed that the inclined cracks were passing over the tips of the sliding shear reinforcement, propagating towards the construction joint. The presence of sliding shear reinforcement kept the concrete around each bar intact and led to the development of a sawtooth like appearance along the construction joint. This resulted in concrete "shear keys". These keys fully developed at $2\Delta_y$. Beyond this load stage the presence of joint reinforcement had no contribution to the flexural resistance of the wall. These shear keys shown in Fig 4.4, prevented shear sliding of the wall.

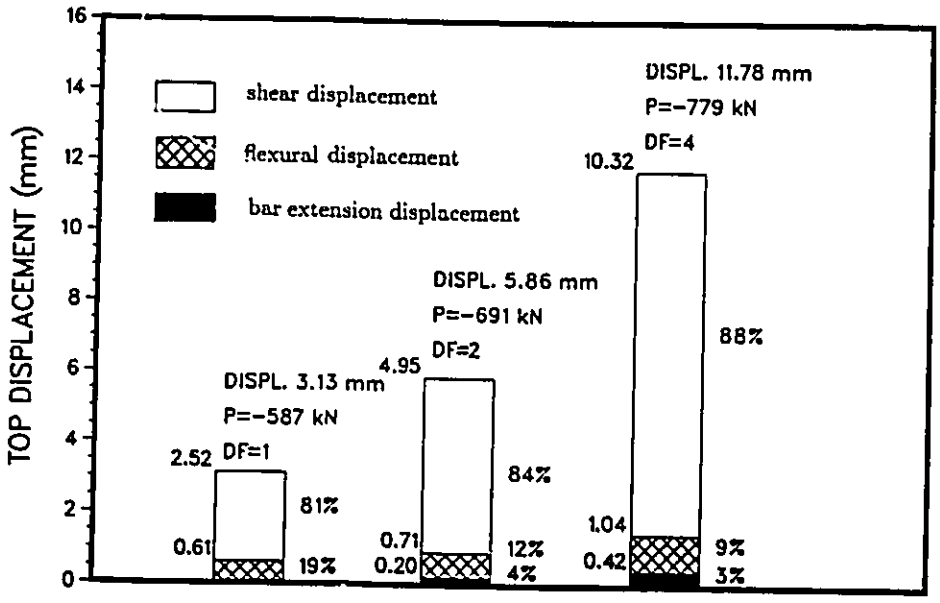

Figure 4.5: Top displacement components in Wall 3 at $1\Delta_y$, $2\Delta_y$, $4\Delta_y$

4.3 Relative Significance of Deformation Components in Wall 3

The significance of each of the four deformation components, discussed in sec.3.3, is investigated. It is concluded that the sliding shear reinforcement provided in Wall 3 prevented the sliding shear. The remaining three components, namely: due to flexure, shear and reinforcement extension have been evaluated. Figure 4.5 shows the significance of each deformation component. As evidenced in this figure 80 - 90% of total horizontal displacement is due to shear.

4.4 Summary and Discussion of Wall 3 behavior

Wall 3, with an aspect ratio of 1/4 and a flexural capacity of 706 kN·m determined on the basis of the beam theory, was subjected to inelastic load reversals. The design moment capacity correspond to a shear force of 1080 kN and associated nominal shear stress capacity of $1.13\sqrt{f'_c}$ MPa. Concrete shear capacity, based on a 45 degree truss analogy, was $0.40\sqrt{f'_c}$ MPa. Special sliding shear reinforcement , well anchored into the foundation beam and extending 100 mm into the wall was used to prevent sliding shear.

Maximum load of 907 kN, and associated shear stress of $0.97\sqrt{f'_c}$ MPa were resisted by the wall during the first cycle of $4\Delta_y$ deformation level. Top horizontal displacement was 9.73 mm, translating into a drift ratio of 2%. Progressive yielding of vertical reinforcement took place during the test. The design capacity based on the beam theory could not be developed by the wall. The wall essentially behaved in the shear mode, shear displacement forming 80 – 90% of the total horizontal displacement. Load cycles and criss crossing of inclined shear cracks led to diagonal compression failure at a deformation level of $6\Delta_y$, when the displacement was 13.08 mm, corresponding to 2.6% drift ratio. The failure load was 834 kN at a shear stress of $0.89\sqrt{f'_c}$ MPa.
Highlights of some of the observations are listed below:

- Shear sliding was prevented by the use of "sliding shear reinforcement" which led to the development of shear keys under cyclic loading.
- The wall behaved in a ductile manner up to $4\Delta_y$.
- The major component of deformation was the shear deformation,

forming in excess of 80% of the total horizontal displacement.

- Ties to prevent buckling of exterior vertical bars are essential.
- ACI [1] or CSA [10] Building Code limit of $0.80\sqrt{f'_c}$MPa, for diagonal compression failure appears to be adequate, for walls with an aspect ratio of 1/4, provided that sliding shear is prevented by special reinforcement.

4.5 Comparison of Wall 2 and Wall 3 Behaviors

The behavior of Wall 3 is compared with that of Wall 2, which was a companion specimen, and tested in an earlier program. These two specimens were designed to be similar.
The following were the major differences in the two specimens:

1. Special reinforcement against sliding shear was provided in Wall 3
2. Lateral ties were used to prevent buckling of extreme vertical bars in Wall 2

The comparison, including predicted and experimental results, is shown in Table 4.1. The comparison indicates a superior response for Wall 3 with the sliding shear reinforcement.
Table 4.1 indicates:

- Wall 3 was much more effective in resisting the applied force, developing 86% of design capacity computed using flexural beam theory, compared with 66% for Wall 2.

Objectives	WALL 2	WALL 3
Theoretical flexural capacity	661 kNm	706 kNm
Shear force associated with theoretical flexural capacity	1017 kNm	1080 kNm
Designed nominal shear stresses at ultimate	$1.36\sqrt{f'_c}$	$1.13\sqrt{f'_c}$
Positive yield displacement	2.5 mm	2.5 mm
Negative yield displacement	3.0 mm	3.1 mm
Maximum shear force sustained	675 kN	910 kN
Ductility attained at maximum load	1.0	4.0
Maximum nominal shear stresses sustained	$0.90\sqrt{f'_c}$	$0.97\sqrt{f'_c}$
Maximum nominal shear stresses sustained / designed nominal shear stresses	66%	86%
Drift ratio attained at maximum sustained load	0.5%	2.0%
Shear capacity including concrete contribution based on CSA Code [10]	376 kN	324 kN

Table 4.1: Comparison between Wall 2 and Wall 3

- Wall 3 attained displacement ductility factor of 4.0 (drift ratio of 2%) at the maximum sustained load, while Wall 2 started sliding after the first cycle at a deformation level of $1\Delta_y$ (drift ratio of 0.50%)

4.6 Mechanism of Load Resistance in Wall 6

4.6.1 Flexural Response

Flexural behavior of Wall 6 is determined by examining the strain gauge data taken from vertical reinforcement, as well as by examining the moment–rotation relationship, recorded by LVDTs.

Some of the recorded strain data for vertical reinforcement of Wall 3 are reported in sec.3.7. Progression of yielding in vertical reinforcement at the critical section is illustrated in Fig 4.6. Experimentally obtained strain profiles are shown in Fig 4.7 at different load stages. Moment – curvature relationship, obtained from this data is compared with that obtained theoretically, in the same figure. The theoretical curve is based on the beam theory and is intended for members where shear effect is negligible. The comparison indicates that a substantially softer response was obtained in the test than that indicated by the beam theory. This is attributed to the flexure – shear interaction which is very significant in a squat member, such as Wall 6. Comparison of moment – curvature relationships of Wall 3 and Wall 6 indicates that the flexural response of Wall 6 was better predicted than that of Wall 3. This may be attributed to increased shear span of Wall 6.

The moment – rotation relationship, obtained from the LVDT data is shown

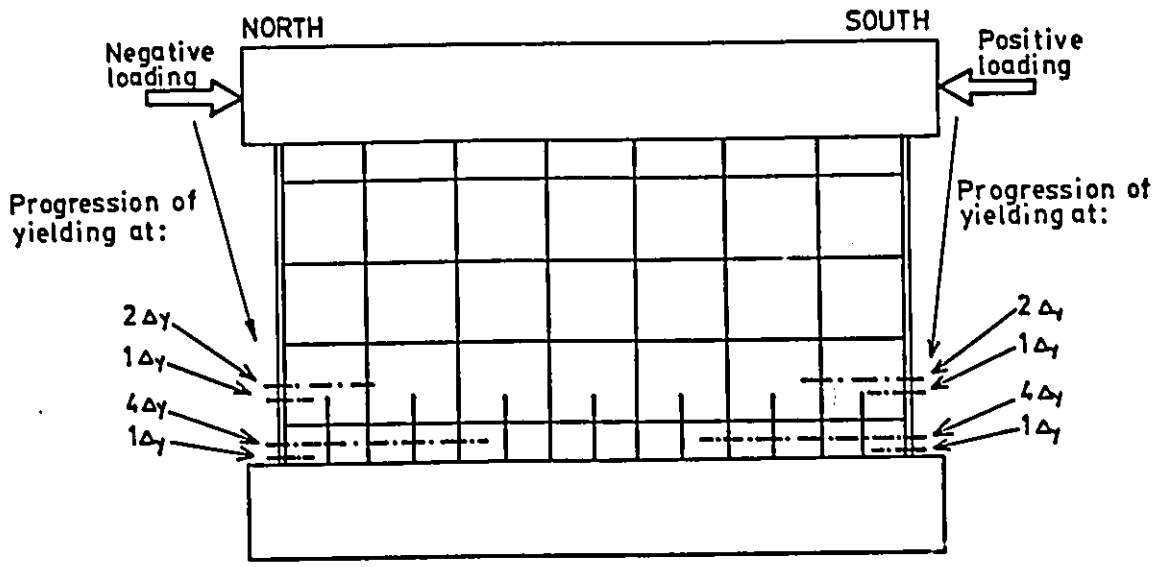

Figure 4.6: Progressive yielding of flexural reinforcement in Wall 6

in Fig 3.46. This relationship excludes the rigid body rotation of the wall caused by extension of vertical reinforcement in the base and hence gives the flexural response. The envelope of the experimental hysteresis curves is compared with that obtained by integration of theoretical moment – curvature relationships, in Fig 4.8. The comparison indicates softer response in flexure than that predicted theoretically. Furthermore, the wall strength observed experimentally is less than that predicted theoretically. The difference between the experimental and theoretical moment – rotation relationship is attributed largely to shear – flexure interaction which is not accounted for in the theoretical prediction. Furthermore, the theoretical prediction is base on the assumption that the wall is fully fixed at the base along the entire length. The experimental set – up, on the other hand, was such that the wall was fixed only at the ends. Furthermore additional softening in the wall was caused during the experiment by the vertical component of lateral load as discussed in sec 3.3.4.

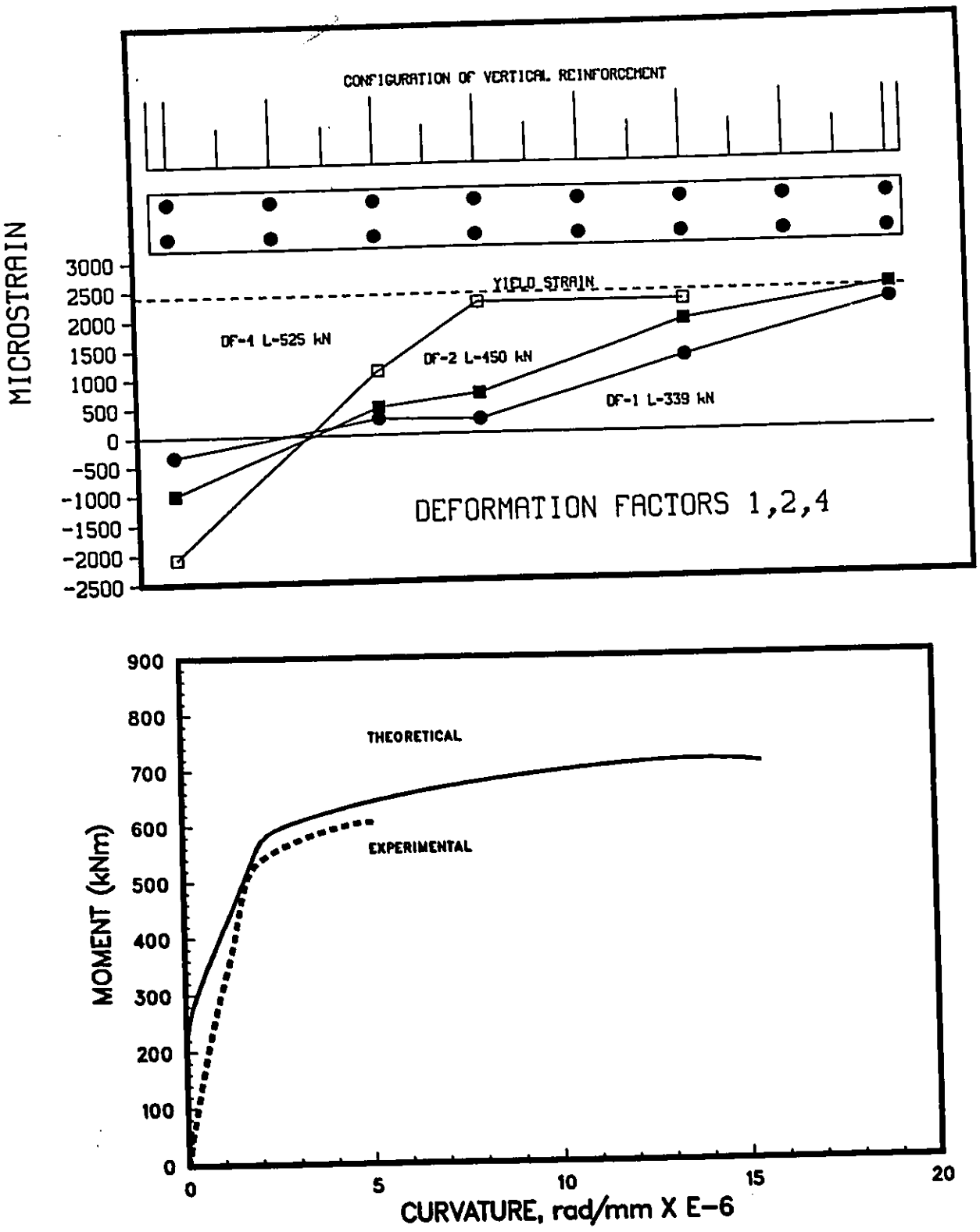

Figure 4.7: Strain profiles in flexural reinforcement and experimental and theoretical moment curvature relationship in Wall 6

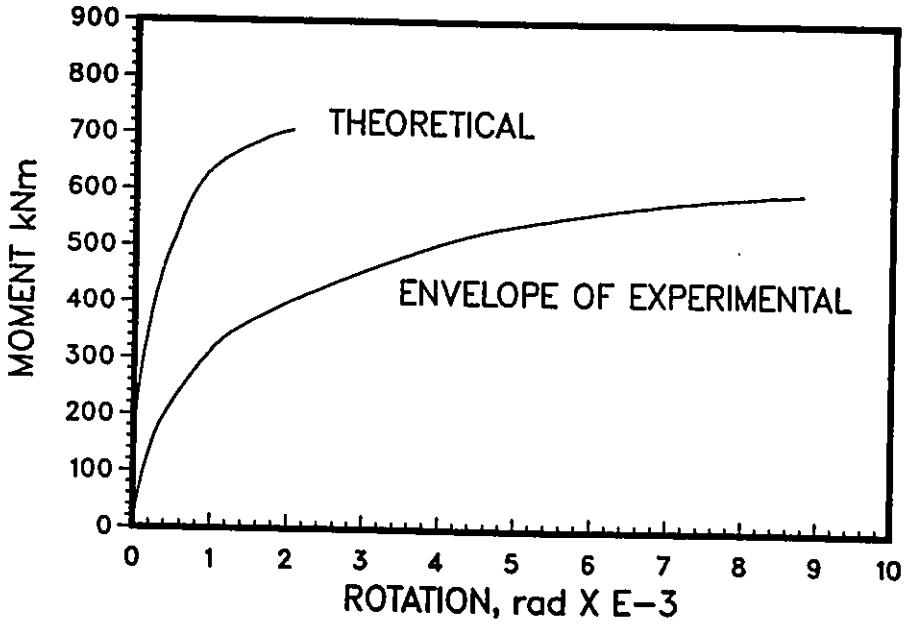

Figure 4.8: Theoretical and experimental envelopes of moment – rotation relationships for Wall 6

4.6.2 Shear Response

Wall 6 with an aspect ratio 1/2 was critical in shear. Shear deformations were calculated from LVDT readings as discussed in sec.3.6.2 and Appendix C. Shear force – shear displacement hysteretic relationship is shown in Fig 3.41. Examination of this relationship indicates a significant degradation of shear stiffness under cyclic loading. Pinching of force – displacement hysteresis loops is evident, indicating sliding of cracked surfaces under shear.

Examination of strain gage data taken from horizontal reinforcement and crack patterns indicates that the horizontal reinforcement did not yield during the test. The maximum shear crack widths up to cycles of $2\Delta_y$ was approximately 0.30 mm. At load stage $4\Delta_y$ the crack widths ranged between 1.5 to 4.0 mm. These wide open cracks did not cross horizontal reinforcement, having tendency to open wider between locations of horizontal bars. There was an evident yielding of vertical bars at the location

where the wide open shear cracks were passing through vertical reinforcement. This led to the conclusion that at load stage $4\Delta_y$, the load was being transmitted to the base by diagonal struts, and the wall was rotating about the flexural compression zone. Cyclic loading reduced diagonal compression capacity of the wall and resulted in diagonal compression failure.

4.6.3 Contribution of sliding shear reinforcement

Sliding shear failure was observed in one of the walls tested earlier [21]. This wall, labelled as Wall 4 was companion to Wall 6. The only difference between the two walls was the presence of sliding shear reinforcement in Wall 6 at the construction joint.

The details of the sliding shear reinforcement are discussed in sec. 2.2.3. These bars extended into the wall by about 200 mm. Their short lengths would prevent them to develop their full strengths and hence would not contribute to the flexural capacity appreciably.

The strain gage data indicate that the sliding shear reinforcement developed a maximum stress of approximately 70% of the yield stress. At $1\Delta_y$ it was observed that the inclined cracks were passing over the tips of the sliding shear reinforcement extending to approximately 100 mm from the construction joint. The presence of joint bars kept the concrete around each bar intact and led to the development of a sawtooth like appearance along the construction joint. This resulted in concrete "shear keys". These keys fully developed at $2\Delta_y$. Beyond this load stage the presence of sliding shear reinforcement had no contribution to the flexural capacity resistance of the wall. These shear keys shown in Fig 4.9, prevented shear sliding of the wall.

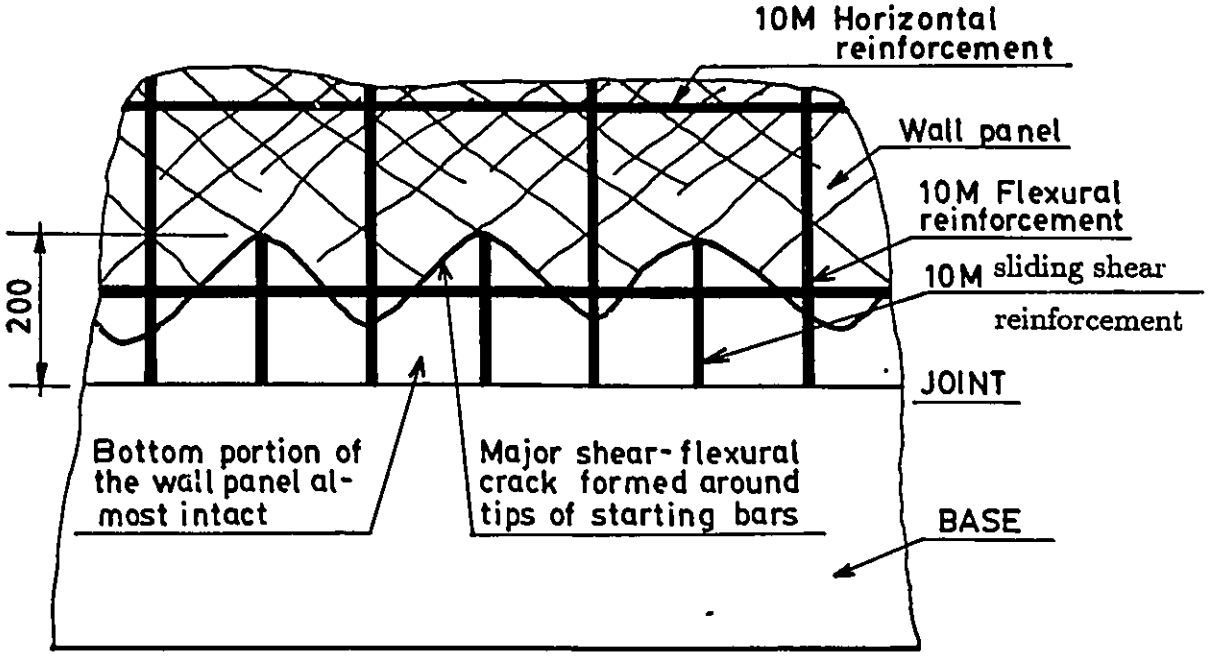

Figure 4.9: The mechanism of formation of "shear keys in Wall 6

4.7 Relative Significance of Deformation Components in Wall 6

The significance of each of the four deformation components, discussed in sec.3.6, is investigated. It is concluded that the sliding shear reinforcement provided in Wall 6 prevented the sliding shear. The remaining three components, namely: due to flexure, shear and reinforcement extension have been evaluated. Figure 4.10 shows the significance of each deformation component. As evidenced in this figure over 80% of total horizontal displacement is due to shear.

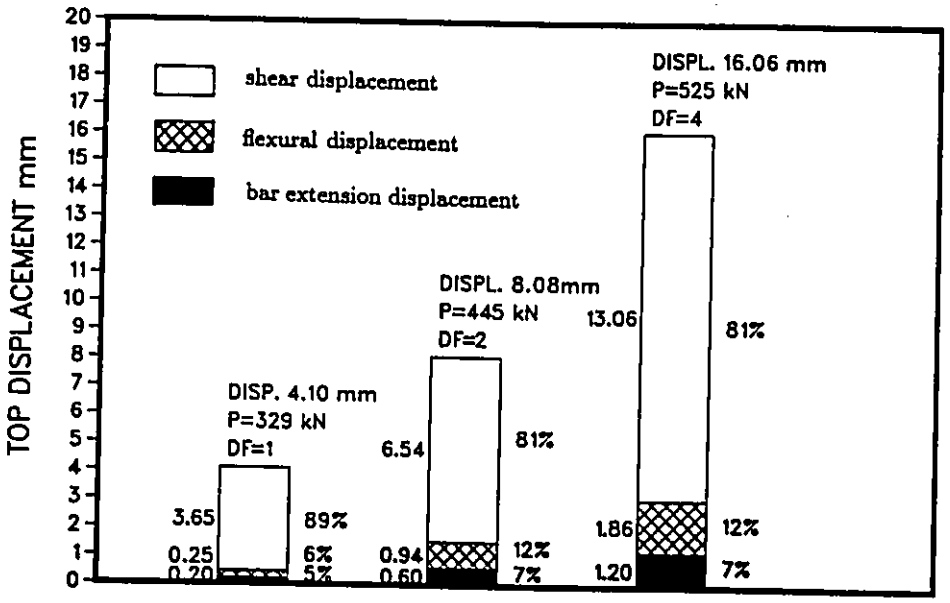

Figure 4.10: Top displacement components in Wall 6 at $1\Delta_y$, $2\Delta_y$, $4\Delta_y$

4.8 Summary and Discussion of Wall 6 behavior

Wall 6, with an aspect ratio of 1/2 and a flexural capacity of 706 kN·m, determined on the basis of the beam theory, was subjected to inelastic load reversals. The design moment capacity correspond to a shear force of 612 kN and associated nominal shear stress capacity of $0.65\sqrt{f'_c}$ MPa. Concrete shear capacity, based on a 45 degree truss analogy, was $0.85\sqrt{f'_c}$ MPa. Special reinforcement, well anchored into the foundation beam and extending 200 mm into the wall was used to prevent sliding shear.

Maximum load of 529 kN, and associated shear stress of $0.56\sqrt{f'_c}$ MPa were resisted by the wall during the first cycle of $4\Delta_y$ deformation level. Top horizontal displacement was 16.1 mm, translating into a drift ratio of 1.6%. Progressive yielding of vertical reinforcement took place during the test. The design capacity based on the beam theory could not be

developed by the wall. The wall essentially behaved in the shear mode, shear displacement forming 80% of the total horizontal displacement. Load cycles and criss crossing of inclined shear cracks led to diagonal compression failure at a deformation level of $5\Delta_y$, when the displacement was 19.67 mm, corresponding to 2.0% drift ratio. The failure load was 438 kN at a shear stress of $0.47\sqrt{f_c'}$ MPa.
Highlights of some of the observations are listed below:

- Shear sliding was prevented by the use of sliding shear reinforcement which led to the development of shear keys under cyclic loading.
- The wall behaved in a ductile manner up to $4\Delta_y$.
- The major component of deformation was the shear deformation, forming in excess of 80% of the total horizontal displacement.
- Ties to prevent buckling of exterior vertical bars are essential.
- ACI [1] or CSA [10] Building Code limit of $0.80\sqrt{f_c'}$ MPa, for diagonal compression failure appears to be inadequate for walls with aspect ratio 1/2 when the wall is subjected to inelastic load reversals, and the sliding shear is prevented.

4.9 Comparison of Wall 6 and Walls 1, 4, and 5 Behaviors

The behavior of Wall 6 is compared with those of Walls 1, 4, and 5 which were companion specimens, and tested in earlier programs.
The following were the differences in the four specimens when compared with Wall 6:

1. In Walls 1, 4, 5 special reinforcement to prevent shear sliding was not provided.

2. Wall 1 had a minimum horizontal reinforcement ratio of 0.0025.

3. Wall 5 was designed for approximately 40% higher flexural capacity and associated shear force.

The comparison, including predicted and experimental results, is shown in Table 4.2. Reinforcement layouts for all four walls is shown in Fig. 4.11 The comparison indicates a superior response for Wall 6 with the sliding shear reinforcement.
Table 4.2 indicates:

- Wall 3 was much more effective in resisting the applied force, developing 86% of design capacity computed using flexural beam theory, compared with 70% for Wall 4 and 69% for Wall 5.

- Wall 6 attained displacement ductility factor of 4.0 (drift ratio of 1.6%) at the maximum sustained load, while Wall 4 and Wall 5 started sliding after the first cycle at a deformation level of $2\Delta_y$ (drift ratios of 0.80% and 1.10% respectively).

- Wall 1 with minimum horizontal reinforcement developed full flexural capacity and failed in diagonal tension.

- Wall 1 attained drift ratio of 0.8% at maximum sustained load which was two times smaller than that of Wall 6.

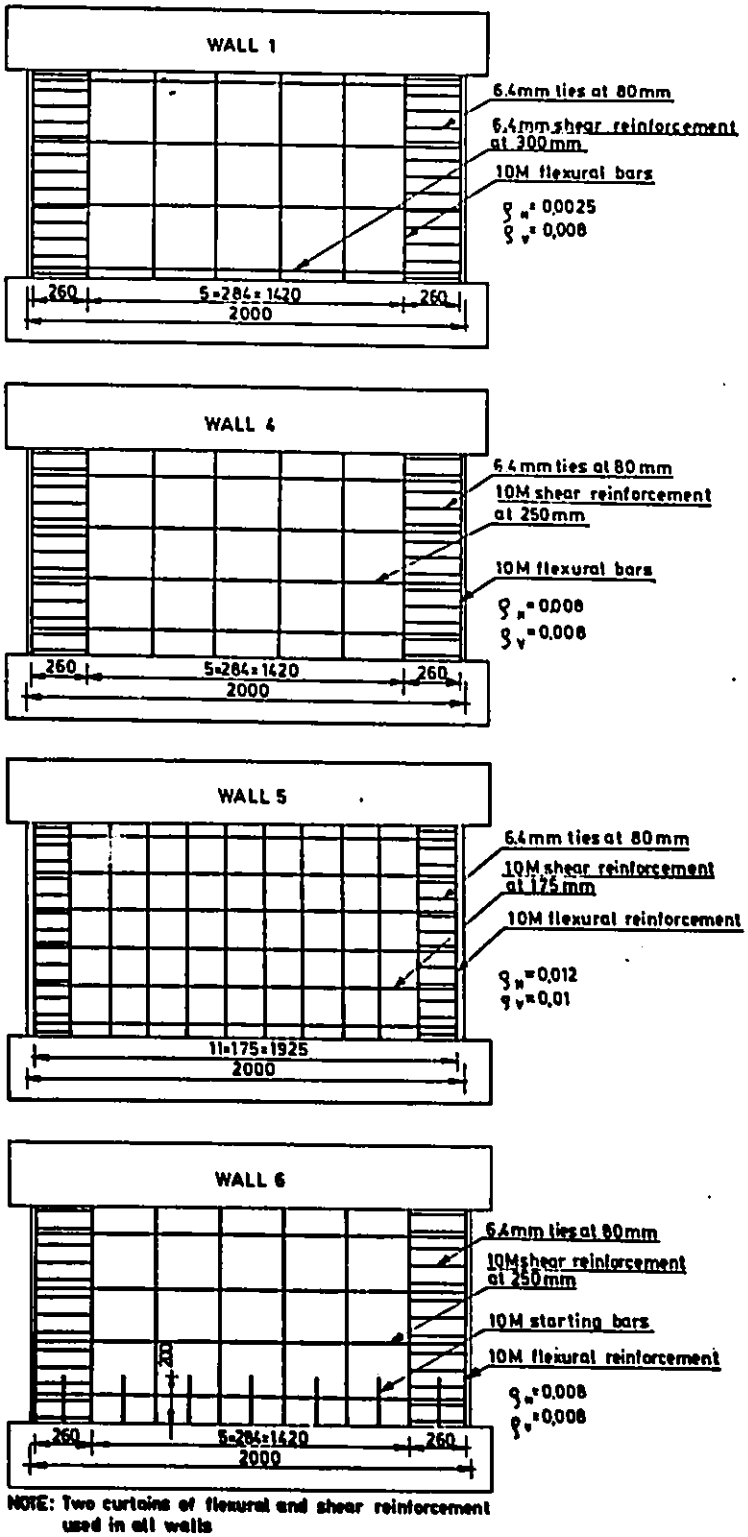

Figure 4.11: Reinforcement layout in Walls 1, 4, 5, and 6

Objectives	WALL 1	WALL 4	WALL 5	WALL 6
Theoretical flexural capacity	660 kNm	698 kNm	955 kNm	706 kNm
Shear force associated with theoretical flexural capacity	575 kNm	612 kNm	838 kNm	612 kNm
Designed nominal shear stresses at ultimate [MPa]	$0.72\sqrt{f'_c}$	$0.66\sqrt{f'_c}$	$1.01\sqrt{f'_c}$	$0.65\sqrt{f'_c}$
Yield displacement	2.50 mm	4.00 mm	10.0 mm	4.0 mm
Maximum shear force sustained	575 kN	419 kN	586 kN	529 kN
Ductility attained at maximum load	$+4\Delta_y$	$-2\Delta_y$	$+2\Delta_y$	$+4\Delta_y$
Maximum nominal shear stresses sustained	$0.72\sqrt{f'_c}$	$0.46\sqrt{f'_c}$	$0.70\sqrt{f'_c}$	$0.56\sqrt{f'_c}$
Maximum nominal shear stresses sustained / designed nominal shear stresses	100 %	70 %	69 %	86 %
Drift ratio attained at maximum sustained load	0.8 %	0.8 %	1.1 %	1.6 %
Shear capacity including concrete contribution based on CSA Code [10]	305 kNm	798 kNm	1044 kNm	800 kNm

Table 4.2: Comparison between Walls 1, 4, 5 and 6

Chapter 5

Design recommendations to prevent sliding shear

5.1 Previous recommendations

Only a limited number of research projects have been undertaken in the past that produced design recommendations. Synge [20] in 1980 recommended use of specially detailed diagonal reinforcement to suppress shear sliding. Figure 5.1 shows the solution recommended by Synge which involves the use of inclined reinforcement. This type of reinforcement configuration involves a few shortcomings:

- Diagonal reinforcement in specimens tested by Synge did not completely eliminate shear sliding, but only reduced its magnitude.
- Diagonal bars have to be included in calculation of flexural resistance of the wall, which makes design procedure more complicated.

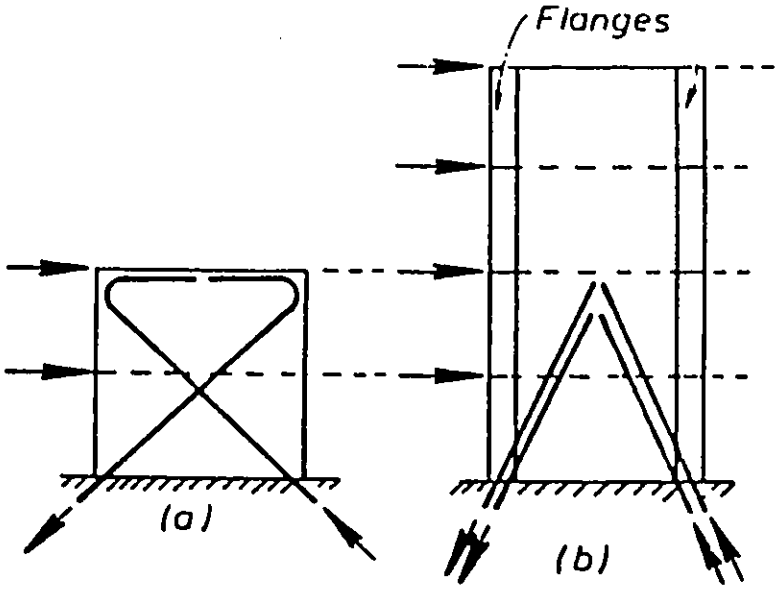

Figure 5.1: Solution proposed by Synge to suppress sliding shear

- Higher cost of workmanship to place diagonal reinforcement than orthogonal reinforcement.

Trounce and Pristley recommended the use of steel angles crossing the base crack, to prevent shear sliding in masonry squat walls. It seems that there are no obstacles to adopt this type of solution to reinforced concrete shear walls, and it can be effective in eliminating shear sliding. However, this recommendation has not been verified experimentally. It may not be suitable for reinforced concrete construction from practical point of view.

5.2 Design recommendations

Based on previous researchers studies and results obtained from this investigation, design recommendations are made for design of squat shear walls. These recommendations reflect the current design practice with the exception of those that are intended to prevent shear sliding. The current

building codes [1,10] do not address the issue of shear sliding for earthquake resistant shear walls.

The following are the recommendations:

1. The minimum thickness of squat walls assigned as a primary load resisting component should be at least 200 mm.

2. Vertical reinforcement should be distributed uniformly throughout the section, and the vertical reinforcement ratio should be at least 0.0025.

3. The spacing of flexural reinforcement shall be not more than 300 mm, or 30 times the diameter of bars, whichever is less.

4. All uniformly distributed flexural reinforcement should be included in the calculation of flexural capacity.

5. Conventional beam theory shall be employed to calculate flexural capacity of the wall.

6. Two rows of vertical reinforcement at the extreme ends of a wall should be supported by lateral ties to prevent buckling. These ties should extend throughout the entire height of the wall. Spacing between the ties shall not exceed the smaller of:

   - wall thickness
   - 16 times the tie diameter

7. Double layers of flexural reinforcement shall be placed at least in two rows on either side of the wall.

8. Clear concrete cover for vertical reinforcement shall not be less than:

   - 3 times the flexural bar diameter

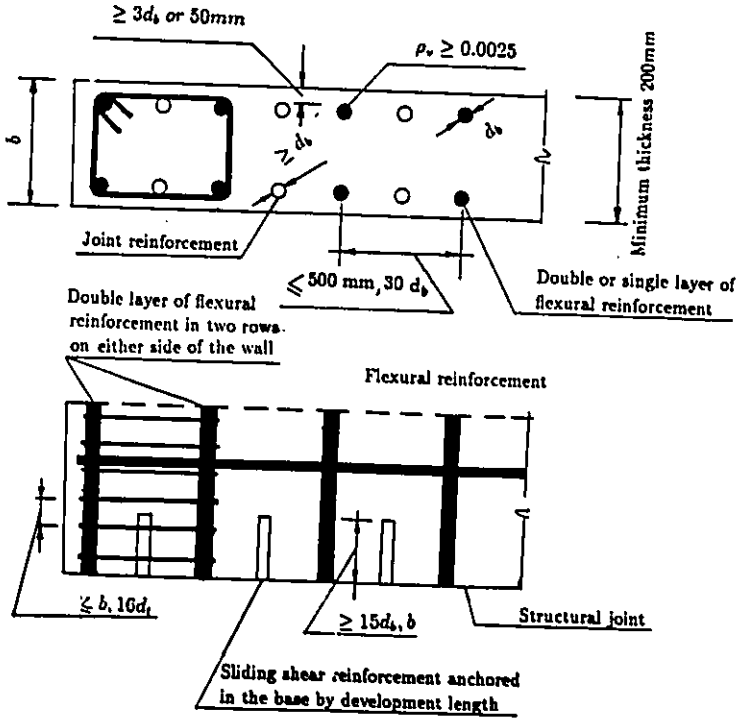

Figure 5.2: Design recommendations

- 50 mm

9. To suppress sliding shear special sliding shear reinforcement will be placed in between each adjacent rows of flexural reinforcement at the construction joint. These bars should be anchored into the base by extending them at least the development length. The extension into the wall shall be equal to the larger of:

   - 15 times the bar diameter
   - wall thickness

10. Bar size for sliding shear reinforcement should not be smaller than that provided for vertical bars.

11. Concrete cover provided for sliding shear reinforcement should not be smaller than that provided for flexural bars.

Figure 5.2 summarizes all the design recommendations for squat shear walls subjected to lateral load reversal.

Chapter 6

Conclusions

Two squat shear walls with aspect ratios of 1/2 and 1/4, were subjected to reversed loading. Both walls contained specially detailed reinforcement at the base to suppress shear sliding. The wall with an aspect ratio of 1/4 contained minimum horizontal reinforcement, while the wall with an aspect ratio of 1/2 was designed for shear force associated with ultimate flexural capacity. Based on the results of this investigation the following conclusions can be made:

1. Sliding shear failure can be eliminated by the use of specially detailed vertical reinforcement at the construction joint. This reinforcement, details of which were developed in this investigation, should consist of vertical bars properly anchored into the foundation, extending into the wall at least 15 bar diameter or the wall thickness, whichever is greater.

2. Sliding shear failure of low – rise walls, occurs under cyclic loading at a shear force approximately equal to 70% of that corresponding to flexural capacity.

3. The use of the recommended sliding shear reinforcement at the construction joint improves load resisting mechanism of squat walls, increasing the lateral load capacity while suppressing shear sliding. Both specimens, with aspect ratios of 1/4 and 1/2 were able to develop approximately 85% of their flexural capacities when reinforced with sliding shear reinforcement.

4. Displacement ductility of squat walls improves by a factor of 2.0 to 4.0 when reinforced with the sliding shear reinforcement.

5. Diagonal tension failure in walls with an aspect ratio of less than 1.0 is prevented by the presence of top beam or floor. Walls with high aspect ratio, while still having an aspect ratio of less than 1.0, may develop a second tension failure plane between opposite corners. In these walls, adequate reinforcement should be placed to maintain the integrity of the wall under inelastic deformation cycles.

6. Walls with low aspect ratios, having aspect ratios lower than 1/2, can not develop corner – to – corner failure plane, and hence need not be reinforced with more than the minimum reinforcement ratio of 0.0025 in the horizontal direction.

7. Walls in which diagonal tension and sliding shear failures are prevented, failure occurs by crushing of diagonal compression struts. Diagonal compression failure, in walls with an aspect ratio of 1/2 and less, takes place at a shear force level approximately equal to 85% of that corresponding to flexural failure.

8. Low rise shear walls subjected to inelastic deformations behave essentially in the shear mode. The specimens tested in this investigation showed that when shear sliding is prevented, approximately 85% of total deformation was due to shear, while the remaining was made

up of deformations due to flexure and reinforcement extension in the foundation.

Bibliography

[1] American Concrete Institute, *Building Code Requirements For Reinforced Concrete ACI 318-83*, Detroit, 1983, pp 111.

[2] American Concrete Institute, *Commentary on Building Code Requirements For Reinforced Concrete ACI 318-83*, Detroit, 1983, pp 151.

[3] Arnold C. , *Configuration And Seismic Design: A General Review*, Proceedings of the 2^{n}d U. S. National Conference on Earthquake Engineering, August 22-24, 1979, Stanford, California, pp 22-36.

[4] Associate Committe on the National Building Code, *National Building Code of Canada 1985*, National Research Council of Canada, 1985, Part 4, pp 151-180.

[5] Associate Committe on the National Building Code, *Supplement to the National Building Code of Canada 1985*, National Research Council of Canada, 1985, Chapter 4, Commentary J, pp 221-241.

[6] Barda Felix, Hanson John M. , and Corley W. Gene. , *Shear Strength Of Low-Rise Walls With Boundary Elements*, Reinforced Concrete Structures In Seismic Zones, Publication SP-53, American Concrete Institute, Detroit, 1977, pp 149-202.

[7] Bertero V. V. , *An Overwiew Of The State-Of-The-Art In Earthquake-Resistant Reinforced Concrete Building Construction*, Proceedings of

the 2^nd U. S. National Conference on Earthquake Engineering, August 22-24, 1979, Stanford, California, pp 838-852.

[8] Bertero V. V. , *Seismic Behavior Of R/C Wall Structural Systems*, Proceedings of the 7^th World Conference on Earthquake Engineering, September 8-13, 1980, Istanbul, Turkey, Part III, pp 323-330.

[9] Bertero V. V. , *State Of The Art In The Seismic Resistant Construction Of Structures*, Third International Earthquake Microzonation Conference Proceedings, Vol. 2, June 28-July 1, 1982, Seattle, U. S. A. ,pp 767-799.

[10] Canadian Standard Association, *Design Of Concrete Structures For Buildings CAN3-A23.3-M84*, Rexdale, 1984, 281 pp.

[11] Cardenas A. E. , Hanson j. M. , Corley W. G. , and Hognestead E., *Design Provisions For Shear Walls*, ACI Journal, Proceedings, Vol. 70, March 1973, pp 221-230.

[12] Cardenas A. E. , Russell H. G. and Corley W. G. , *Strength Of Low-Rise Structural Walls*, Reinforced Concrete Structures Subjected To Wind And Earthquake Forces, Publication SP-63, American Concrete Institute, Detroit, 1980, pp 221-241.

[13] Fiorato A. E. , Oesterle R. G. and Carpenter J. E. , *Reversing Load Tests Of Five Isolated Structural Walls*, Proceedings of the International Symposium on Earthquake Structural Engineering,St-Louis, Missouri, U. S. A. ,Vol. 1, August 1976, pp 437-453.

[14] Oesterle R. G. , Fiorato A. E. , Aristizabal-Ochoa J. D. and Corley W. G. , *Hysteretic Response Of Reinforced Concrete Structural Walls*, Reinforced Concrete Structures Subjected To Wind And Earthquake Forces, Publication SP-63, American Concrete Institute, Detroit, 1980, pp 243-273.

[15] Park R. and Paulay T. , *Reinforced Concrete Structures*, John Wily and Sons Inc. , New York, 1975.

[16] Pauley T. , *The Design Of Reinforced Concrete Ductile Shear Walls For Earthquake Resistance*, Research Report 81-1, Department of Civil Engineering, University of Canterbury, New Zealand, February 1981.

[17] Paulay T. , *Earthquake-Resisting Shearwalls — New Zealand Design Trends*, ACI Journal, Proceedings, Vol. 77, No. 3, May-June 1980.

[18] Paulay T. , *Design Aspects Of Shear Walls For Seismic Areas*, Canadian Journal of Civil Engineering, Vol. 2, No. 3, September 1975.

[19] Paulay T. and Uzumeri S. M. , *A Critical Review Of The Seismic Design Provisions For Ductile Shear Walls Of The Canadian Code And Commentary*, Canadian Journal of Civil Engineering, Vol. 2, 1975, pp 592-601.

[20] Synge A. J. , *Ductility Of Squat Shear Walls*, Research report 80-8, Department of Civil Engineering, University of Canterbury, New Zealand, February 1980.

[21] Pilette C. , *Behavior of earthquake resistant squat shear walls*, M. A. Sc. Thesis, Department of Civil Engineering, University of Ottawa, 1987.

[22] Wiradinata S. , *Behavior Of Squat Walls Subjected To Load Reversals*, M. A. Sc. Thesis, Department of Civil Engineering, University of Toronto, January 1985.

[23] Wiradianata S. and Saatcioglu M. , *Tests Of Squat Shear Wall Under Lateral Load Reversal*, Proceedings of the Third U. S. National Conference on Earthquake Engineering, August 24-28, 1986, Charleston, South Carolina, pp 1395-1406.

[24] Alexander C. ,Heidebrecht A. C. and Tso K. , *Cyclic loading on shear wall panels*, Proceedings of The Fifth World Conference on Earthquake Engineering, Rome 1973, Italy, pp 1116 - 1119

[25] Fintel et. al. , *Handbook of concrete engineering*, Second Edition, Van Nostrand Reinhold Company, N. Y. ,pp 460 -462, 485 - 487

[26] Bertero V. V. and Popov E. P. , *Seismic behavior of ductile moment resisting reinforced concrete frames*, American Concrete Institute, Publication SP - 53 "Reinforced Concrete Structures in Seismic Zones"

[27] DZ 3101: Part 1 and Part 2, *Second Draft New Zealand Standard Code of Practice for the Design of Concrete Structures* Standards Association of New Zealand, 1980

[28] Trounce, M. J. *Seismic behavior of reinforced concrete masonry shear walls*, M. E. Report, University of Canterbury. Civil Eng. Dept. , Research Report No. 78 – 19, February 1978

Appendix A

Design of Wall 3

A.1 Flexural capacity of Wall 3

Wall 3 was designed in accordance with CAN3 - A23.3 - M84 [10]. Accordingly, all uniformly distributed reinforcement was taken into account in determining the resistance of the wall. Since the ratio of horizontal reinforcement was one of the variables in this investigation, shear design of Wall 3 does not comply with the code requirements. However, calculation of shear capacity was based on the equation provided in the code [10].

A.2 Theoretical moment – curvature relationship

Primary moment curvature relationship for Wall 3 was analytically established using the conventional beam theory. Values of curvature were obtained assuming yielding of subsequent rows of flexural reinforcement, un-

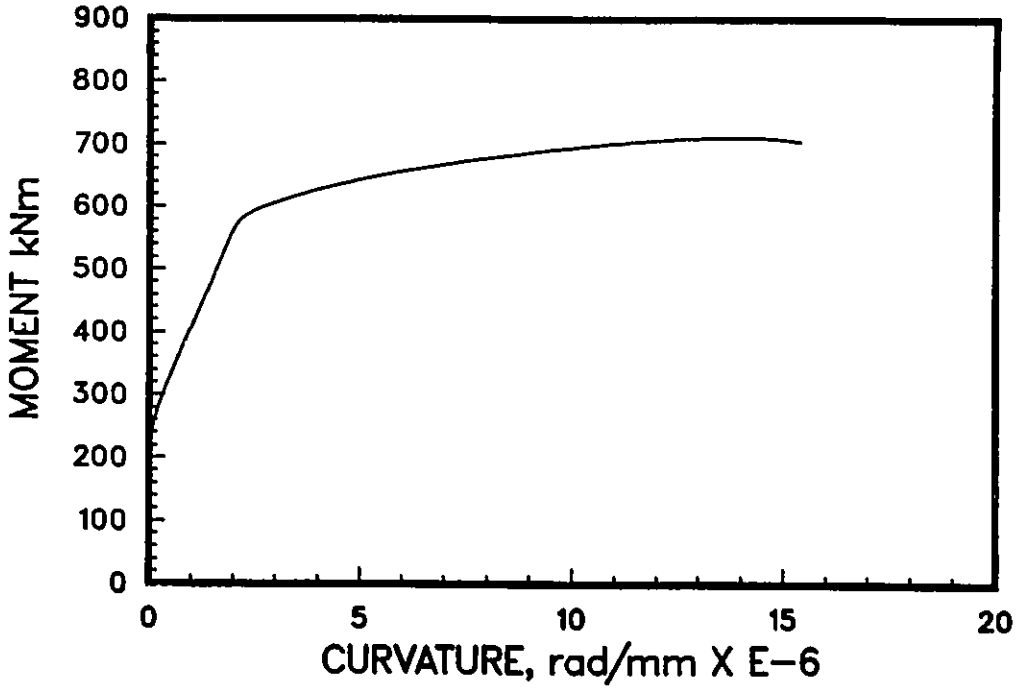

Figure A.1: Theoretical moment curvature relationship for Wall 3 and Wall 6.

der monolitically increasing load. Ultimate concrete strain was assumed to be 0.003, strain hardening of steel and tensile strength of concrete were neglected. Figure A.1 shows the theoretical moment curvature relationship for Wall 3. The values obtained from the sectional analysis are presented in Table A.1. Following material properties were used in the calculation:

$f'_c = 34.5\ MPa$

$f_y = 480\ MPa$

$\varepsilon_y = 0.24\%$

$E = 200000\ MPa$

$E_c = 5000\sqrt{f'_c} = 29580$ MPa

$\varepsilon_o = 0.00178$

Eight pairs of 10M deformed bars were used as the flexural reinforcement. Total area of flexural reinforcement was:

$$A_{sv} = 16 \times 100 = 1600\ mm^2$$

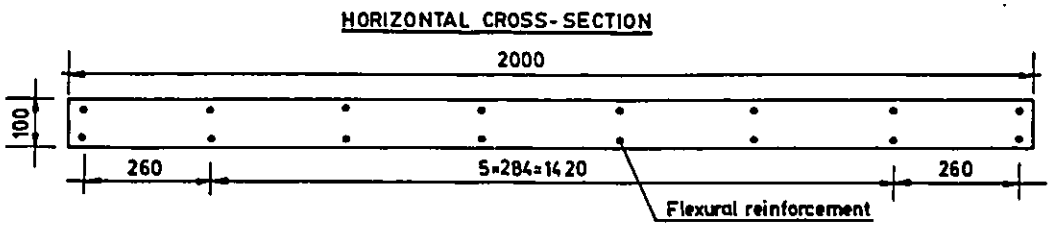

Figure A.2: Cross section of Wall 3 and Wall 6

c [mm]	ϕ [$\frac{rad}{mm}$ $\times$ 10^{-3}]	M [$kN \cdot m$]	F [kN] Wall 3	Notes
1000	0.12	260.0	398.0	Moment cracking
350	1.45	477.0	729.0	# 1 yields
350	1.69	517.0	791.0	# 1,2 yield
335	2.11	575.0	870.0	# 1,2,3 yield
280	4.0	627.0	959.0	#1, 2, 3, 4, 5 yield
194	15.4	706.0	1080.0	Ultimate

Table A.1: Calculation of theoretical curvature of Wall 3

Provided ratio of uniformly distributed flexural reinforcement:

$$\rho_{sv} = \frac{1600}{2000 \times 100} = 0.8\%$$

Cross–section of the wall with uniformly distributed flexural reinforcement is shown in Figure A.2.

In Table A.1:

c – depth of compression zone

ϕ – curvature

M – applied moment

F – applied force

Resultant compression force in concrete and its location was established using Hognestad's equations:

$$C_c = b\, f'_c\, c^2\, \frac{\phi}{\epsilon_o}\left(1 - \frac{\phi\, c}{3\, \epsilon_o}\right)$$

$$\bar{x} = c\left[\frac{8\, \epsilon_o - 3\, \phi\, c}{12\epsilon_o - 4\, \phi\, c}\right]$$

where $\bar{x}$ is the distance of resultant compression force in concrete from extreme compression fibre.

A.3 Theoretical moment rotation relationship

Moment rotationship relationship was determined by integrating curvature along the height of the specimen:

$$\theta = \int_0^{h_w} \phi dx$$

where; θ – rotation of the top of the wall

ϕ – curvature along the height of the wall

h_w – wall height

Variation of curvature along the height of the wall was determined from theoretical moment curvature relationship for selected magnitude of base moment. Analytically, the value of rotation was calculated as the area under curvature along the height of the wall. Theoretical moment rotation relationship for Wall 3 is presented in Figure A.3

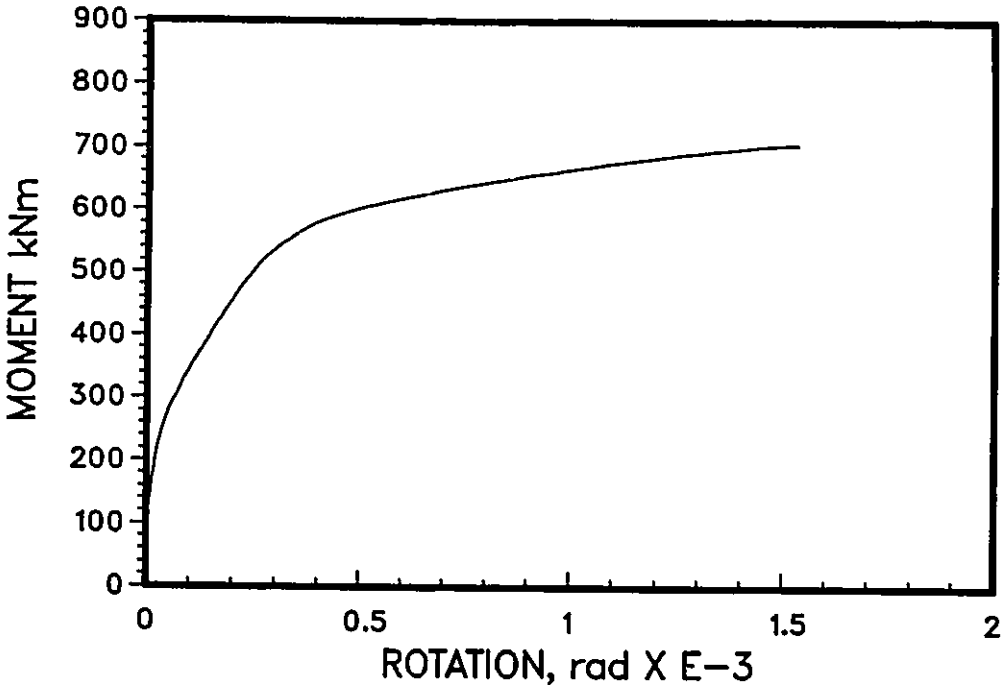

Figure A.3: Theoretical moment rotation relationship for Wall 3.

A.4 Theoretical force – flexural deformation relationship

Theoretical flexural displacement was calculated from equation:

$$\delta = \int_o^{h_w} x \, \phi \, dx$$

Figure A.4 shows consecutive stages in calculation of theoretical flexural deformation.

Figure A.4:

a) cantilever action of the wall

b) bending moment diagram

c) bending moment diagram for a given base moment

d) distribution of curvature along the height of the wall

The following figures are presented:

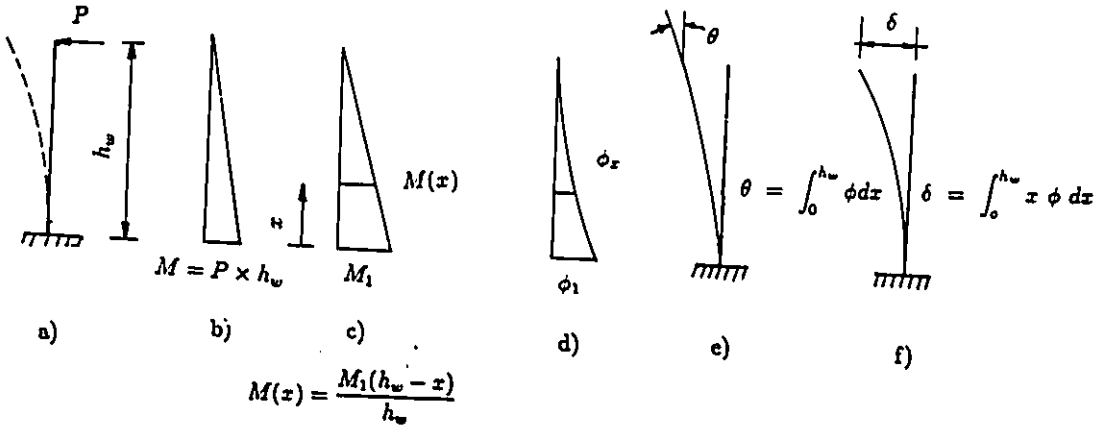

Figure A.4: Calculation of flexural deformation in the specimen

found from theoretical moment curvature relattionship
for a moment M(x)
e) rotation of the wall
f) flexural deformation of the top of the wall

Figure A.5 shows the relationship between applied load and theoretical flexural displacement.

A.5 Shear capacity of Wall 3

The shear capacity of Wall 3 was calculated based on the equation provided in CSA A23.3 - M84 [10]. The characteristcs of shear reinforcement used are described in section 2.5.7. The horizontal steel contribution to shear

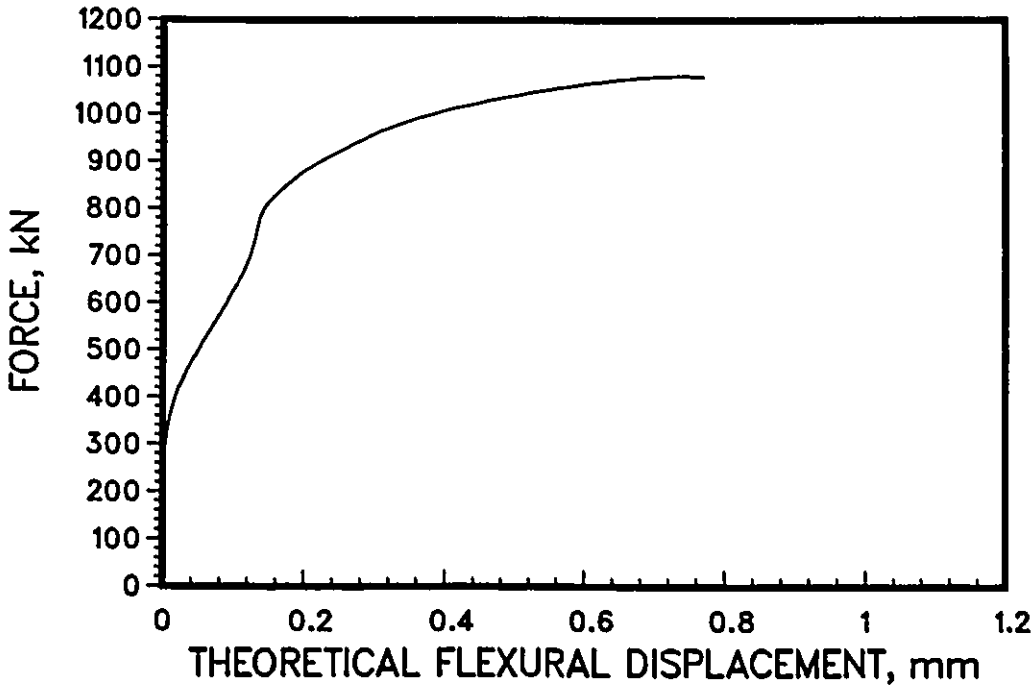

Figure A.5: Force vs. theoretical flexural deformation in Wall 3

capacity accordingly to p. 21.7.3.1. [10] was calculated from equation:

$$V_s = \frac{A_v\, f_y\, d}{s}$$

The steel contribution to shear capacity was the same as that provided in Wall 2. Three pairs of 6.4 mm diameter reinforcing bars, placed at a spacing of 150 mm, were used as shear reinforcement. Effective depth of the section was assumed as $0.8l_w$.

Hence;

$$V_s = \frac{A_v\, f_y\, d}{s} = \frac{2 \times 32.17 \times 248.0 \times 0.8 \times 2000}{150.0} = 170kN$$

The reinforcement ratio was factored to give the same shear capacity as that with $f_y = 400\ MPa$.

$$\rho_{sh} = \frac{A_{sh}}{A_{cv}} \times \frac{f_y}{400.0} = \frac{2 \times 32.17 \times 3 \times 248}{500 \times \times 100 \times 400} = 0.0024$$

This complies with minimum horizontal reinforcement requirements in CSA code [10].

Concrete contribution to shear capacity was determined based on equation

(11 – 7)of the CSA Code [10].

$$V_c = 0.2\,\lambda\,\sqrt{f'_c}\,b_w\,d = 0.2 \times 1.0 \times \sqrt{34.5} \times 100.0 \times 0.8 \times 2000.0 = 188.0\,kN$$

Total shear capacity:

$$V = V_c + V_s = 170 + 188 = 358\,kN$$

The designed nominal ultimate shear stresses calculated for shear force associated with ultimate flexural capacity:

$$\tau_n = \frac{F}{0.8\,l_w\,b_w} = \frac{1080 \times 10^3}{100 \times 0.8 \times 2000.0} = 6.75\,MPa = 1.13\sqrt{f'_c}\,MPa$$

A.6 Detailing

Seven pairs of 10M joint bars were provided between the vertical reinforcement to prevent shear sliding. These bars were anchored into the base by extending them at least their development length. These bars extended into the wall panel by 100 mm.

Appendix B

Design of wall 6

B.1 Flexural capacity of Wall 6

Wall 6 was designed in accordance with CAN3 – A23.3 – M84 [10]. The specimen was designed to resist a shear force greater than that corresponding to ultimate flexural capacity.

Following material properties were used in designing Wall 6:

$f'_c = 34.7\ MPa$

$f_y = 480\ MPa$

$\epsilon_y = 0.24\%$

$E = 200000\ MPa$

$E_c = 5000\sqrt{f'_c} = 29453$ MPa

$\epsilon_o = 0.00169$

Since, there was a negligible difference in the concrete strengths, of Wall 3 and Wall 6, and vertical reinforcement layout was identical, moment curvature relationship established in Appendix A for Wall 3 is applicable to Wall 6. See Figure A.1. The values obtained from sectional analysis are presented in Table B.1.

c [mm]	ϕ [$\frac{rad}{mm}$ $\times$ 10^{-3}]	M [$kN \cdot m$]	F [kN] Wall 3	Notes
1000	0.12	260.0	225.0	Moment cracking
350	1.45	477.0	413.0	# 1 yields
350	1.69	517.0	448.0	# 1,2 yield
335	2.11	575.0	498.0	# 1,2,3 yield
280	4.0	627.0	543.0	#1, 2, 3, 4, 5 yield
194	15.4	706.0	612.0	Ultimate

Table B.1: Calculation of theoretical curvature of Wall 6

Moment rotation and force flexural deformation relationships were obtained the same way as explained in Appendix A. Moment vs. rotation for Wall6 is presented in Figure B.1. Force vs. theoretical flexural displacement in Wall 6 is presented in Figure B.2. Ultimate moment capacity of Wall 6 was identical to Wall 3, i. e. 706 $kN \cdot m$. The shear force corresponding to the ultimate moment capacity was:

$$V_u = \frac{M_u}{h_w} = \frac{706.0}{1.154} = 612\ kN$$

B.2 Shear capacity of Wall 6

Four rows of 10M deformed bars at a spacing of 250 mm were used as shear reinforcement in Wall 6.

Therefore;

$$V_s = \frac{A_v\ f_y\ d}{s} = \frac{200\ \times\ 480\ \times\ 0.8\ \times\ 2000}{250.0} = 614\ kN$$

$$\rho_{sh} = \frac{4\ \times\ 200}{100\ \times\ 1000} = 0.008$$

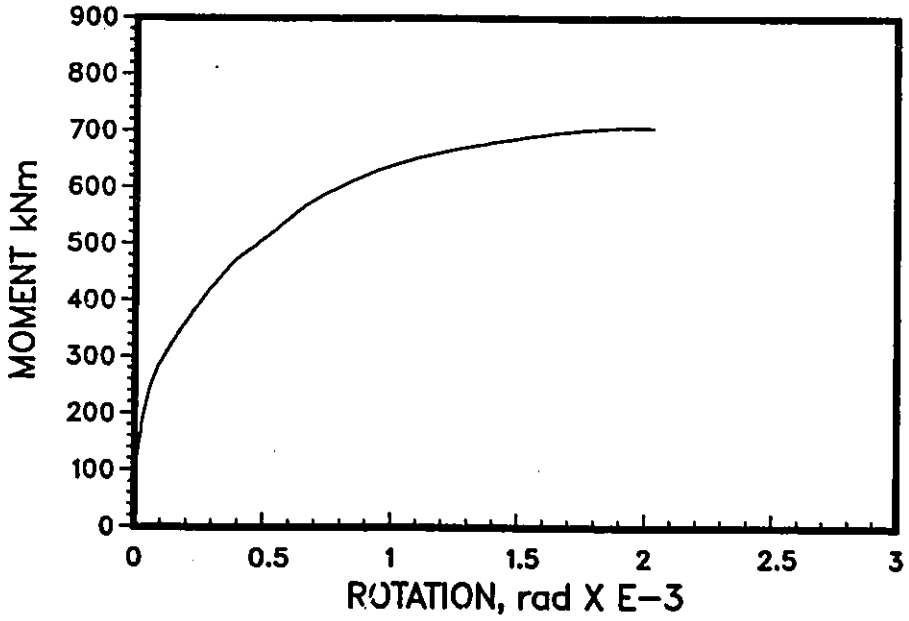

Figure B.1: Theoretical moment vs. rotation relationship in Wall 6.

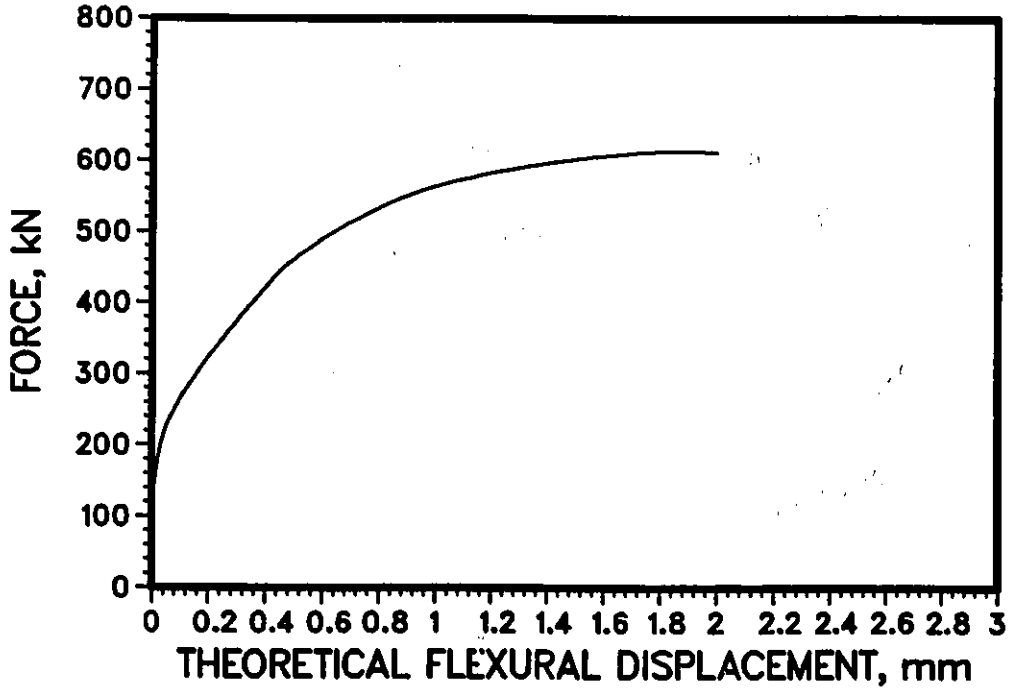

Figure B.2: Theoretical force vs. flexural deformation relationship in Wall 6.

Concrete contribution to shear capacity:

$$V_c = 0.2\,\lambda\,\sqrt{f'_c}\,b_w\,d = 0.2 \times 1.0 \times \sqrt{34.7} \times 100.0 \times 0.8 \times 2000 = 189\,kN$$

Total shear capacity :

$$V = V_s + V_c = 614 + 189 = 803\,kN > 612\,kN$$

The nominal ultimate shear stress the wall was designed to sustain:

$$\tau_n = \frac{612 \times 10^3}{100 \times 0.8 \times 2000.0} = 3.83\,MPa = 0.66\,\sqrt{f'_c}\,MPa$$

B.3 Detailing

Seven pairs of 10M joint bars were provided in between the vertical reinforcement to prevent shear sliding. These bars were anchored into the base by extending them at least their development length. These bars extended into the wall panel by 200 mm.

Ties made of 6.4 mm diametr plain bars were placed around two exterior rows of flexural reinforcement on either side of the wall. Spacing between the ties was 80 mm. These ties were provided to prevent premature buckling of exterior vertical bars.

Appendix C

Shear deformation

C.1 Shear deformation in Wall 3

As mentioned in section 2.5.5. four targets forming a rectangular grid were placed on the east side of the wall. Relative displacements of these targets were measured during the test. See Figure 2.19. Using the notations shown in Figure C.1 the strains in the x, and y directions were computed from equations:

$$\epsilon_x = \frac{1}{2}(\epsilon_{2-4} + \epsilon_{1-3})$$

$$\epsilon_y = \frac{1}{2}(\epsilon_{2-1} + \epsilon_{4-3})$$

$$\epsilon_{\theta 1} = \epsilon_{2-3}$$

$$\epsilon_{\theta 2} = \epsilon_{1-4}$$

The shear deformations were calculated from equations:

$$\Delta_{sh1} = \gamma_{xy1}\, h_w$$

$$\Delta_{sh2} = \gamma_{xy2}\, h_w$$

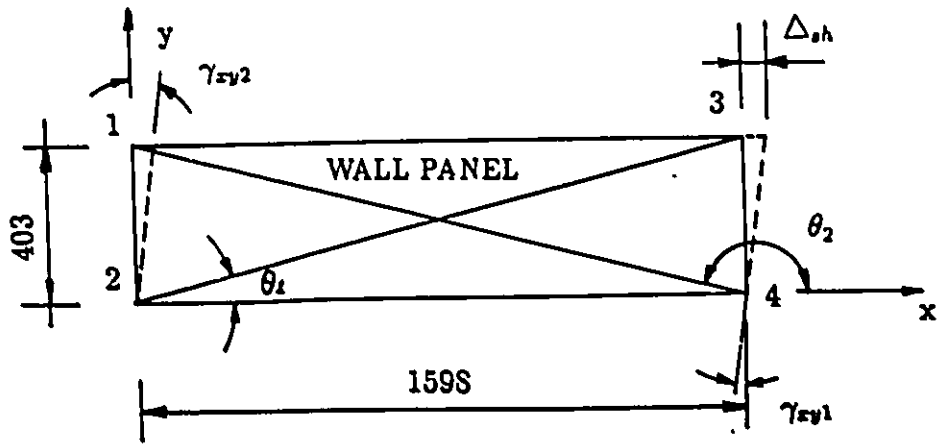

Figure C.1: Calculation of shear deformation in Wall 3

Angle of shear distortion was calculated from the transformation equation:

$$\epsilon_{\theta 1} = \epsilon_x \cos^2\theta_1 + \epsilon_y \sin^2\theta_1 - \gamma_{xy1} \sin\theta_1 \cos\theta_1$$

$$\epsilon_{\theta 2} = \epsilon_x \cos^2\theta_2 + \epsilon_y \sin^2\theta_2 - \gamma_{xy2} \sin\theta_2 \cos\theta_2$$

However;

$$\sin\theta_2 = \sin\theta_1$$

$$\cos\theta_2 = -\cos\theta_1$$

and

$$\Delta_{sh1} = \frac{h_w}{\sin\theta_1 \cos\theta_1} (\epsilon_{\theta 1} - \epsilon_x \cos^2\theta_1 - \epsilon_y \sin^2\theta_1)$$

$$\Delta_{sh2} = -\frac{h_w}{\sin\theta_2 \cos\theta_2} (\epsilon_{\theta 2} - \epsilon_x \cos^2\theta_2 - \epsilon_y \sin^2\theta_2)$$

Hence;

$$\Delta_{sh} = \frac{1}{2} (\Delta_{sh1} + \Delta_{sh2})$$

Therefore;

$$\Delta_{sh} = \frac{h_w}{\sin\theta_1 \cos\theta_1} \left(\frac{\epsilon_{\theta 1} + \epsilon_{\theta 2}}{2} - \epsilon_x \cos^2\theta_1 - \epsilon_y \sin^2\theta_1 \right)$$

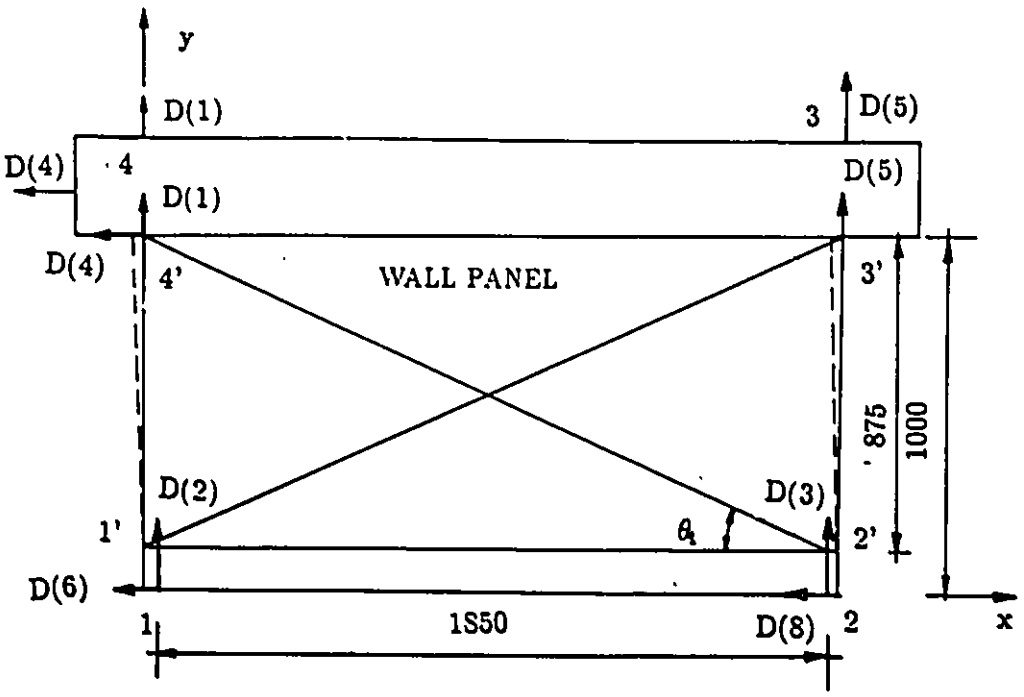

Figure C.2: Calculation of shear component in Wall 6

C.2 Shear deformation in Wall 6

Calculation of shear component in total deformation was performed based on readings of LVDT's placed at each corner of the specimen. As mentioned previously, major part of deformation took place in the upper portion of the wall above the sliding shear reinforcement. (See Figure C.2) This area was approximately 125 mm above the joint. Displacement of points 1', 2', 3', 4', were assumed as identical to those of points 1, 2, 3, 4.
Therefore the strains in x, y, and diagonal directions were calculated from:

$$\epsilon_x = \frac{1}{2}\,\frac{D(6) - D(8)}{1850}$$

$$\epsilon_y = \frac{1}{2}\,\frac{D(1) - D(2) + D(5) - D(3)}{875}$$

$$\epsilon_{\theta 1} = [D(6) - D(4)]\,\cos\theta_1 + [D(5) - D(2)]\,\sin\theta_1$$

$$\epsilon_{\theta 2} = [D(4) - D(8)]\,\cos\theta_1 + [D(1) - D(3)]\,\sin\theta_1$$

Calculation of shear component was similar to procedure used for Wall 3.